

# Validation of one-dimensional loss models for axial gas turbines

---

LUND UNIVERSITY

Kim Hirsch, Ramin Moghadam

Thesis for the Degree of Master of Science  
Division of Thermal Power Engineering  
Department of Energy Science  
Lund Institute of Technology | Lund University



This degree project for the degree of Master of Science in Engineering has been conducted at the Division of Thermal Power Sciences, Department of Energy Sciences, Faculty of Engineering, Lund University, and at Siemens Industrial Turbomachinery AB.

Supervisor at the Division of Thermal Power Sciences was Prof. Magnus Genrup. Supervisors at Siemens Industrial Turbomachinery AB were Lars Hedlund, Ken Flydalen and Navid Mikailian.

Examiner at Lund University was Assoc. Prof. Marcus Thern

© 2016 Kim Hirsh, Ramin Moghadam

Division of Thermal Power Engineering  
Department of Energy Sciences  
Lund University – Lund Institute of Technology  
P.O. Box 118  
SE-221 00 Lund  
Sweden

ISRN LUTMDN/TMHP-16/5362-SE  
ISSN 0282-1990

## **Abstract**

This thesis for the degree of Master of Science is a collaboration between Siemens Industrial Turbomachinery (SIT) and Lund Institute of Technology (LTH). This thesis concerns validation of a new SIT in-house code Mean Line Tool (MLT) and especially the secondary loss models used by this tool. The validation was made by investigating and comparing predictions from MLT with experiments carried out on a test turbine rig at the Royal Institute of Technology (KTH). The main goal of this investigation was to identify sources of bad prediction in order to find areas in need of improvement. To broaden the scope of this investigation, secondary loss model used in MLT were also compared to models used in other SIT in-house codes as well as models available in the open literature.

The Experiments were carried out on a single stage test rig at KTH by Johan Dahlgvist. In this thesis two different stages have been analyzed, stage 4b and stage 5. Stage 4b is a low reaction stage modelled after typical SIT steam turbine. Stage 5 modelled after a typical SIT gas turbine and therefore has a significantly higher degree of reaction.

The overall conclusion is that the secondary loss model used by MLT is greatly under predicting the secondary losses. It is believed that this is caused by a weak dependence on aspect ratio and that a more modern approach with models utilizing boundary layers should be more accurate, but no best alternative model could be determined. In addition, it has also been concluded that there is an over-sensitivity to incidence in the codes used in MLT.

## Sammanfattning

Denna masteruppsats är ett samarbete mellan Siemens Industrial Turbomachinery (SIT) och Lunds Tekniska Högskola (LTH). Uppsatsen berör validering av ett nytt in-house verktyg på SIT som heter "Mean Line Tool" (MLT), framför allt sekundärförlustmodellerna som verktyget använder. Valideringen gjordes genom att undersöka och jämföra predikteringar från MLT med experiment utförda på en testturbin vid Kungliga Tekniska Högskolan (KTH). Målet med examensarbetet var att identifiera de bakomliggande orsakerna till de dåliga predikteringarna. För att bredda vidden av denna undersökning så har förlustmodellerna som används i MLT jämförts med modeller i öppen litteratur.

Experimenten utfördes på en enstegsturbin på KTH av Johan Dahlqvist. I denna masteruppsats har två olika steg analyserats, steg 4b och steg 5. Steg 4b är ett lågreaktionssteg designat för att efterlikna typiska SIT-ångturbiner. Steg 5 är modellerat efter en typisk SIT-gasturbin har därför en högre reaktionsgrad.

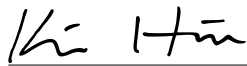
Den övergripande slutsatsen är att den predikterade sekundärförlusten från MLT är kraftigt underpredikerad. Detta tros vara en effekt av en för svag inverkan av höjdbreddförhållande. En modell med ett modernare tillvägagångssätt som tar hänsyn till gränsskikt ser ut att vara bättre på att prediktera förlusterna, men vilken testad modell som är bäst har inte kunnat fastställas. Ytterligare en slutsats är att förlustmodellerna i MLT är överkänsliga för fel anströmningsvinkel.

### **Acknowledgements**

We would like to thank Siemens Industrial Turbomachinery for their cooperation in making this thesis. We would like to extend our sincerest thanks and appreciation to our supervisors Lars Hedlund (SIT), Ken Flydalen (SIT) and Navid Mikailian (SIT) for your great support. A special thank you to Navid Mikailian, who always took his time to help us with computer related problems, regardless of time of day, or day of the week. We would also like to thank Magnus Persson (SIT) for all the good talks and coffee breaks.

Furthermore, we would like to thank our supervisor Prof. Magnus Genrup (LTH) and our examiner Assoc. Prof. Marcus Thern (LTH) for two amazing and exciting years at LTH. Without you, none of this would be possible.

Last but not least, we would like to thank our respective girlfriends and families for all the love and support during our time at Siemens Industrial Turbomachinery in Finspång.



Kim Hirsch



Ramin Moghadam

*"It is expensive to live, but the price includes a trip around the sun every year"*  
–Marcus Thern (1977–present)

# Contents

<b>1</b>	<b>Introduction</b>	<b>1</b>
1.1	Background . . . . .	1
1.2	Objective . . . . .	1
1.3	Limitation . . . . .	2
<b>2</b>	<b>Method</b>	<b>3</b>
2.1	Data comparisons . . . . .	3
2.2	TIT scaling . . . . .	4
2.3	Extra loss addition . . . . .	5
2.4	Profile loss validation . . . . .	5
2.5	Open literature comparison . . . . .	6
2.5.1	BSM . . . . .	6
<b>3</b>	<b>Theory</b>	<b>7</b>
3.1	Gas Turbine Basics . . . . .	7
3.1.1	Gas turbine work extraction . . . . .	9
3.1.2	The momentum equation . . . . .	10
3.1.3	Moment of momentum . . . . .	11
3.1.4	Euler turbomachinery equation . . . . .	11
3.2	Blade profiles . . . . .	12
3.2.1	Blade notation . . . . .	12
3.2.2	Velocity triangles . . . . .	13
3.2.3	Axial blade notation in MLT and Beta2 . . . . .	14
3.2.4	Blade Spacing . . . . .	15
3.3	Turbine Theory . . . . .	16
3.3.1	Rothalpy . . . . .	16
3.3.2	Mollier Diagram . . . . .	16
3.3.3	Radial equilibrium . . . . .	17
3.3.4	Meridional profiling . . . . .	18
3.3.5	Choke . . . . .	20
3.3.6	Limit loading . . . . .	21
3.3.7	Averaging . . . . .	21
3.4	Turbine characteristics . . . . .	21
3.4.1	Turbine efficiency . . . . .	21

3.4.2	Total-to-static isentropic efficiency . . . . .	22
3.5	Dimensionless parameters . . . . .	23
3.5.1	Dimensionless speed . . . . .	23
3.5.2	Dimensionless massflow . . . . .	23
3.5.3	Flow coefficient . . . . .	24
3.5.4	Stage Loading . . . . .	24
3.5.5	Degree of reaction . . . . .	24
3.5.6	Reynolds number . . . . .	25
3.5.7	Turbine scaling . . . . .	25
3.5.8	Loss coefficient . . . . .	26
3.5.9	Streamtube thickness variation . . . . .	26
3.5.10	Mach number . . . . .	26
3.5.11	Laval number . . . . .	27
3.6	Relative stagnation pressure . . . . .	27
3.7	Loss sources . . . . .	28
3.7.1	Boundary Layer formation . . . . .	28
3.7.2	Displacement thickness . . . . .	29
3.7.3	Secondary flow . . . . .	30
3.7.4	Rotor pump work . . . . .	32
3.7.5	Rotor purge flow . . . . .	32
3.8	Loss models . . . . .	33
3.8.1	MLT model . . . . .	33
3.8.2	BSM loss model . . . . .	33
3.8.3	Mukhatarov, Krichakin . . . . .	34
3.8.4	Traupel . . . . .	34
3.8.5	Sharma and Butler . . . . .	35
<b>4</b>	<b>Computational programs</b>	<b>37</b>
4.1	MLT . . . . .	37
4.2	Beta2 . . . . .	37
4.3	CATO . . . . .	38
4.4	MISES . . . . .	38
4.5	AutoMLT . . . . .	38
<b>5</b>	<b>The test turbine</b>	<b>39</b>
5.1	Geometries . . . . .	40
5.1.1	Test Turbine stage 4b . . . . .	40
5.1.2	Test Turbine stage 5 . . . . .	42
5.2	Measuring equipment . . . . .	44
<b>6</b>	<b>Experiment validation</b>	<b>46</b>
6.1	Global and traversed data comparison . . . . .	46
6.2	Traverse errors . . . . .	47



<b>7</b>	<b>Results</b>	<b>50</b>
7.1	TIT scaling	50
7.1.1	Scaling method validation	52
7.2	Stage 4b	57
7.2.1	Global evaluation – PR = 1.23	57
7.2.2	Global stage evaluation – PR = 2.06	61
7.2.3	Traversed data analysis – PR = 1.23	62
7.2.4	Analysis of radial distribution - Stator	63
7.2.5	Rotor and stator loss coefficients	65
7.2.6	Extra loss addition – PR = 1.23	67
7.2.7	Extra loss addition – PR = 2.06	72
7.3	Global evaluation of stage 5	73
7.3.1	Extra losses	75
7.4	Comparison stage 5 and 4b	75
7.4.1	Total-to-static efficiency	75
7.4.2	Total-to-total efficiency	76
7.5	Profile loss validation	77
7.6	Alternative loss models	78
7.6.1	BSM	78
7.6.2	MuKr	79
7.6.3	Traupel	80
7.6.4	ShBu	82
7.6.5	Comparison between secondary loss models	83
7.6.6	Secondary loss investigation	89
7.7	Cavity purge flow impact	93
<b>8</b>	<b>Discussion</b>	<b>94</b>
8.1	Conclusions	94
8.2	Future work	96

# List of Figures

Figure 3.1	Schematic single shaft gas turbine . . . . .	8
Figure 3.2	Ideal closed Brayton cycle . . . . .	8
Figure 3.3	Real Brayton Cycle . . . . .	9
Figure 3.4	Flow turning and its effect on flow area . . . . .	10
Figure 3.5	Control volume for deriving of moment of momentum law	11
Figure 3.6	Turbine blade angles and notation . . . . .	13
Figure 3.7	Velocity triangles describing a turbine cascade with an- gles defined from both axial and tangential plane . . . . .	14
Figure 3.8	Blade notation used in MLT and Beta2, n = Throat sections	14
Figure 3.9	Viscous and diffusion losses as functions of pitch chord ratio . . . . .	15
Figure 3.10	Mollier diagram for a schematic expansion process . . . . .	17
Figure 3.11	Fluid element in radial equilibrium . . . . .	18
Figure 3.12	Static pressure lines for a blade row with lean . . . . .	19
Figure 3.13	Effect of radial force on streamline over a blade . . . . .	20
Figure 3.14	Stator outlet static pressure profile, conceptual drawing . . . . .	20
Figure 3.15	Wall boundary layer build-up . . . . .	29
Figure 3.16	Illustration of Displacement thickness . . . . .	29
Figure 3.17	Secondary flows in a blade row . . . . .	31
Figure 3.18	Flow paths in a rotor cavity with two moving walls . . . . .	32
Figure 3.19	Graph used in Traupel's loss coefficient . . . . .	35
Figure 5.1	KTH's test rig with stage 5's rotor visible . . . . .	40
Figure 5.2	Stage 4b's stage geometry profiles . . . . .	41
Figure 5.3	Drawing of KTH's test turbine with stage 4b mounted, hot dimensions . . . . .	41
Figure 5.4	Stage 5's stage geometry profiles . . . . .	43
Figure 5.5	Drawing of KTH's test turbine with stage 5 mounted, hot dimensions . . . . .	43
Figure 6.1	Comparison between datasets for stage 4b, $\Pi \approx 1.23$ . . . . .	47
Figure 6.2	Comparison between predicted and measured radial pres- sure distribution . . . . .	48

Figure 6.3	Expansion calculated from global measurements and measured loss coefficients for stage 4b's rotor and stator, $\Pi_{ts} \approx 1.23$ and $v_{ts} \approx 0.55$ . . . . .	49
Figure 6.4	Impact of stator tangential position on measured global reaction . . . . .	49
Figure 7.1	Varying temperatures at two different turbine speeds, $\Pi \approx 2.06$ , stage 4b . . . . .	52
Figure 7.2	Comparison of scaling accuracy for total-to-static efficiency, stage 4b, $\Pi_{ts} \approx 1.23$ . . . . .	53
Figure 7.3	Comparison of scaling accuracy for total-to-static efficiency, stage 4b, $\Pi_{ts} \approx 1.23$ . . . . .	54
Figure 7.4	Comparison of scaling accuracy for total-to-static efficiency, stage 4b, $\Pi_{ts} \approx 1.23$ . . . . .	55
Figure 7.5	Differences between scaled and unscaled simulation using different loss models, stage 4b, $\Pi_{ts} \approx 1.23$ . . . . .	56
Figure 7.6	Total-to-static efficiency for stage 4b, $\Pi \approx 1.23$ . . . . .	58
Figure 7.7	Pressure based degree of reaction as function of dimensionless speed, stage 4b, $\Pi \approx 1.23$ . . . . .	59
Figure 7.8	Dimensionless mass flow as function of dimensionless speed, stage 4b, $\Pi \approx 1.23$ . . . . .	60
Figure 7.9	Turbine characteristics as function of dimensionless speed, stage 4b, $\Pi \approx 2.06$ , correlation based loss, TIT scaled to 345 K . . . . .	61
Figure 7.10	Pressures within stage 4b, $\Pi \approx 1.23$ . . . . .	62
Figure 7.11	Total stator exit velocity for stage 4b, $\Pi \approx 1.23$ . . . . .	63
Figure 7.12	Radial distribution at stator exit, stage 4b, $\frac{N}{\sqrt{T^*}} = 161$ , $\Pi \approx 1.23$ . . . . .	64
Figure 7.13	Radial distribution and iso plots over the stator exit, stage 4b, $\Pi \approx 1.23$ . . . . .	64
Figure 7.14	Total loss coefficients for the uncooled 4b stage, $\Pi \approx 1.23$ . . . . .	65
Figure 7.15	Secondary loss coefficient, stage 4b stator, $\Pi \approx 1.23$ . . . . .	67
Figure 7.16	Loss coefficients for stage 4b rotor, $\Pi \approx 1.23$ . . . . .	67
Figure 7.17	Total-to-static efficiencies for different extra loss additions, stage 4b, $\Pi \approx 1.23$ . . . . .	69
Figure 7.18	Pressure degree of reaction for different extra loss additions, stage 4b, $\Pi \approx 1.23$ . . . . .	70
Figure 7.19	Dimensionless mass flow for different extra loss additions, stage 4b, $\Pi \approx 1.23$ . . . . .	71
Figure 7.20	Turbine characteristics with 7.23 % extra loss in the rotor, stage 4b, $\Pi_{ts} = 2.06$ . . . . .	72
Figure 7.21	Turbine characteristics for stage 5 as function of dimensionless speed, $\Pi_{ts} \approx 1.23$ . . . . .	73

Figure 7.22	Stage 5 characteristics as function of pressure ratio, $\frac{N}{\sqrt{T^*}} \approx 577$ , scaled to $T^* = 350$ K . . . . .	74
Figure 7.23	Total-to-static efficiency for stage 5 with stator losses matched to stage 4b, $\Pi_{ts} \approx 1.23$ . . . . .	75
Figure 7.24	Comparison of total-to-static efficiency between stage 5 and stage 4b, $\Pi_{ts} \approx 1.23$ . . . . .	76
Figure 7.25	Total-to-total efficiency as function of dimensionless speed, $\Pi_{ts} \approx 1.23$ . . . . .	77
Figure 7.26	Traupel's and MLT profile loss, AVDR compensated, stage 4b, $\Pi \approx 1.23$ . . . . .	78
Figure 7.27	Total loss coefficients with BSM's secondary loss model, stage 4b, $\Pi_{ts} \approx 1.23$ . . . . .	79
Figure 7.28	Turbine characteristics with BSM's loss model for the stator, stage 4b, $\Pi_{ts} \approx 1.23$ . . . . .	79
Figure 7.29	Total loss coefficients for the MuKr model, stage 4b, $\Pi_{ts} \approx 1.23$ . . . . .	80
Figure 7.30	Comparison between experiment, unmodified MLT and MLT with MuKr's secondary loss model, stage 4b, $\Pi_{ts} \approx 1.23$ . . . . .	80
Figure 7.31	Total loss coefficients with Traupel's secondary loss model, $\Pi_{ts} \approx 1.23$ . . . . .	81
Figure 7.32	Comparison between experiment, unmodified MLT and MLT with Traupel's secondary loss model, stage 4b, $\Pi_{ts} \approx 1.23$ . . . . .	81
Figure 7.33	Traupel's secondary loss graph with stator and rotor operating points marked, stage 4b, $\Pi \approx 1.23$ , $\frac{N}{\sqrt{T^*}} \approx 295$ . . . . .	82
Figure 7.34	Total loss coefficients with ShBu secondary loss model, stage 4b, $\Pi_{ts} \approx 1.23$ . . . . .	82
Figure 7.35	Comparison between experiment, unmodified MLT and MLT with ShBu's secondary loss model, stage 4b, $\Pi_{ts} \approx 1.23$ . . . . .	83
Figure 7.36	Total-to-static efficiency for stage 4b, $\Pi_{ts} \approx 1.23$ with 4 different loss models . . . . .	85
Figure 7.37	Degree of reaction for stage 4b, $\Pi_{ts} \approx 1.23$ with 4 different loss models . . . . .	85
Figure 7.38	Total-to-static efficiency for stage 5, $\Pi_{ts} \approx 1.23$ with 4 different loss models . . . . .	86
Figure 7.39	Degree of reaction for stage 5, $\Pi_{ts} \approx 1.23$ with 4 different loss models . . . . .	86
Figure 7.40	Total-to-static efficiency for stage 4b, $\Pi_{ts} \approx 2.06$ with 4 different loss models . . . . .	87
Figure 7.41	Degree of reaction for stage 4b, $\Pi_{ts} \approx 2.06$ with 4 different loss models . . . . .	87

Figure 7.42	Total-to-static efficiency as function of $\Pi_{ts}$ , stage 5, $\frac{N}{\sqrt{T^*}} \approx 560$ . . . . .	88
Figure 7.43	Degree of reaction as function of $\Pi_{ts}$ , stage 5, $\frac{N}{\sqrt{T^*}} \approx 560$ . . . . .	88
Figure 7.44	Comparison between secondary loss coefficients with varying aspect ratio for stage 4b's stator . . . . .	90
Figure 7.45	Comparison between secondary loss coefficients with varying exit angle for stage 4b's stator . . . . .	90
Figure 7.46	Comparison between secondary loss coefficients with varying aspect ratio for stage 4b's rotor . . . . .	91
Figure 7.47	Comparison between secondary loss coefficients with varying exit angle for stage 4b's rotor . . . . .	91
Figure 7.48	Comparison between secondary loss coefficients with varying aspect ratio for stage 5's rotor . . . . .	92
Figure 7.49	Comparison between secondary loss coefficients with varying exit angle for stage 5's rotor . . . . .	92
Figure 7.50	Impact of cavity purge flow, stage 4b, $v_{ts} \approx 0.47$ . . . . .	93

# List of Tables

5.1	Geometry parameters for test turbine stage 4b (CATO) . . . . .	42
5.2	Geometry parameters for test turbine stage 5 (CATO) . . . . .	44
7.1	Scaled non-dimensional turbine speed for the speed sweep, stage 4b, $\Pi \approx 2.06$ . . . . .	51
7.2	Scaled non-dimensional turbine speed for the pressure ratio sweep, stage 5 . . . . .	51

# Nomenclature

## Latin symbols

---

A	[m <sup>2</sup> ]	Area
a	[m/s],[m]	Local sonic velocity, throat distance
B	[m]	Axial chord
b, C	[m]	Chord
c	[m/s]	Absolute velocity
$c_p$	[kJ/(kgK)]	Specific heat capacity at constant pressure
$c_v$	[kJ/(kgK)]	Specific heat capacity at constant volume
D	[-]	Diffusion factor
d	[m]	Diameter
H	[-],[m]	Shape parameter, blade height
h	[kJ/kg]	Enthalpy
I	[kJ/kg]	Rothalpy
M	[-]	Mach number
$\dot{m}$	[kg/s]	Mass flow
N	[rpm]	Rotational speed
n, z	[pcs]	Number of blades
o	[m]	Throat area
p	[Pa]	Pressure
P	[W]	Power
R	[kJ/(kgK)]	Specific gas constant
r	[m]	Radius
Re	[-]	Reynolds number
s	[J/K], [m]	Entropy, surface distance
T	[K]	Temperature
TI	[%]	Turbulence intensity
t, s	[m]	Pitch, spacing
U, u	[m/s]	Blade speed
v	[m/s]	Velocity
w	[m/s]	Relative velocity, specific work
x	[m]	Axial distance
Zw	[-]	Zweifel coefficient

### Greek symbols

---

$\alpha$	[°]	Absolute flow angle
$\beta$	[°]	Relative flow angle
$\gamma$	[-]	Ratio of specific heats
$\Delta$	[-]	Difference
$\delta$	[°]	Uncovered turning angle
$\delta^*$	[m]	Displacement thickness
$\zeta$	[-]	Enthalpy based loss Coefficient
$\eta$	[-]	Efficiency
$\theta$	[m]	Momentum thickness
$\kappa$	[-]	Ratio of specific heats
$\Lambda$	[-]	Degree of reaction
$\lambda$	[-]	Laval number
$\mu$	[Ns/m <sup>2</sup> ]	Dynamic viscosity
$\Pi$	[-]	Pressure ratio (total-to-static)
$\nu$	[-]	Isentropic velocity ratio
$\rho$	kg/m <sup>3</sup>	Density
$\tau$	[N m]	Torque
$\Phi$	[-]	Flow coefficient
$\Psi$	[-]	Stage loading coefficient
$\omega$	[°], [rad/s]	Wedge angle, angular velocity

### Superscripts

---

\*

Total, critical



## Subscripts

---

0	Turbine inlet, vane inlet
1	Vane outlet, blade outlet
2	Blade outlet, turbine outlet
a, ax, x	Axial
av	Average
des	Design
e	Effective
f	Friction
h	Enthalpy
is, s	Isentropic,
i	Incidence
m	Metal, blade, meridional
max	Maximum
opt	Optimum
p	Pressure
pr	Profile
r	Radial
ref	Reference
rel	Relative
s	Specific
T	Temperature
ts	Total-to-static
tt	Total-to-total
$\theta$	Tangential

## Abbreviations

---

4b	Test Turbine stage 4b
BSM	Benner, Sjolander, Moustapha
CATO	Common Airfoil Tool
KTH	Royal Institute of Technology
LE	Leading edge
MLT	Mean Line Tool
MuKr	Mukhatarov, Krichakin
p.p.	Percentage point
PS	Pressure side
ShBu	Sharma, Butler
SIT	Siemens Industrial Turbomachinery
SS	Suction side
TE	Trailing edge
TIT	Turbine Inlet Temperature

# Chapter 1

## Introduction

### 1.1 Background

In gas turbine development, it is of great importance to estimate turbine performance and efficiency at an early stage in the design process. Since exact geometries for blades and channel will not be available until much later in the process, some method to evaluate designs based on simple parameters must be used. This is where 1- and 2-dimensional analysis is of great importance. Since final blade geometries are not present, CFD based computations are not feasible. CFD is also problematic since it takes far too much computing power to be used as a tool for initial design. Instead, simplified models for 1- and 2-dimensional design must be used. The models use basic information such as flow coefficient, blade loading and gas angles to determine performance during the initial design phase where turbine features such as number of stages, number of blades per stage, gas angles and throat areas are decided. These models will inevitably greatly simplify reality and need to be constantly validated and updated to keep up with turbine development. A new tool known as MLT or *Mean Line Tool* is being developed on site and this new tool needs to be validated before it starts being used.

### 1.2 Objective

The objective will be to verify the validity of the new mean line design tool. The main goal is to identify sources of prediction error in the models used by this tool by comparing data from a test turbine rig with predictions.

### **1.3 Limitation**

Calculations will mainly focus on 1D. Only stationary effects will be considered and only data from a test turbine at KTH will be used for model building. The data used is the best available as of writing this thesis.

# Chapter 2

## Method

The goal of this thesis has been to verify the loss models used in a new mean line design tool against tests performed in a test turbine located at KTH in Stockholm. The tests were performed by Ph.D. student Johan Dahlqvist and not by the authors themselves. Tests were still being performed when this thesis started, and which data would be available and when was not known from the beginning. Since it was not known what the validation would result in, and with the objective of identifying sources of error in mind, results obtained during the work has dictated the work flow and what to investigate further. This made a prescribed method impractical and a flexible approach has therefore been used. A general outline of the workflow will be presented here.

The work started with theoretical studies of gas turbine models, especially models used at SIT. This was made by studying internal reports, software manuals and also open literature. The initial literature study was complemented with small parametric studies with MLT to learn how to use it and to gain a "feel" for how it behaves. Results from these initial studies were deemed as unimportant and are not included in this thesis.

### 2.1 Data comparisons

With basic theoretical studies done, the actual thesis work began. A lot of data comparisons were made, with a lot of different hypotheses to try out. To limit the amount of manual work and risk of human errors, the data comparison was decided to be made with computer programs. The tools needed did not previously exist and during the first two weeks, a new tool called AutoMLT was written in MATLAB. This tool was then used to make comparisons between in house codes and experimental measurements. The comparisons are made by using the experimental data as input boundary conditions to MLT. In order to gain the most accurate results,

new boundary conditions have been used for each data-point. This makes MLT mimic the experiment conditions exactly every time. As a result of this, only dimensionless groups are used for data visualization since they account for slight variations in inlet conditions. The number of data-points was limited, and to make comparisons easier, polynomials were constructed to fit the data-points using MATLAB's built in toolbox for statistical analysis. These polynomials were then used to plot the graphs used for the comparisons.

The study started with global data in 1-D for an easier overview. Then, more detailed data in the form of traversed data averaged to 1-D data and 2-D was used for more detailed analysis. The comparisons were used to identify areas of weakness in the models. Once a weakness had been found, theoretical studies and occasional SIT employee input was used to form one or several hypotheses for the observed behavior. After that, the hypotheses were tested by doing new comparisons, sometimes with more detailed data and sometimes with modifications or even new methods. The exact way of testing hypotheses varies depending on what has been evaluated. After the evaluation, a new round of observations, hypothesis formation and evaluation started.

## 2.2 TIT scaling

The in-house codes MLT and Beta2 are made with industrial gas turbines in mind. This means that the codes are written and tested for conditions normally found in such turbines. The test turbine on the other hand is driven by compressed air and does only reach temperatures around 80°C at the turbine inlet. This causes the models to not converge properly for the higher pressure ratios. The output from MLT suggested a higher static than total pressure at the turbine outlet and a total-to-static efficiency well above 100%. Both of these results are non-physical and clearly wrong. Closer examination of raw result data found that during the expansion, negative values for enthalpy occurred in the throat areas. This makes the gas table equations lose validity and returns non-physical results. Utilization of non-dimensional groups was used as a workaround. As explained in section 3.5, similitude can be used to take scaled test results and apply them on a real machine to predict performance. This could be used to scale up the *Turbine inlet temperature* (TIT) for the calculations if turbine speed is adjusted accordingly. The scaling is done as described in section 3.5.1. A higher temperature is selected and the appropriate speed determined.

To determine at approximately which temperature MLT will get good convergence, a small parametric study was made. First, the TIT was varied at a fixed speed and pressure ratio and the result plotted to see the nature of the convergence problem. The variation was made at two different speeds in the known problematic area and

the curves analyzed to determine a TIT which would give satisfying results.

The scaling method was then validated by applying it to a case already converging and comparing the results. If the scaling method works as intended, only negligible differences between the scaled and unscaled case should be spotted. The four different friction loss models available in MLT were analyzed to assess how they react to scaling, namely the old correlation based model, and three version of the boundary layer based loss model. The three boundary layer based versions tested are with default settings, with forced transition point and one where the model itself calculates the transition point and velocity level.

### **2.3 Extra loss addition**

To evaluate the impact of rotor and stator loss on turbine characteristics, the calculations were run again with extra loss manually added. The losses were added in two ways. First, loss was added until the predicted efficiency reached experimental values in the optimal operating point. This extra loss was then added to all data-points. This was done for both the rotor and the stator. The second approach was to match the loss coefficients measured in the experiments. This was done by adding the difference between predicted and measured experimental loss coefficients. This addition was made for stator and rotor separately to observe individual impact, but also for both simultaneously to assess if only loss coefficients are behind the observed differences.

### **2.4 Profile loss validation**

Loss model systems usually split loss generating mechanisms into different coefficients that are calculated individually. However, in reality, losses cannot be split up into small pieces as they are in calculations. Instead, an investigation of what is affecting losses must be made by trying to separate loss creating mechanisms. Studying internal reports show that the models used in MLT are highly complicated. This complexity makes it hard to investigate the different parts individually since an alteration cannot be simply made without altering the rest of the results. In order to start investigating which loss source is contributing to eventual errors, an easily separated loss source was validated. It was chosen to start investigating profile losses, and the stator is the most suitable candidate for a profile loss investigation.

The stator is stationary, and the flow has had some distance to even out before it enters the stator. This makes it reasonable to assume that there will be a 2-D flow section in the middle of the vane. This makes it possible to evaluate the blade

accurately with 2-D CFD tools. MISES was chosen for this 2-dimensional blade-to-blade CFD analysis. A 2-D section means the flow in the radial direction is negligible, making profile related losses the only significant loss source. Results from this CFD calculation were compared to MLT predictions, and also to traversed data. MISES was fed boundary conditions by importing Beta2 files based on experiments. The stator and rotor has variation in channel height. Because of this, there will be a change in flow area MISES cannot consider by the imported geometry alone. As a workaround for this, the stream-tube thickness can be altered. The loss coefficient from MISES is based on Traupel's equations for turbine loss since low Mach numbers are expected. From MLT, friction, edge, rough and Reynolds loss were summarised and the results plotted as a function of each other.

## 2.5 Comparison to open literature loss models

The work was finished by making comparisons with secondary loss models available in open literature to assess how these models performed, and what they could tell about possible modifications to be made. This comparison was done by implementing the open literature secondary loss models in MATLAB, calculating new secondary loss coefficients and tweaking the "extra loss" input in MLT to adjust the level of total loss. MLT was then run again with the modified extra loss to get an estimate of how the loss models would perform if they were used instead of the current model used in MLT. A study of how MLT and open literature secondary loss models react on altering parameters important for secondary losses, namely the aspect ratio and exit angle, was made to obtain insight into how the compared models differ. The aspect ratio was varied by altering the height of the blade, keeping the chord fixed.

### 2.5.1 BSM

BSM secondary loss model is a loss system which requires more information than just basic data about the stage geometry. A boundary layer displacement thickness is also required as input. It was assumed that the turbine inlet could be approximated as a smooth flat plate. A validation of this assumption was made by comparing calculated boundary layer thickness to a  $0.99U_{ref}$  value measured by Navid Mikailian. This comparison is not very precise, but it gives a hint whether large errors occurred due to faulty assumptions. The model was then implemented in MATLAB and tested according to the methodology described in 2.5.

# Chapter 3

## Theory

### 3.1 Gas Turbine Basics

Gas turbines are conceptually simple machines. A typical gas turbine flow diagram is illustrated in Figure 3.1. Today, gas turbines are mainly used for power generation in powerplants, for peak power-plants and for aircraft propulsion. A gas turbine consist of three main components; a compressor, a combustor and a turbine. The compressor is the first component; it compresses the working fluid to an elevated pressure level. After the compressor, the working fluid is led into the combustion chamber where heat is added to increase the temperature. The hot working fluid is expanded down to the exhaust pressure in the turbine, extracting work to power the compressor and attached load. The compressor, the turbine and load are usually on a common shaft for simplicity, but separate turbines for the compressor and external load is also a common arrangement. There are more complex arrangements, but the general principle is still the same for all gas turbines. The thermodynamic cycle a gas turbine operates on is known as the *Brayton cycle*. A T-s diagram for a simple ideal Brayton cycle is presented in Figure 3.2. The working fluid is isentropically compressed from ambient pressure  $p_1$  to an elevated pressure level  $p_2$ . Heat is then added to the working fluid in an isobaric heat addition process. The working fluid is then expanded back to the ambient pressure in an isentropic expansion. The working fluid then rejects its left over heat to the surroundings in an isobaric heat rejection process [1, pp. 503–505].



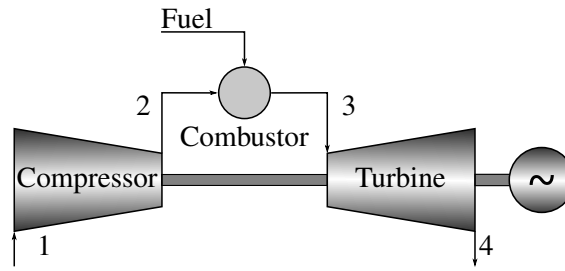


Figure 3.1: Schematic single shaft gas turbine

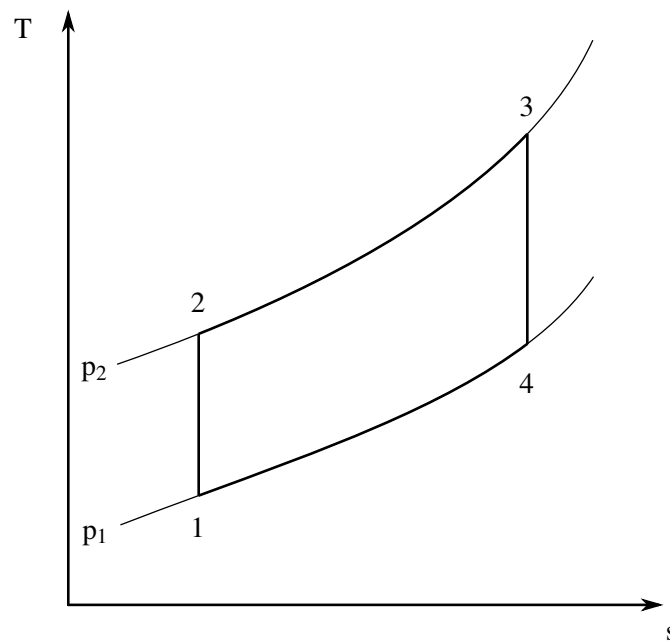


Figure 3.2: Ideal closed Brayton cycle

A practical gas turbine works on the real Brayton cycle. The cycle is normally of the open type, but closed cycles exist. An open cycle uses the working fluid once in an open loop, while a closed cycle uses the same working fluid in a closed loop. Thermodynamically, there is no difference between the two and the closed cycle is used as a model for both since it is easier to model a closed system. Furthermore, the real cycle does not have an ideal compression or expansion, nor are the heat addition and rejection isobaric processes. A T-s diagram for a modelled real cycle is illustrated in Figure 3.3. The working fluid is compressed from state 1 to state 2 and heat is added to bring the working fluid to state 3 at a slightly lower pressure than  $p_2$ . The fluid is then expanded down to state 4 and the heat is rejected to bring the fluid back to state 1. The expansion and compression both have losses associated with them, hence increasing fluid entropy. The losses in the heat addition and rejection processes are mainly pressure losses in ductwork [1, p.509].

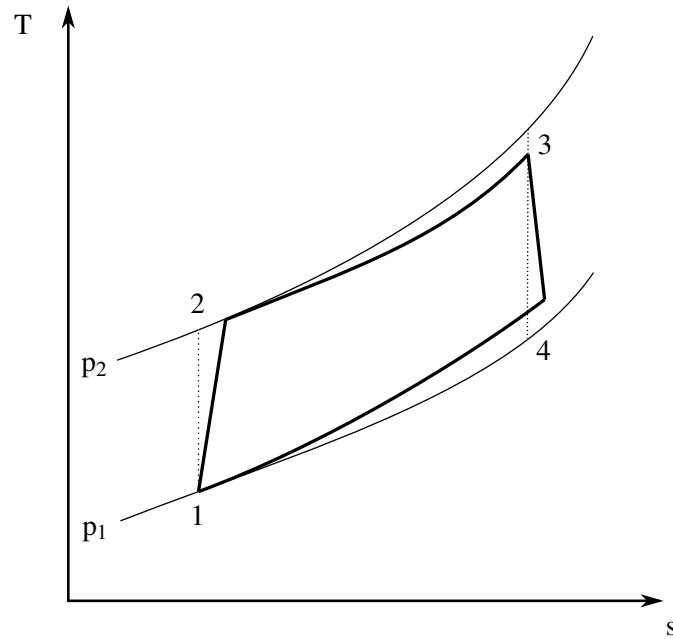


Figure 3.3: Real Brayton Cycle

### 3.1.1 Gas turbine work extraction

A turbine extracts work by expanding the working fluid. The expansion process is done by accelerating the fluid through a nozzle. A nozzle is a contracting channel where the smaller area forces the fluid to accelerate at the expense of static pressure [1, p. 228]. In a turbine, this contraction is accomplished by turning the flow away from the axial direction. Figure 3.4 illustrates two airfoils, or blades as they are called in turbine terminology. The smallest area, known as the *throat*, can easily be seen to be smaller than the inlet as an effect of the flow turning. A turbine stage is made up of two rows of blades, a stationary row called the stator, and a rotating set of blades known as the rotor. The flow turning in the rotor exerts a torque on the rotor, which can be utilized as work. The rotor torque can either come from the force required to change the fluid direction alone, or from a combination of direction change and acceleration. The turbine work and differences between operating mode will be described in section 3.1.4 and 3.5.5.

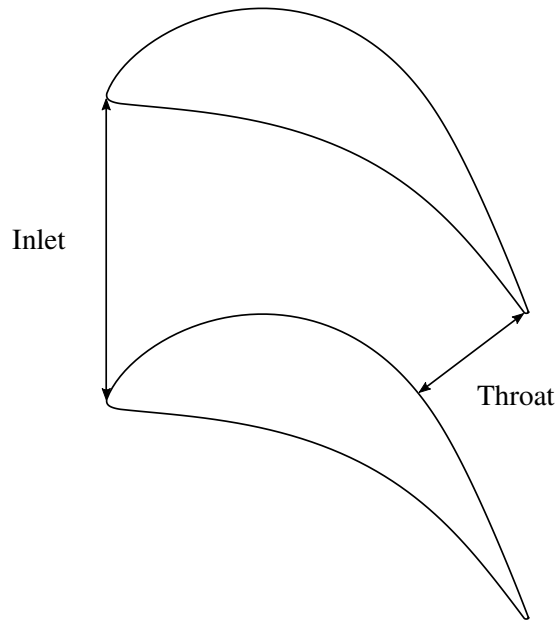


Figure 3.4: Flow turning and its effect on flow area

### 3.1.2 The momentum equation

One of the most fundamental laws in mechanics is *Newton's second law of motion*. The law describes the relation between the external forces acting on a body and its change of momentum, i.e. its acceleration. This body can for the purpose of this thesis be a fluid element. Newton's second law will be useful in deriving the forces acting on parts of the machine, for instance a turbine blade. Consider a fluid element with mass  $m$ . Along an arbitrary direction  $x$ , the sum of the body and surface forces is equal to the time rate of momentum change along this axis as described by Equation (3.1) [2, p. 9]

$$\sum F_x = \frac{d}{dt}(mc_x) \quad (3.1)$$

For a control volume with steady entering of fluid at a uniform velocity  $c_{x1}$ , and leaving at a uniform velocity  $c_{x2}$ , Equation (3.1) is re-written to

$$\sum F_x = \dot{m}(c_{x2} - c_{x1}) \quad (3.2)$$

This equation is known as the *momentum equation* in its one-dimensional form.

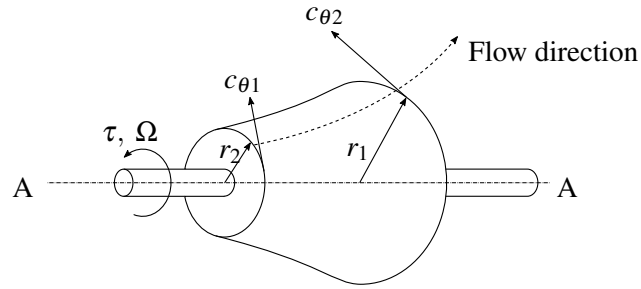


Figure 3.5: Control volume for deriving of moment of momentum law

### 3.1.3 Moment of momentum

In turbomachinery, it is useful to rewrite Newton's second law so that it applies to moments of forces. With this, it is possible to derive an expression for energy transfer in an arbitrary turbomachine. For a system with a fluid element  $m$ , the vector sum of all external forces about an axis  $A - A$  is equal to the time rate of change of angular momentum about that very same axis [2, p. 10].

$$\tau_A = m \frac{d}{dt}(rc_\theta) \quad (3.3)$$

Where  $r$  is the distance from the axis and  $c_\theta$  is the velocity perpendicular to both the axis and the radius vector. In the same way as for the momentum equation, the *law of moment of momentum* can be obtained. A control volume for a theoretical turbomachine is presented in Figure 3.5. Fluid enters with a swirling velocity  $c_{\theta 1}$  at a radius  $r_1$ . The fluid element exits the control volume at a radius  $r_2$  and a swirl velocity  $c_{\theta 2}$ . For one dimensional steady flow, the torque on the axis is expressed as

$$\tau_A = \dot{m}(r_2 c_{\theta 2} - r_1 c_{\theta 1}) \quad (3.4)$$

This equation simply states that for a fluid element inside the control volume, the time rate of momentum change is equal to the external moments acting on the element. This equation can be used to create *Euler's turbomachinery equation*, a very important equation in turbomachine design.

### 3.1.4 Euler turbomachinery equation

In a turbine, the working fluid is doing work on the rotor blades. This work can be determined by the *Euler work equation*, which will be derived in this section. This thesis will derive it as described by [2, p. 10]. The work done on a blade row can be described by the change of tangential momentum over that row. Newton's second law of motion dictates that this momentum change exerts a torque on the

blade row as described in Equation (3.4). The power output can be described by the product of the torque and angular velocity of the blade row

$$P = \tau \cdot \omega \quad (3.5)$$

The angular velocity can be expressed as  $\omega = u/r$ , where  $u$  represents the blade speed. Combining Equation (3.4) and (3.5) gives the following expression

$$P = \dot{m} \cdot (u_2 \cdot c_{\theta 2} - u_1 \cdot c_{\theta 1}) \quad (3.6)$$

If Equation (3.6) is divided by the massflow, the specific work equation is obtained

$$w = u_2 \cdot c_{\theta 2} - u_1 \cdot c_{\theta 1} \quad (3.7)$$

This equation is normally referred to as Euler's turbomachinery equation and is defined to express the work a rotor does on the fluid which would be the case in a compressor. In turbine terminology, it is therefore usually rewritten to give a positive work output. The equation is simply rewritten to

$$w = u_1 \cdot c_{\theta 1} - u_2 \cdot c_{\theta 2} \quad (3.8)$$

The resulting equation clearly shows that in a turbine, only the rotor row is extracting work from the fluid since the stationary row has a velocity of zero. Stator rows are however still subjected to torque from the momentum change over the stator row.

## 3.2 Blade profiles

### 3.2.1 Blade notation

In order to understand the contents of this thesis, blade notation is important to remember. The notation used in this thesis and at SIT is defined in Figure 3.6

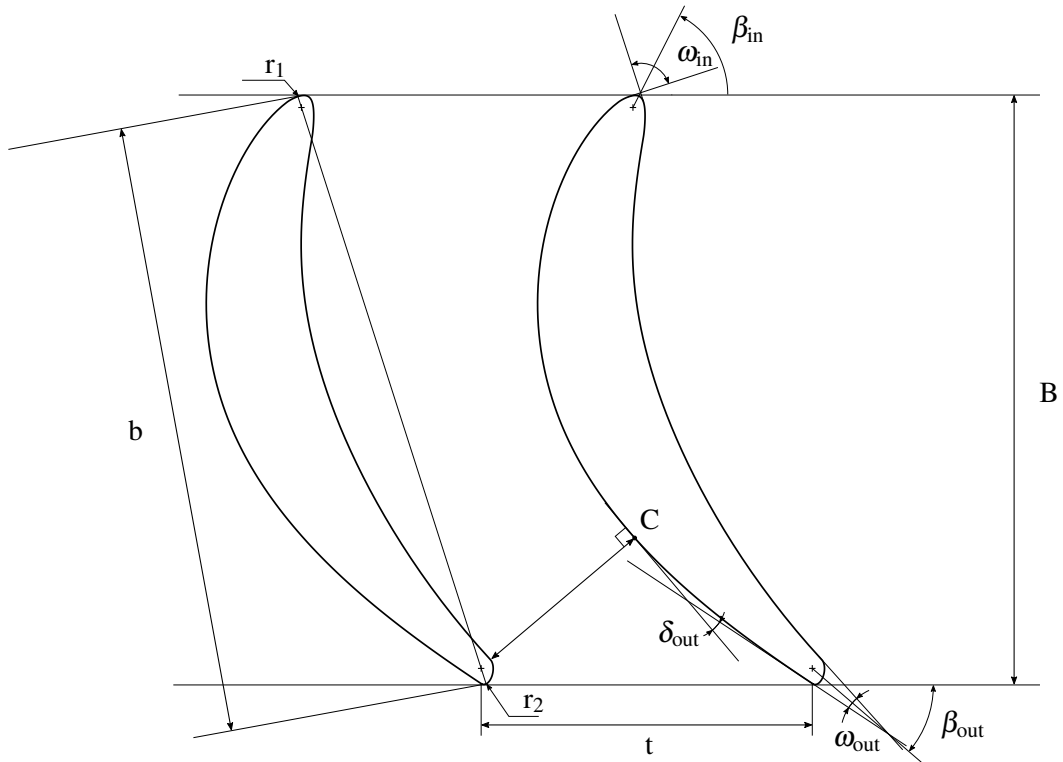


Figure 3.6: Turbine blade angles and notation

### 3.2.2 Velocity triangles

SIT designers use an angle definition not usually encountered in gas turbine literature. At SIT, the angles are defined from the tangential plane as opposed to the more common definition from the axial plane. It is of great importance that the reader does not confuse these two since using the wrong definition will give large errors. In Figure 3.7 both angle definitions are illustrated. This thesis will in general use the SIT definition with the tangential plane as reference plane as illustrated in the right half of the figure.

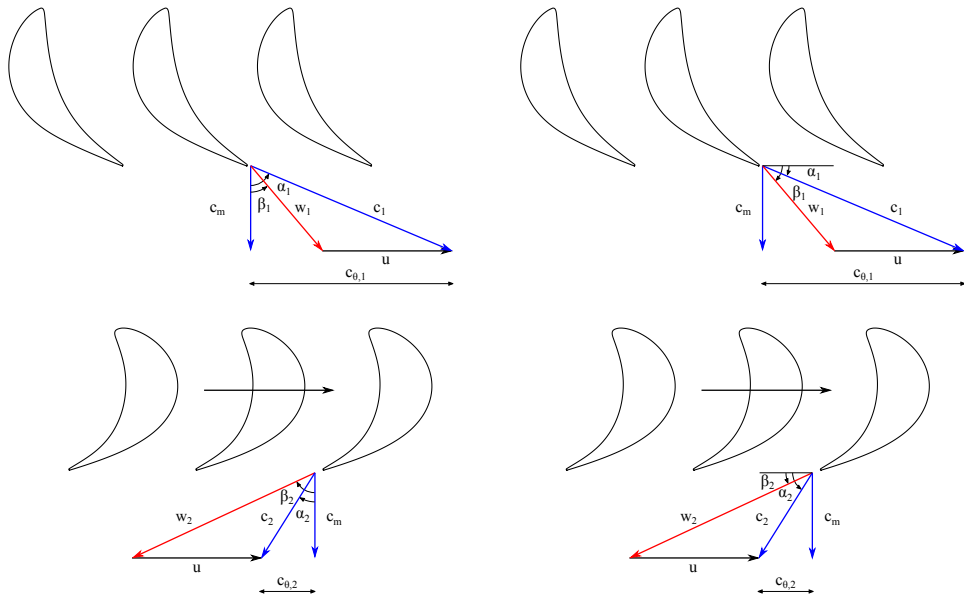


Figure 3.7: Velocity triangles describing a turbine cascade with angles defined from both axial and tangential plane

### 3.2.3 Axial blade notation in MLT and Beta2

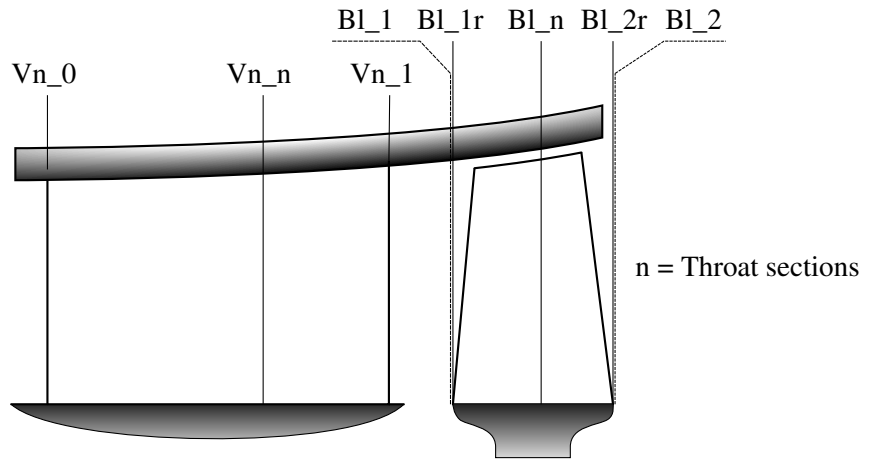


Figure 3.8: Blade notation used in MLT and Beta2,  $n = \text{Throat sections}$

Figure 3.8 show the axial blade notations used by the in-house codes. These definitions of blade sections will be extensively used in this thesis.

### 3.2.4 Blade Spacing

The blade spacing, or *pitch*, depends on how many blades are attached to the disc and at which radius the blades are mounted. The equation for blade pitch is given in [3, p. 20]

$$t = \frac{2 \cdot \pi \cdot r}{n} \quad (3.9)$$

Where  $r$  is the radius and  $n$  is the number of blades.

Given a certain rotor disc radius, decreasing the number of blades will increase the pitch. With a lower number of blades, the wetted area will decrease and thus the viscous losses will also decrease. On the other hand, a larger pitch will mean less flow guidance and turning of the flow which can lead to a higher velocity on the blade suction side resulting in larger diffusion which in turn increases the risk for boundary layer separation. Given the same rotor disc as above, increasing the number of blades will have the opposite effect. The wetted area increases, resulting in increased viscous losses. This is offsetted by better flow guidance, which decreases diffusion losses. It is therefore imperative to find an optimum pitch. This concept is demonstrated by Figure 3.9. The optimal point is where the total loss is lowest, not where one loss type is minimal. [4, p. 21]

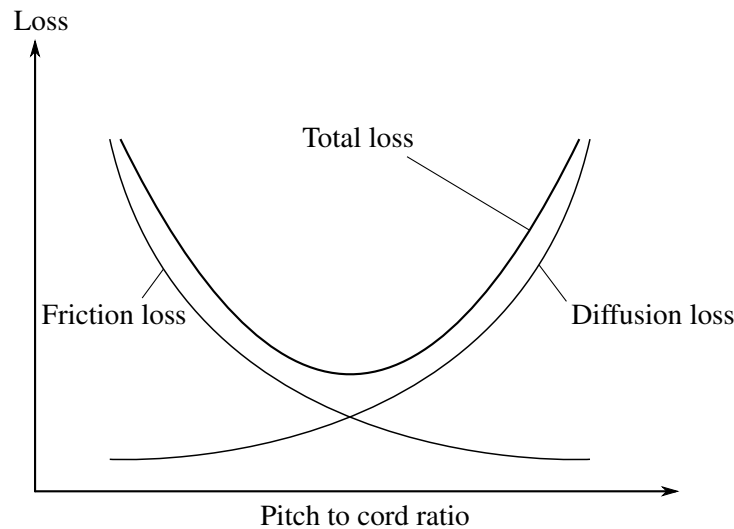


Figure 3.9: Viscous and diffusion losses as functions of pitch chord ratio (redesign of [4, Figure 1.13 p. 21])



### 3.3 Turbine Theory

#### 3.3.1 Rothalpy

The Euler work equation can be rewritten as

$$I = h^* - U c_\theta \quad (3.10)$$

where  $I$  is constant along a streamline. The quantity  $I$  is usually called *rothalpy* and is a very useful property for analyzing rotating systems. It can also be rewritten as static enthalpy, and is then defined as

$$I = h + \frac{1}{2} c^2 - U c_\theta \quad (3.11)$$

It can also be modified to incorporate relative terms to account for a rotating frame of reference, such as in a rotor. The relative tangential velocity can be obtained from the velocity triangles in Figure 3.7 by vector subtraction. The relative tangential velocity is written as

$$w_\theta = c_\theta - U \quad (3.12)$$

Substituting Equation (3.12) into Equation (3.11)

$$I = h + \frac{1}{2} (w^2 + U^2 + 2U w_\theta) - U (w_\theta + U) = h + \frac{1}{2} w^2 - \frac{1}{2} U^2 \quad (3.13)$$

This can be simplified if a relative stagnation enthalpy is defined as

$$h_{\text{rel}}^* = h + \frac{1}{2} \frac{w^2}{2} \quad (3.14)$$

Simplified, the rothalpy can be written as

$$I = h_{\text{rel}}^* - \frac{1}{2} U^2 \quad (3.15)$$

#### 3.3.2 Mollier Diagram

A Mollier diagram can be used to illustrate turbine expansions. The diagram has the fluid entropy on the abscissa and enthalpy on the ordinate. Mollier diagrams are used to illustrate processes involving fluids, such as a compression or expansion. They can also be used to draw complete cycles. Figure 3.10 illustrates a schematic expansion process over a turbine stage in a Mollier diagram. The diagram illustrates both the stagnation enthalpy drop over the stage as well as both absolute and relative isentropic velocities. It also illustrates the real stage velocities and corresponding pressure levels and enthalpies. Assuming an adiabatic turbine stage, the

specific work done on the rotor is the stagnation enthalpy drop over the stage. The specific work can thus be written as

$$w_s = \Delta h^* = h_0^* - h_2^* \tag{3.16}$$

Since an isentropic, adiabatic stator does no work, the total enthalpy in and out of a stator row is equal.

$$h_0^* = h_1^* \tag{3.17}$$

Thus

$$w_s = h_1^* - h_2^* \tag{3.18}$$

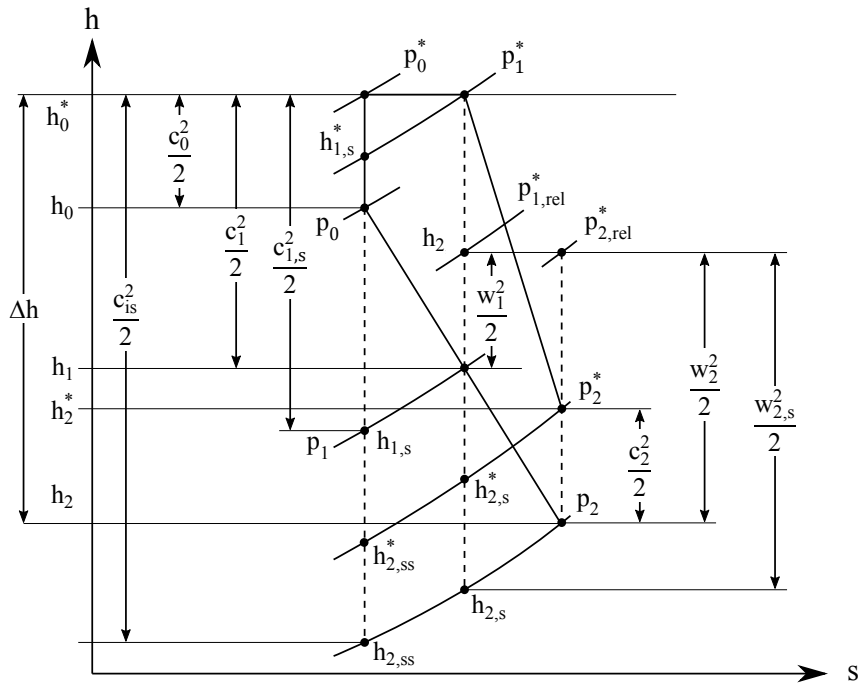


Figure 3.10: Mollier diagram for a schematic expansion process

### 3.3.3 Radial equilibrium

The radial equilibrium equation is a fundamental equation for understanding of turbomachinery. The derivation of the radial equilibrium equation is made as described in [2, p. 215]. Consider a small element of fluid  $dm$ , with the depth of a unit and a tangential width of a small angle  $d\theta$  illustrated in Figure 3.11. The element rotates about the axis at a radius of  $r$  with the tangential velocity  $c_\theta$ . The element is assumed to be in radial equilibrium, meaning centrifugal and pressure forces are

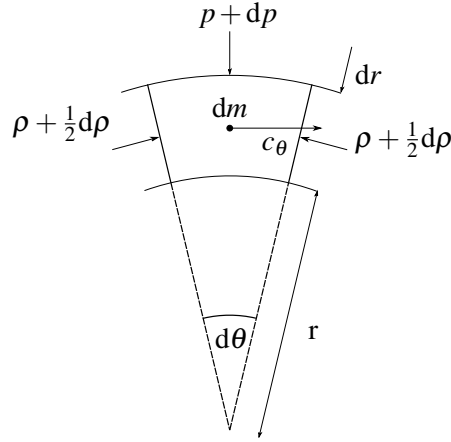


Figure 3.11: Fluid element in radial equilibrium

in balance. A force balance can now be stated as

$$(p + dp)(r + dr) \cdot d\theta - prd\theta - \left(p + \frac{1}{2}dp\right) drd\theta = \frac{dmc_\theta^2}{r} \quad (3.19)$$

By writing  $dm = \rho r d\theta dr$  and ignoring terms of second order smallness, the equation reduces to

$$\frac{1}{\rho} \frac{dp}{dr} = \frac{c_\theta^2}{r} \quad (3.20)$$

### 3.3.4 Meridional profiling

The stator vane analyzed in this thesis is of a typical SIT steam turbine design. This is evident from the contraction in the channel height in the stator in conjunction with blade lean. This is known as *meridional profiling* and is used to counter the effect of the radial equilibrium by lowering the static pressure gradient over the blade height with the goal of lowering secondary and leakage losses. How this works is described in [5], [pp. 100–105] [6] and [7] but a short explanation follows in this section.

The meridional profiling is made by combining two blade row features, a leaned blade and a contracting gas channel. Blade lean is normally used to improve the flow through a stator row by introducing a span-wise pressure gradient in the flow field. This gradient will increase the pressure at the hub and decrease it at the tip compared to a row with straight blades. This effect is exploited for a number of reasons, one of the most popular being to increase the degree of reaction at the root. This is very useful in stages with low hub-to-tip ratio where the degree of reaction can vary very much between hub and tip, and even become negative at

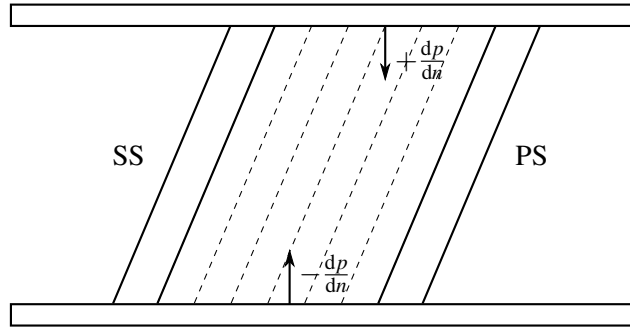


Figure 3.12: Static pressure lines for a blade row with lean

the hub. This is especially true in the last LP stages in steam turbines. In order to understand how blade lean works, imagine a 2-dimensional cascade with leaned blades as illustrated in Figure 3.12. The leaned blade will create a pressure field as illustrated by the dashed lines of constant static pressure. As can clearly be seen, this lean will introduce a pressure gradient perpendicular to the wall, which will accelerate the fluid towards the tip of the blade. This acceleration moves the streamlines inside the blade row as shown in Figure 3.13. With this radial force added, the radial equilibrium equation will be written as

$$F_r + \frac{1}{\rho} \cdot \frac{dp}{dr} = \frac{V_\theta^2}{r} + \frac{V_m^2}{r_c} \quad (3.21)$$

$$F_r + \frac{1}{\rho} \cdot \frac{d\Delta p}{dr} = \frac{V_m^2}{r_c} \quad (3.22)$$

Where  $\Delta p$  is the static pressure change by lean. Detailed derivation of the approximate relationship between blade geometry and streamline behavior is described in [5], the end result is

$$\frac{\text{Change in curvature term}}{\text{Change in pressure gradient term}} = \frac{K}{8} \cdot \left( \frac{H \cos \alpha}{C_x} \right) \quad (3.23)$$

Where  $K$  is on the order of 10, and last term in the order of  $A_x^2 \cdot \cos \alpha$  where  $A_x$  is the axial chord. This shows that for a short chord, the change in static pressure gradient will dominate. The change is local to the blade row and does not have a significant impact on the up or downstream rows. This is the case for the evaluated stator blade. For a longer chord, the change in streamline curvature will dominate with a more significant effect on up- and downstream rows since the streamline changes decays comparatively slowly. Equation (3.23) is an approximate solution, but captures the general trend important for understanding.

In the stage analyzed in this thesis, lean has been used in conjunction with a curved casing wall to reduce secondary losses and leakage losses. How this reduction in

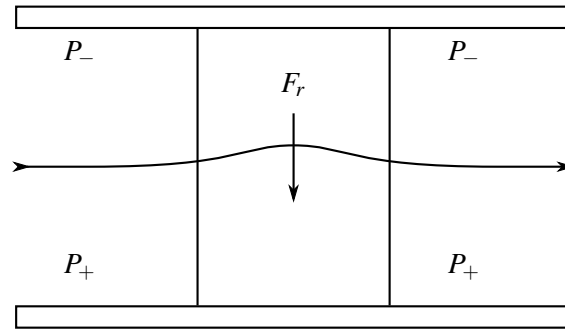


Figure 3.13: Effect of radial force on streamline over a blade

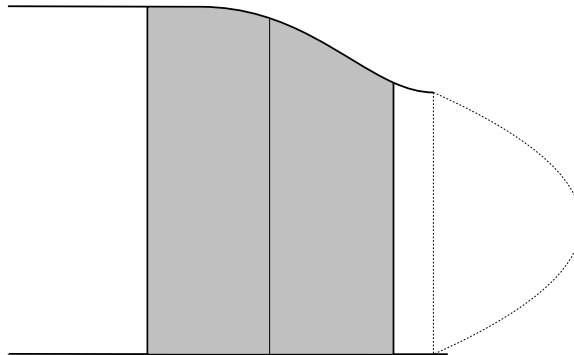


Figure 3.14: Stator outlet static pressure profile, conceptual drawing

secondary losses occurs is disputed, but it is thought to be an effect of lowered inlet velocity and reduced front loading, both of which should have a positive effect on endwall losses. The reduced leakage losses is an effect of the resulting static pressure distribution. The static pressure obtains a "bubble" shape as illustrated in Figure 3.14. The bubble shape make the pressure drop over rotor tip seals lower than normal, reducing the driving pressure and therefore leakage [5].

### 3.3.5 Choke

A turbine is said to be choked when some turbine row exhibits choked flow. Choked flow occurs when the flow reaches Mach 1 in the smallest section and means that regardless of increased pressure ratio, the velocity through this section cannot increase without changing inlet stagnation conditions [2, p. 21]. For a turbomachine, this means that once the velocity through the throats in some blade row reaches Mach 1, the mass flow has reached its maximum and can only be increased by increasing inlet temperature. A higher temperature will increase the local sonic velocity and hence the velocity at which choking occurs. The turbine has however not yet reached *limit loading*.

### 3.3.6 Limit loading

Limit loading is the point when a higher pressure drop cannot occur over the turbine and is reached when the Mach number for the axial velocity becomes unity. Since the fluid is exiting the row with an angle from the axial direction, the total velocity reaches sonic conditions long before limit loading is reached. The supersonic flow exiting the rotor creates a shock system originating from the trailing edges. As the velocity is increased, the shock rotates about the trailing edge, closer and closer to the trailing edge of the blade underneath. When the axial Mach number reaches unity, the shock is tangential and stands between the trailing edges. After this point, any further pressure drop will occur over this shock. This means that it is impossible for additional pressure drop to travel further upstream, effectively subjecting the whole blade row to the conditions at Mach 1 in axial velocity regardless of further stage pressure drop [8, pp. 70–71].

### 3.3.7 Averaging

In order to use traversed experimental data in a 1-dimensional analysis, some method for creating an average value of the approximately 1200 measurement points must be used. This might seem like an easy task, but selection of a method is difficult and might have a significant impact on the final results. In this case, the measurement and data processing was made by Ph.D. student Johan Dahlqvist at KTH. The method chosen by him was Dzungs averaging method which is described in [9]. This method averages based on the stream momentum, and mathematically mixes all exit fluid into a uniform stream, adding the mixing loss to the upstream component.

## 3.4 Turbine characteristics

### 3.4.1 Turbine efficiency

There are two main ways to describe turbine efficiency, isentropic total-to-total and isentropic total-to-static. The isentropic efficiency is defined as the ratio of actual work done to the isentropic (ideal) work. Whether the total-to-static or total-to-total efficiency is used depends on the application. In a stage where the exit kinetic energy can be utilized, the total-to-total definition is commonly used. Such applications could be in an aircraft engine where exit kinetic energy is used for propulsion or a turbine stage with another stage behind it. In the second definition, the exit kinetic energy is considered a loss in addition to the internal losses. From this, naturally, it follows that the total-to-total efficiency is always higher than the total-to-static [2, p. 24]. Total-to-static is commonly used for applications where the exit

kinetic energy cannot be utilized. One such example would be the entire turbine in stationary applications, or for the last stage. In this thesis, total-to-static will be used predominantly since the data supplied has total-to-static for all cases and there is no easy conversion between the two. Mathematically, the two definitions are written as

$$\eta_{tt} = \frac{h_0^* - h_2^*}{h_0^* - h_{2,is}^*} \quad (3.24)$$

$$\eta_{ts} = \frac{h_0^* - h_2}{h_0^* - h_{2,is}} \quad (3.25)$$

### 3.4.2 Total-to-static isentropic efficiency

In many calculation tools used in this thesis, gas states are given as total pressures and total temperatures. Because of this, a more useful definition of efficiency is required. The total-to-static efficiency can be expressed as in Equation (3.25). Assuming a perfect gas, the stagnation enthalpy can be expressed as

$$h^* = c_p \cdot T^* \quad (3.26)$$

and in the same way, the static enthalpy can be expressed as

$$h = c_p \cdot T \quad (3.27)$$

Combining Equations (3.24), (3.26) and (3.27), the total-to-static efficiency can be written as

$$\eta_{ts} = \frac{h_0^* - h_2}{h_0^* - h_{2,is}} = \frac{c_p(T_0^* - T_2)}{c_p(T_0^* - T_{2,is})} \quad (3.28)$$

Gas turbines usually operate with air as the working fluid. Over a limited pressure and temperature range, ideal gases such as air can be treated as a *perfect gas*. A perfect gas has a constant value for  $c_p$ . In turbomachinery, it is generally assumed that the air can be described as a perfect gas if average values for the process are used [2, p. 16]. The constant  $c_p$  can be used to simplify Equation (3.28) to

$$\eta_{ts} = \frac{T_0^* - T_2}{T_0^* - T_{2,is}} \quad (3.29)$$

Using the isentropic relation defined in [10, p. 56]

$$\frac{p_0^*}{p_2} = \left( \frac{T_0^*}{T_2} \right)^{\frac{\gamma}{\gamma-1}} \quad (3.30)$$

With this, the total-to-static efficiency can be rewritten as

$$\eta_{ts} = \frac{T_0^* - T_2}{T_0^* \cdot \left( 1 - \left( \frac{p_2}{p_0^*} \right)^{\frac{\gamma}{\gamma-1}} \right)} \quad (3.31)$$

### 3.5 Dimensionless parameters

The purpose of using *dimensionless groups* is that they make analysis of a fluid system much easier. A complete analytical solution of a fluid mechanics problem requires a complete solution of the Navier-Stokes equations, and is for the most cases unfeasible. Instead, experiments are used to obtain data to determine a solution [11, p. 240]. It might be very hard to conduct the large number of experiments required while varying only a single variable. Therefore, a shortcut in the form of dimensionless groups is usually taken. A dimensionless group is a collection of independent variables that combined are dimensionless. How a dimensionless group is created is outside the scope of this report, but it is described in [11, pp. 238–241]. Dimensionless groups can be used to easier determine relations between different variables. It is also possible to use a concept known as *similitude* to scale experiments to real machines and compare different experiments to each other. In this thesis, the concept of similitude will be used to make experimental data comparable and also for some parameter scaling.

Dimensionless groups are also extensively used by turbomachine designers to quickly determine turbine characteristics. The standard groups used for this kind of analysis will be listed below. It should be noted that although these groups are *called* dimensionless, it does not always mean they are completely dimensionless. One example is dimensionless turbine speed  $\frac{N}{\sqrt{T^*}}$  which can be seen to clearly have a dimension. They are however still used as if they were dimensionless. Since it is almost impossible to keep experiment variables constant while varying only one, dimensionless parameters will be used almost exclusively throughout this thesis to take care of these variations in the measurements.

#### 3.5.1 Dimensionless speed

Dimensionless speed can be used as a replacement for regular turbine speed since it gives some flexibility in turbine inlet temperature, and also accounts for the slight variations in total inlet temperature. The dimensionless speed is defined in [10, p. 180] as

$$\frac{N}{\sqrt{T^*}} \quad (3.32)$$

With  $T^*$  as the total temperature at stage inlet.

#### 3.5.2 Dimensionless massflow

Dimensionless mass flow can be used as a replacement for mass flow in the same way as dimensionless speed since it accounts for variations in inlet pressure and



total temperature. It is defined in [10, p. 180] as

$$\frac{\dot{m} \cdot \sqrt{T^*}}{p^*} \quad (3.33)$$

Where  $T^*$  and  $p^*$  are the total states at stage inlet.

### 3.5.3 Flow coefficient

In an axial turbine, the flow coefficient is defined as meridional velocity over blade speed as described in Equation (3.34). The flow coefficient can be used to quickly assess the relative flow angles. A low value suggests highly staggered blades and flow angles close to tangential. High values instead suggest highly axial flow angles, meaning mass flow through a turbine increases with increased flow coefficient [2, p. 41]. This equation is valid for all axial turbines.

$$\phi = \frac{c_m}{u} \quad (3.34)$$

The meridional velocity is written according to Equation (3.35). In a constant radius turbine, the radial component is equal to zero and the expression in Equation (3.34) can be rewritten to use the axial velocity instead. The meridional velocity is defined in [2, p. 3] as

$$c_m = \sqrt{c_a^2 + c_r^2} \quad (3.35)$$

### 3.5.4 Stage Loading

The stage loading is defined as in Equation (3.36). The coefficient expresses the work output from a turbine stage. A high stage loading will be detrimental to stage efficiency but will in turn give a lower number of stages, making a cheaper, lighter turbine possible.

$$\psi = \frac{\Delta h_0}{u^2} \quad (3.36)$$

Assuming a fully axial, adiabatic turbine stage with constant radius the stage loading can also be defined as the flow turning in the rotor. [2, p. 48, 123]

$$\psi = \frac{\Delta h_0}{u^2} = \frac{\Delta c_\theta}{u} \quad (3.37)$$

### 3.5.5 Degree of reaction

The degree of reaction requires caution from the reader since it has numerous definitions. However, all definitions are the ratio of either temperature, pressure or

enthalpy drop across the rotor over the drop across the whole stage. A low degree of reaction means a high acceleration in the stator, with only minor expansion in the rotor. A high degree of reaction means lower stator outlet velocities and higher rotor acceleration. The three definitions presented below,  $\Lambda_p$ ,  $\Lambda_h$  and  $\Lambda_T$  are based on pressure, enthalpy and temperature respectively as defined by [2, 12, p. 123, p. 12].

$$\Lambda_p = \frac{p_2 - p_3}{p_1 - p_3} \quad (3.38)$$

$$\Lambda_h = \frac{h_2 - h_3}{h_1 - h_3} \quad (3.39)$$

$$\Lambda_T = \frac{T_2 - T_3}{T_1 - T_3} \quad (3.40)$$

Since there are different definitions, great care must be taken to use the correct definition since they vary 5-10 % between each other. The degree of reaction also varies over the stage radius as mentioned in section 3.3.4. If nothing else is mentioned, the reaction is defined by pressure and at the blade mean radius.

### 3.5.6 Reynolds number

The Reynolds number is an important property for a moving fluid. It describes the ratio between kinematic and viscous forces in the fluid, and is defined by Equation (3.41). The velocities in a gas turbine vary drastically and the characteristic length can be hard to define. The most common definition however is to use velocity and density at the blade row exit and the cord as characteristic length [12, p. 13].

$$\text{Re} = \frac{c_2 \cdot \rho_2 \cdot b}{\mu} \quad (3.41)$$

A low Reynolds number indicates laminar boundary layers. Laminar boundary layers give lower friction losses, but in turn they in general separate easier. Boundary layers will be discussed further in section 3.7.1

### 3.5.7 Turbine scaling

Similitude was mentioned briefly in section 3.5. According to [2, p. 39] this can be used to scale a turbine, for instance to match a small scale experiment to a full size machine. This can also be used to scale other variables than physical size. For this thesis, the total inlet temperature will be scaled by using the dimensionless speed. Similitude dictates that in order for a scaling to be accurate, the dimensionless groups must be equal. This is expressed as

$$\frac{N_s}{\sqrt{T_s^*}} = \frac{N_{\text{org}}}{\sqrt{T_{\text{org}}^*}} \quad (3.42)$$

A higher temperature will be selected and the appropriate speed should be determined. Moving the simulation temperature to the right hand side gives an expression for scaled turbine speed as

$$N_s = \frac{N_{\text{org}}}{\sqrt{T_{\text{org}}^*}} \cdot \sqrt{T_s^*} = \frac{N_{\text{org}} \cdot \sqrt{T_s^*}}{\sqrt{T_{\text{org}}^*}} \quad (3.43)$$

By using this equation, it is possible to set the inlet temperature freely without altering the turbine characteristics.

### 3.5.8 Loss coefficient

The loss coefficient is a dimensionless coefficient describing the losses over a turbine row. The loss coefficients used in this thesis are enthalpy based as is common practice at SIT. For a stator, the coefficient is defined as

$$\zeta = 1 - 0.5 \cdot \frac{c_1^2}{\Delta h_s + \frac{c_0^2}{2}} \quad (3.44)$$

and the loss coefficient for a rotor is defined in the same way as

$$\zeta = 1 - 0.5 \cdot \frac{w_2^2}{\Delta h_s + \frac{w_1^2}{2}} \quad (3.45)$$

### 3.5.9 Streamtube thickness variation

When considering the flow through a turbine cascade, constant streamtube thickness is normally assumed. This may not be true if the channel is partially blocked by boundary layer growth or by a channel feature that alters the perceived flow area. The variation of stream-tube thickness is described by the *Axial velocity density ratio* (AVDR). It is defined in [2, p. 76] as

$$\text{AVDR} = \frac{\rho_2 \cdot c_{a2}}{\rho_1 \cdot c_{a1}} = \frac{H_1}{H_2} \quad (3.46)$$

Where  $H$  is the axial projection of flow area. This will be used later in blade-to-blade calculations with a contracting stator channel.

### 3.5.10 Mach number

The Mach number is defined as the local speed over the local speed of sound. The Mach number is an important parameter since it governs the properties of the flow,

especially for incompressible flow. For Mach numbers above 0.3, the flow can no longer be considered incompressible and at above Mach 1, shocks will occur. For a perfect gas, the Mach number is defined in [2, page 18] as

$$M = \frac{c}{a} \quad (3.47)$$

where

$$a = \sqrt{\gamma \cdot R \cdot T} \quad (3.48)$$

The Mach number can either refer to the local velocity for the flow, such as in flow fields, or a specific position. If the Mach number is referring to the entire stage it is measured at stage exit for turbines.

### 3.5.11 Laval number

Laval number is a dimensionless parameter much used at SIT. The parameter is related to the Mach number, but without two disadvantages observed for the definition of Mach number. The Mach number is not dependent on local velocity only since local speed of sound is used in the definition, making it temperature dependent. The Mach number also goes towards infinity as the pressure ratio over a supersonic nozzle increases [13] while the Laval number will approach a fixed finite value. The first weakness is important for the application of gas turbines at normal conditions, the second weakness is not so important for normal gas turbine pressure ratios. The Laval number is defined with a reference velocity that is constant throughout the stage, meaning the Laval number for the fluid within a row is dependent only on the local velocity. At SIT, the Laval number is defined in [3] as

$$\lambda = \frac{c}{\sqrt{\gamma \cdot R \cdot T_{\text{critical}}}} \quad (3.49)$$

Where  $T_{\text{critical}}$  is the static temperature at sonic conditions.

## 3.6 Relative stagnation pressure for compressible flows

The total temperature for a moving fluid is expressed as

$$T^* = T + \frac{c^2}{2 \cdot c_p} \quad (3.50)$$

From this, the relative stagnation pressure can be derived as described in [14, pp. 29-30]. By inserting the definition of sonic velocity from Equation (3.48) into Equation (3.50), the following expression is obtained

$$T^* = T + \frac{M^2 \cdot \gamma \cdot R \cdot T}{2 \cdot c_p} \quad (3.51)$$

The definition of the ratio of specific heats and specific gas constants are

$$R = c_p - c_v \quad (3.52)$$

$$\gamma = \frac{c_p}{c_v} \quad (3.53)$$

Combining Equation (3.53) and (3.52) above gives

$$R = c_p - \frac{c_p}{\gamma} = c_p \cdot \left(1 - \frac{1}{\gamma}\right) \quad (3.54)$$

Then, Equation (3.54) can be simplified to

$$\frac{R}{c_p} = 1 - \frac{1}{\gamma} = \frac{\gamma - 1}{\gamma} \quad (3.55)$$

Inserting Equation (3.55) into (3.51)

$$T^* = T \cdot \left(1 + \frac{\gamma - 1}{2} \cdot M^2\right) \quad (3.56)$$

Lastly, the isentropic relation defined in Equation (3.30) can be used to write

$$\frac{p_{\text{rel}}^*}{p} = \left(\frac{T^*}{T}\right)^{\frac{\gamma}{\gamma-1}} = \left(1 + \frac{\gamma - 1}{2} \cdot M_{\text{rel}}^2\right)^{\frac{\gamma}{\gamma-1}} \quad (3.57)$$

## 3.7 Loss sources

### 3.7.1 Boundary Layer formation

To understand how losses occur in turbines, it is very important to understand the process behind the formation of boundary layers. A boundary layer forms when there is a relative motion between a fluid and a solid object. Imagine a stationary wall with a fluid flowing parallel to it with free-stream velocity  $v$ . Viscous flow will mean that the fluid in contact with the surface satisfies the *no slip condition*, meaning it will have a velocity of zero. The velocity difference between the stationary and moving fluid will give rise to a viscous shear force within the fluid. This force will slow down the flow closest to the wall and so on until the velocity differences between stream lines, illustrated in Figure 3.15, give a viscous shear force balanced by pressure forces. The shear force between the stream lines is described in [11, p. 13] as

$$\tau = \mu \frac{du}{dy} \quad (3.58)$$

The shear force transport builds up a boundary layer along the wall until it is fully developed and assumes a shape described by Figure 3.15 This process takes place

in all parts of a turbomachine where there is a velocity difference between the fluid and walls. Boundary layers will cause losses by viscous shear in the boundary layer, also known as skin friction, but also by making the flow less resistant to pressure gradients and turn non-uniform. This is the main mechanism behind what is known as secondary flows and is further described in section 3.7.3.

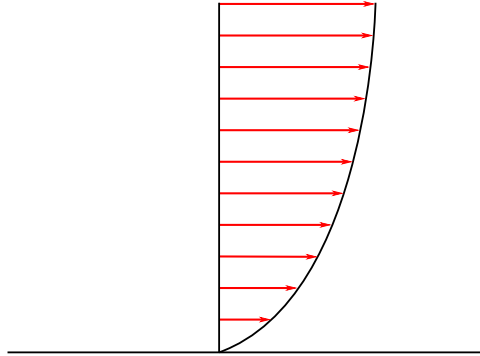


Figure 3.15: Wall boundary layer build-up

### 3.7.2 Displacement thickness

In boundary layer theory, the displacement thickness is an important parameter. It describes the distance a wall must be displaced in order to pass the same mass flow through a passage as if an inviscid calculation is made. The concept is illustrated in Figure 3.16, where the marked grey area represents flow missing compared to an inviscid solution. The square shaped area is the displacement thickness, and represents the distance the wall should be moved to satisfy equal mass flow. The boundary layer displacement thickness is defined in [11, p. 330] as

$$\delta^* = \int_0^{\infty} \left(1 - \frac{u(y)}{U}\right) dy \quad (3.59)$$

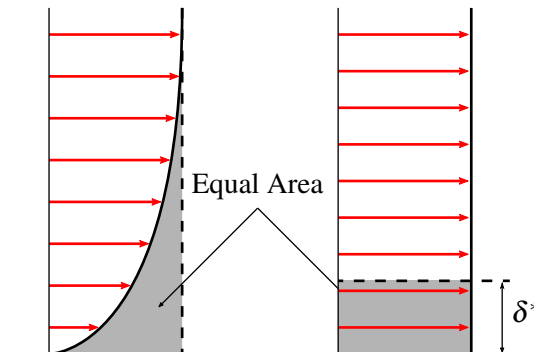


Figure 3.16: Illustration of Displacement thickness

A complete solution requires the velocity profile in the boundary layer to be known. The boundary layer shape can be obtained by solving Navier-Stokes equations, but this is very impractical. Experimental measurements could be used, but the resolution of the available data is too low for satisfactory results. Instead, an approximation of the boundary layers can be used. This approximation is called the Blasius boundary layer solution, and is an approximate solution of Navier-Stokes equations. The approximation is valid for laminar flow, i.e.  $Re < 5 \cdot 10^5$ , over a smooth flat plate and is written as in [15, p.574]

$$\delta^* = \frac{1.72}{\sqrt{Re_x}} \cdot x \quad (3.60)$$

And the total boundary layer thickness is given by

$$\delta = \frac{4.91}{\sqrt{Re_x}} \cdot x \quad (3.61)$$

If the flow is turbulent, the following approximations are used instead

$$\delta^* = \frac{0.048}{Re_x^{1/5}} \cdot x \quad (3.62)$$

$$\delta = \frac{0.38}{Re_x^{1/5}} \cdot x \quad (3.63)$$

### 3.7.3 Secondary flow

Secondary flows are usually a major source of total loss in turbines, usually comparable to that of profile losses [16, pp. 167–168]. Secondary losses are mainly from endwall boundary layer interaction with the passage. In practice, an accurate description of secondary losses could be "losses needed to obtain the correct efficiency once profile and leakage losses has been accounted for" [16, p. 164]. The secondary flow mechanisms are usually divided into two parts since they are created by different mechanisms. The two parts are known as the *horseshoe vortex* and the *passage vortex*. The horseshoe vortex is created by the interaction between the endwall boundary layer and the blade leading edge. Since the boundary layer has been slowed down by wall interaction, the total pressure will be lower than in the free-stream stagnation point where the pressure build up originates from inviscid effects. This leads to a boundary layer separation that causes the wall boundary layer to "roll up" creating a rotating vortex which folds around the leading edge. Downstream of the horseshoe vortex separation line, a new boundary layer starts to form. This layer will be skewed under influence of the pitch-wise pressure gradient which will force low momentum fluid towards the suction side, and possibly up the suction side wall. This vortex is what is usually called the passage vortex. Both of these vortices are illustrated in Figure 3.17. The interaction between these

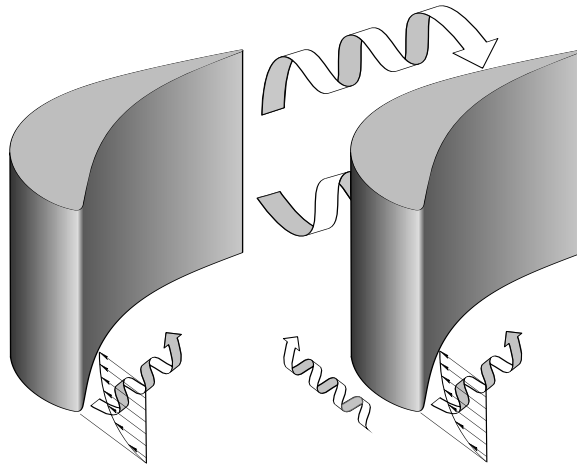


Figure 3.17: Secondary flows in a blade row

two vortices creates large losses by dissipation of the bound kinetic energy. Secondary flow in turbines are still an area with ongoing research, without any specific consensus about the exact mechanisms [17].



### 3.7.4 Rotor pump work

The fluid in the cavity between the turbine discs will be subjected to what is known as *pump work*. Close to the disc, the spinning motion will create a boundary layer following the disc. As established in section 3.3.3, turning fluid will give rise to a pressure gradient, and low momentum fluid will be swept away in the same fashion as secondary flows. The pressure gradient inside the cavity will skew the boundary layer towards the annulus and to satisfy mass continuity, it will return where the fluid velocity is lower. This process forms a cavity flow as described in [18, pp.433–434]. In the case of a moving and a stationary wall, the flow will behave as illustrated in Figure 3.18a, with fluid returning at the stationary wall. In the case of a cavity with two rotating walls, the flow pattern will behave like in Figure 3.18b, with fluid returning in the low velocity core in between the discs. The strong shear in the boundary layer causes windage losses, exerting a breaking torque on the disc. Work is also done by transporting the fluid to a higher radius with greater velocity as described by Eulers turbomachinery equation. Both these effects require work that dissipates in the fluid, becoming heat.

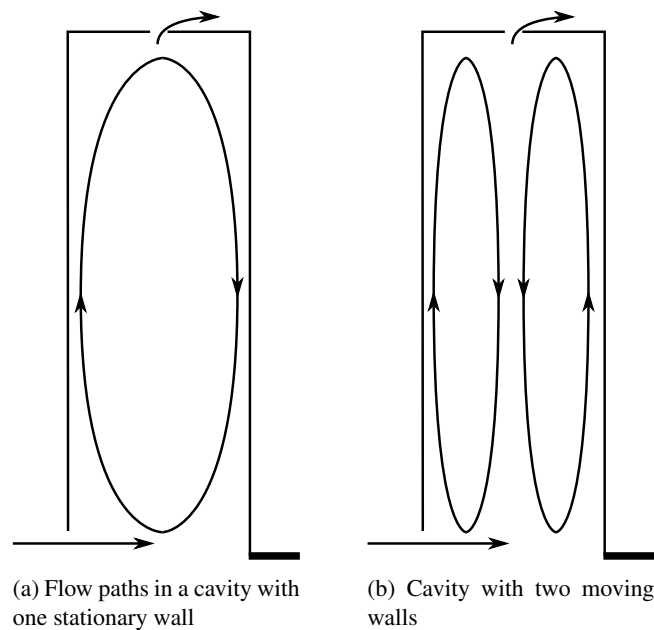


Figure 3.18: Simplified flow paths in a rotating cavity (redesign of [18, p. 443])

### 3.7.5 Rotor purge flow

The rotor is cooled by compressed air bled from the compressor. The air is inserted into the cavity, either straight in radial direction, or with some tangential velocity in the rotation direction. In the latter case, velocity is gained by accelerating the

flow with a guide vane, making required pump work described in section 3.7.4 less. Even an uncooled stage will have a need for purge air, partly to replace air heated by the pump work, but also to ensure a positive flow out of the rotor cavity. If no purge flow exists, there will be a risk that the low pressure caused by the returning flow could suck in hot gases from the turbine annulus. This cannot be allowed to happen since the hot annulus fluid would compromise the structural integrity of the discs. The purge flow is ejected into the free-stream with a velocity and enthalpy different from the free-stream and irreversible mixing of the purge jet creates entropy. The strong jet also disturbs the flow field, creating extra losses further downstream the injection point. The impact of mixing is relatively easy to quantify by mass and energy balances, but the impact of the disturbed flow field is much harder to quantify.

## 3.8 Loss models

A number of different loss models will be presented here for further use later in the thesis. All models except the in-house model are available in the open literature.

### 3.8.1 MLT model

The loss model in MLT is based on a large number of cascade tests. The model uses correlations based on these tests. Most of the tests were carried out in the 1960's and are of course most valid for airfoils typical for this period. The models have later been modified by SIT internal testing to better suit modern profiles.

### 3.8.2 BSM loss model

This loss model is based on the work of Benner, Sjolander and Moustapha who released a paper in 2006. The model uses a new and a bit unconventional loss breakdown scheme. The scheme will be briefly explained here, a full description of the thought behind the new scheme is available in [19] and the secondary loss in particular is described in [17]. The BSM model is very simple and can be implemented using only a few lines of code. In order to use the BSM model, the displacement thickness at blade inlet must be calculated as described in section 3.7.2, for both the stator and rotor row. The model uses one of Equation (3.64) and (3.65) to calculate a secondary loss coefficient, which is then used in conjunction with the *vortex penetration height* calculated with Equation (3.67). In the complete BSM loss system, Equation (3.66) is used to calculate a total loss coefficient. For the purpose of this thesis however, only the unmodified secondary loss coefficient will

be used.

$$Y_{sec} = \frac{0.038 + 0.41 \cdot \tanh(1.20\delta^*/h)}{\sqrt{\cos \gamma(CR)}(h/C)^{0.55} \left(\frac{C \cos \alpha_2}{C_x}\right)^{0.55}} \quad \text{for } h/C \leq 2.0 \quad (3.64)$$

$$Y_{sec} = \frac{0.052 + 0.56 \cdot \tanh(1.20\delta^*/h)}{\sqrt{\cos \gamma(CR)}(h/C) \left(\frac{C \cos \alpha_2}{C_x}\right)^{0.55}} \quad \text{for } h/C > 2.0 \quad (3.65)$$

$$Y_{tot} = Y_{mid} \left(1 - \frac{Z_{TE}}{h}\right) + Y_{sec} \quad (3.66)$$

$$\frac{Z_{TE}}{h} = \frac{0.10(F_t)^{0.79}}{\sqrt{CR} \left(\frac{h}{C}\right)^{0.55}} \quad (3.67)$$

### 3.8.3 Mukhtarov, Krichakin

Mukhtarov and Krichakin (MuKr) made an improved secondary loss model based on the work of Ainley and Mathieson. The secondary loss coefficient suggested by Mukhtarov and Krichakin is written as in [ch.3-5 p.58] [20].

$$\zeta_{S0} = 0.075 * \text{Re}_{des}^{0.2} \cdot \left(\frac{19}{3} - \frac{\alpha_{in,des} + \alpha_{out,des}}{30}\right) \cdot \frac{\sin(\alpha_{out,des})^{1/2}}{\sin(\alpha_{in,des})} \cdot (\zeta_{pr} - \Delta\zeta_i) \cdot \frac{o}{h} \quad (3.68)$$

The secondary loss coefficient calculated from Equation (3.68) is valid for the design point only. If the profile is subjected to incidence, the secondary loss is adjusted by a correction factor expressed by Equation (3.69).

$$\frac{\Delta\zeta_i}{\zeta_{S0}} = 400x^3 + 76x^2 + 5.6x \quad (3.69)$$

where

$$x = \frac{\alpha_{in,des} - \alpha_{in}}{\alpha_{in,des} + \alpha_{out,des}} \cdot \frac{\sin \alpha_{out,des}^{2/3}}{\sin \alpha_{in,des}} \quad (3.70)$$

### 3.8.4 Traupel

Traupel's loss model is a relatively old loss model system, containing all relevant loss sources for complete evaluation of turbine designs. In this thesis, only the secondary loss model will be used to compare in-house codes with open models. The secondary loss model is described in [21, pp. 410–412], with some in-house tweaking described in [22, pp. 11–12].

$$\zeta_S = \frac{\zeta_p}{\zeta_{p0}} \cdot F \cdot \frac{t}{l} + \zeta_\alpha \quad (3.71)$$

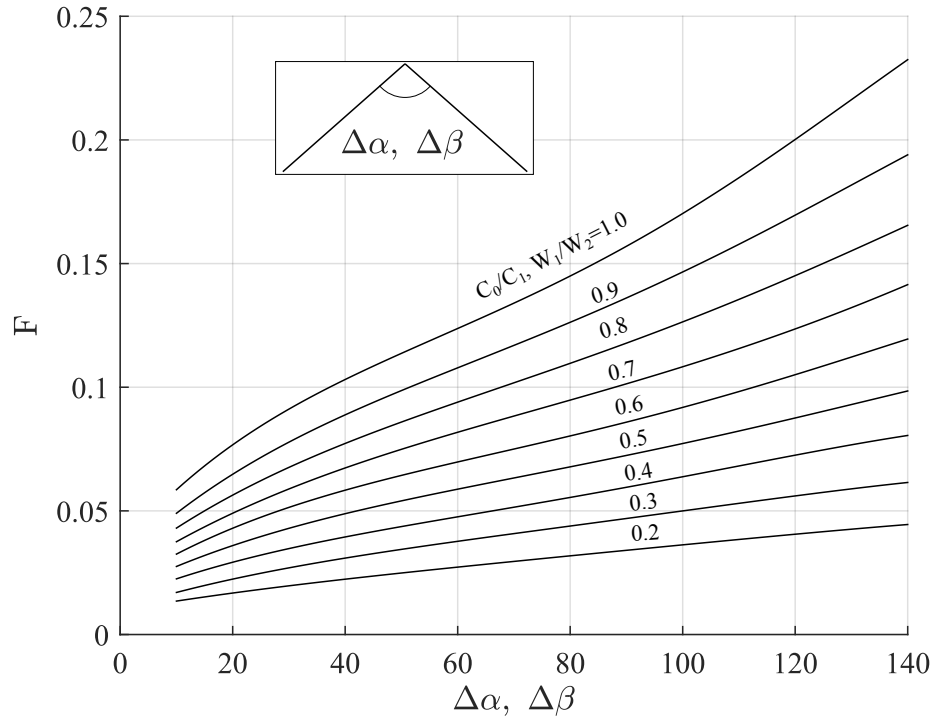


Figure 3.19: Graph used in Traupel's loss coefficient (redesign of [21, p. 411])

The model system uses loss coefficients for profile loss obtained elsewhere. The parameter  $F$  is a function of deflection and velocity ratio and can be read from the graph in Figure 3.19.

### 3.8.5 Sharma and Butler

This loss model is described in [23] and is an attempt to include viscous effects into the loss model. The MLT models as well as MuKr are older, which in general mainly considered the inviscid effects on the inlet boundary layer vorticity. The derivation of the secondary loss model is described in [23, p. 234] and is written as.

$$(1 - \phi^2)_{ew} = (1 - \phi^2)_{2D} \cdot \frac{\tau \sin \beta_2 - TET}{h} \cdot \left( 1 + 4 \frac{\varepsilon}{\sqrt{CR}} \right) \quad (3.72)$$

where

$$(1 - \phi^2) = \zeta \quad (3.73)$$

The energy loss in the endwall is analogous to the secondary loss and the 2-D loss to the airfoil profile loss. Inserting Equation (3.73) into (3.72) gives ShBu's

secondary loss coefficient in SIT notation

$$\zeta_s = \zeta_p \cdot \frac{\tau \sin \beta_2 - \text{TET}}{h} \cdot \left( 1 + 4 \frac{\varepsilon}{\sqrt{\text{CR}}} \right) \quad (3.74)$$

## **Chapter 4**

# **Computational programs**

During this thesis a couple of SIT in-house codes have been used, MLT, Beta2, CATO, MISES and AutoMLT.

### **4.1 MLT**

SIT's new code MLT is a mean line code. This code was used to analyze losses and to generate data to be compared with the test results from the test turbine at KTH. A slightly modified version of MLT v.0.9 was used for this work. The slight modification was made to allow for single stage turbines by overriding an error message causing poor convergence. However, the models are not modified, so results are directly comparable to the original version of MLT v.0.9.

### **4.2 Beta2**

SIT in-house code Beta2 is a 2-dimensional through flow solver, with correlations for 3-D effects, that is based on prof. Mamaev's correlations. Beta2 has a large number of built in loss models the user can choose between as well as different cooling schemes and whether cooling air should be injected or not. Beta2 does also give the user the opportunity to fine tune the convergence of the solution with a set of relaxation parameters. Beta2 has been used to create input files to MISES. During this thesis Beta2 v.2.07.05 was used.

### 4.3 Common Airfoil Tool (CATO)

SIT in-house code CATO is a two dimensional profiling tool used for both compressor and turbine blades. CATO uses Bezier polynomials to describe the blade geometry of the profile at each section. A section can be created either from scratch or by importing an existing set of coordinates. In CATO there is also the possibility to visualize the whole turbine including vanes, blades and channel geometry in 3-D [14]. During this thesis CATO v.6.4.0 was used to generate profile coordinates that were used in input files to Beta2.

### 4.4 MISES

MISES is a collection of programs for cascade analysis and design which includes programs for grid generation and initialization, flow analysis, plotting and interpretation of results [24]. The program is written by Mark Drela at MIT and has been used at SIT for years. MISES is a coupled viscid/inviscid solver, where the boundary layers are described by compressible integral boundary layer equations. The flow outside the boundary layers is modelled with the steady Euler equations with viscous corrections. The two are coupled and solved together by a Newton-Raphson solver. MISES was used as a second source of profile loss validation since it is an accurate 2-D blade-to-blade CFD tool.

### 4.5 AutoMLT

This code is written by the authors and is used to simplify both the result extraction process and the data comparison process. The existing in-house code sweep can be used for parametric studies but does only allow for two input parameters to be changed at a time and can only store three output parameters for each run. With AutoMLT it is possible to change as many input parameters as needed to calculate with the same conditions as the experimental case being investigated. It is also possible to store as many output parameters as desired. Another advantage of great importance to the authors is AutoMLT's possibility to automatically plot the desired results. The program is written in MATLAB.

## Chapter 5

# The test turbine

The test turbine at KTH was commissioned in 1989. It comprises of an external compressor that is compressing air and a turbine section. There is no combustion chamber so the rig operates at very low temperatures compared to those of an actual gas turbine. The 1 MW compressor can deliver a maximum pressure of 4 bar and the inlet temperature can be set between 30-80 °C by use of a cooler after the compressor exit. The rig can be used in different configurations by altering either the number of stages up to three or by changing the turbulence grid upstream of the inlet [25]. In this thesis the test rig has only been run in a single stage configuration. The rotor has been swapped between two geometries, creating what is referred to as stage 4b and stage 5. The stages use the same stator for cost considerations. The geometries are more thoroughly described in section 5.1. A drawing illustrating the channel of the test turbine can be seen in Figure 5.5 and a photograph of the turbine disassembled for rotor swap is presented in Figure 5.1.



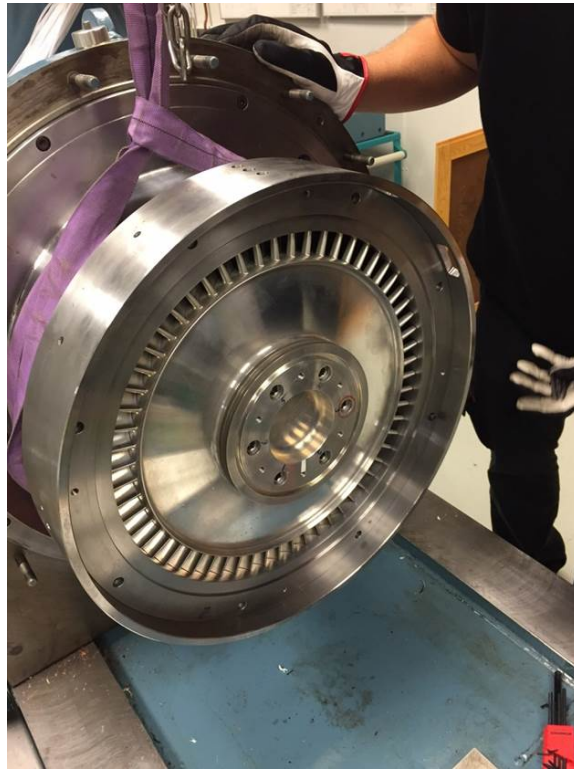


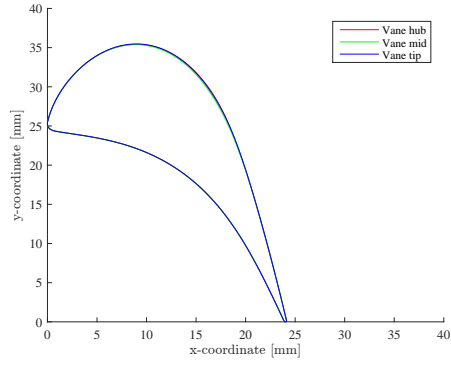
Figure 5.1: KTH's test rig with stage 5's rotor visible

## 5.1 Geometries

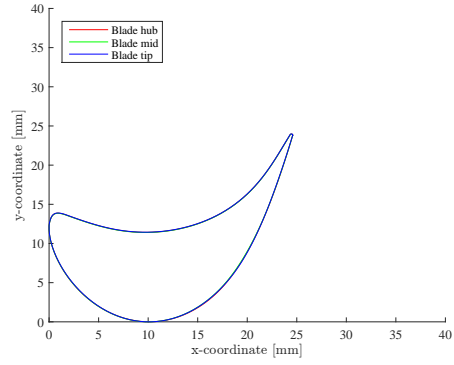
During this thesis data for two different turbine stages has been analyzed, 4b and 5. The test data analyzed is gathered by Ph.D. student Johan Dahlquist at KTH.

### 5.1.1 Test Turbine stage 4b

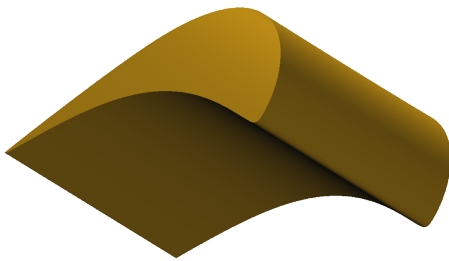
Stage 4b has been designed with straight blades. The blades are mounted radially on the rotor disc while the vanes have been stacked with a certain lean angle with respect to the stator disc radial direction [25]. Stage 4b has 42 vanes and 58 blades and is a low reaction stage designed to represent a turbine stage normally used in Finspång steam turbines. In Figure 5.2 both the vane and blade profiles are presented as well as a 3D-view from CATO. Some section parameters are also presented in Table 5.1.



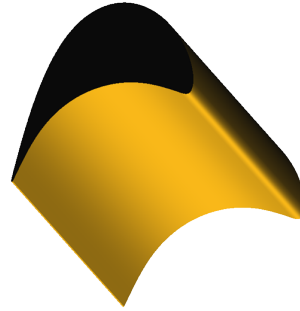
(a) Stage 4b's vane sections geometry (CATO)



(b) Stage 4b's blade sections geometry (CATO)



(c) 3D-view of stage 4b's vane profile



(d) 3D-view of 4b blade profile

Figure 5.2: Stage 4b's stage geometry profiles

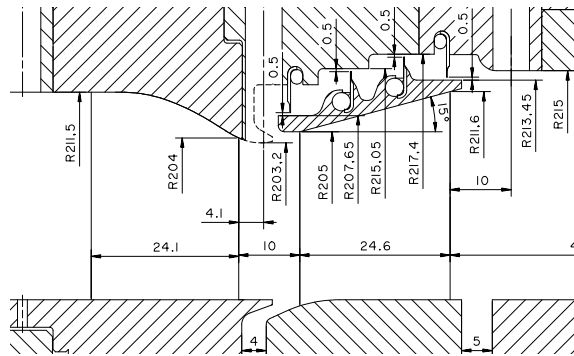


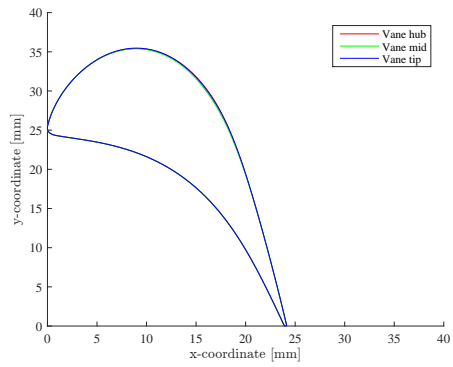
Figure 5.3: Drawing of KTH's test turbine with stage 4b mounted, hot dimensions

	Vane		Blade	
	Tip	Hub	Tip	Hub
Area 2D [mm <sup>2</sup> ]	252.41	252.72	217.85	217.71
Area 2D / Chord 2D <sup>2</sup>	0.21	0.21	0.32	0.32
Axial width [mm]	24.13	24.13	24.59	24.59
Chord 2D [mm]	34.41	34.40	26.08	26.08
Chord 3D [mm]	34.41	34.40	26.08	26.08
Effective exit angle [°]	14.4	12.24	19.88	16.90
Exit angle [°]	15.35	15.35	19.63	19.63
Inlet angle [°]	56.54	56.54	31.70	31.70
Inlet wedge [°]	92.38	92.38	67.37	67.37
Lean [°]	4.07	5.23	-3.37	-4.34
LE diameter [mm]	2.16	2.16	2.85	2.85
LE row distance [mm]	11.88	11.89	10.87	10.88
Main axis angle [°]	0.66	0.66	1.16	1.16
Max. thick. / Chord 2D	0.37	0.37	0.44	0.44
Pitch / Chord 2D	0.96	0.74	0.91	0.71
Pitch / Chord 3D	0.96	0.74	0.91	0.71
Radius TE [mm]	220	170	220	170
Stagger [°]	44.00	44.00	66.94	66.95
TE diameter [mm]	0.25	0.25	0.27	0.27
Throat distance [mm]	8.07	5.33	8.13	5.38
Uncovered turn [°]	16.90	7.10	21.56	12.86

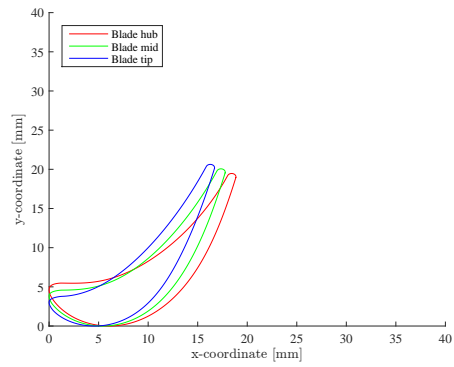
Table 5.1: Geometry parameters for test turbine stage 4b (CATO)

### 5.1.2 Test Turbine stage 5

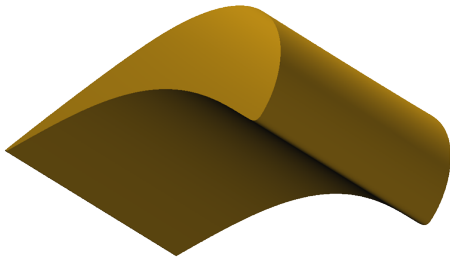
Stage 5 is a combination of the stator from stage 4b and the blade profile BC7M. The blade is built up from three radial sections; hub, mid and tip, where each section has been designed as a cylindrical section [14]. Stage 5 has 42 vanes, 60 blades and is designed to more accurately represent a modern gas turbine stage. The blade is designed to mimic a modern industrial gas turbine and therefore has a significantly higher degree of reaction than stage 4b as well as a higher design speed. In Figure 5.4 both vane and blade profile sections are presented as well as a 3D-view of both exported from CATO. Some section parameters are also presented in Table 5.2.



(a) Stage 5's vane sections geometry (CATO)



(b) Stage 5's blade sections geometry (CATO)



(c) 3D-view of stage 5's vane profile



(d) 3D-view of stage 5's blade profile

Figure 5.4: Stage 5's stage geometry profiles

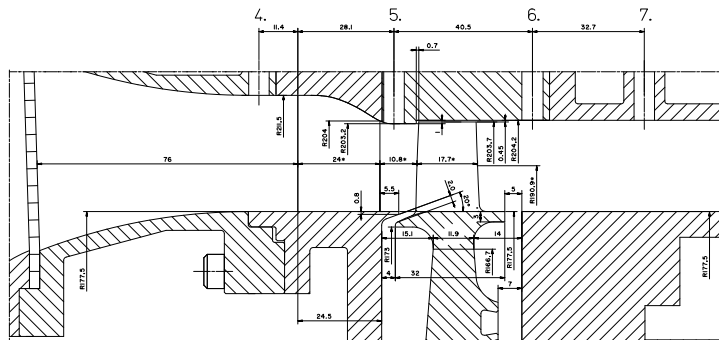


Figure 5.5: Drawing of KTH's test turbine with stage 5 mounted, hot dimensions

	<b>Vane</b>		<b>Blade</b>		
	Tip	Hub	Tip	Mid	Hub
Area 2D [mm <sup>2</sup> ]	252.41	252.72	84.74	91.44	104.08
Area 2D / Chord 2D <sup>2</sup>	0.21	0.21	0.15	0.16	0.19
Axial width [m]	24.13	24.13	16.70	17.78	18.86
Chord 2D, [mm]	34.41	34.40	23.86	23.6	23.38
Chord 3D [mm]	34.41	34.40	23.87	23.61	23.39
Effective exit angle [°]	14.4	12.24	19.27	19.21	19.22
Exit angle [°]	15.35	15.35	18.57	18.61	18.64
Inlet angle [°]	56.54	56.54	65	61	56
Inlet wedge [°]	92.38	92.38	54.32	59.12	66.41
Lean, [°]	4.07	5.23	-2.46	-2.46	-2.48
LE diameter [mm]	2.16	2.16	2.31	2.32	2.32
LE row distance [mm]	11.88	11.89	8.89	9.34	9.65
Main axis angle [°]	0.66	0.66	0.67	0.75	0.84
Max. thick. pos. / Chord 2D	0.08	0.08	0.19	0.18	0.19
Max. thick. / Chord 2D	0.37	0.37	0.21	0.23	0.26
Pitch / Chord 2D	0.96	0.74	0.90	0.85	0.79
Pitch / Chord 3D	0.96	0.74	0.90	0.85	0.90
Radius TE, [mm]	220	170	205	191	177
Stagger [°]	44.00	44.00	43.29	47.54	52.07
TE diameter [mm]	0.25	0.25	0.87	0.87	0.87
Throat distance [mm]	8.07	5.33	7.07	6.58	6.10
Uncovered turn [°]	16.90	7.10	23.31	22.63	22.36

Table 5.2: Geometry parameters for test turbine stage 5 (CATO)

## 5.2 Measuring equipment

The test turbine has a lot of measurement equipment connected to it. For the global measurements, the test turbine relies on pressure and temperature gauges. The pressure is mostly measured through holes drilled in the casing and hub, with tubes connecting them to the data sampling equipment. There are pressure taps in the inlet before the vane row, both in the tip and hub. There is also pressure sensing holes behind the stator row. The pressure is measured with four holes drilled in the casing and four holes drilled in the hub. As a consequence of the construction of the turbine, the pressure sensors in the hub will follow when the stator is turned, i.e. they are fixed in relation to the stator TE. The holes in the tip however, are a part of the casing, meaning they will measure in different parts of the wake as the stator is turned. Care must be taken to make sure the stator is in an appropriate position when global measurements are taken. If this is not done, the measurements in the tip might be taken in a position it was not expected to, leaving the measured value

for static pressure after the stator incorrect. There are also holes drilled to measure static pressure after the rotor in the same way as for the stator. These are however not sensitive to position since the rotor is spinning relative to them. There is also temperature probes located in the same places as static pressure gauges as well as a mass measurement flange in the turbine housing exit.

The turbine can also be measured with traversing probes. A traverse probe is used to measure the static and total pressures in a 2-D plane at two positions in the machine. One plane is after the stator and one is after the rotor. The probes are moved up and down to traverse radially, and the stator can be turned to measure in the tangential direction. The probes are made with 5 holes drilled into them in order to measure total pressure in the axial, tangential and radial direction as well as static pressure. This makes it possible to determine all the velocities in the stage as well. It is however important to remember that the measurement planes are placed a short distance away from the blades for practical reasons, while as evident from Figure 3.8, the planes for output data from in-house codes are placed at blade entry and exit. This small distance can have an impact on the measurement, especially if it is placed in a region where the channel geometry is not smooth and straight.

## Chapter 6

# Experimental data validation

The experimental data used in this thesis is given in three forms. *Raw data*, which is acquired by traversing a probe radially and tangentially. This method captures radial and tangential variations and is the most accurate, but very slow and hard to analyse. *Traversed data*, which is acquired by transforming the raw data by averaging. Traversed data can be transformed to 1D or 2D. The last form, *global data* uses pressure gauges only in the hub and tip walls to measure stage performance. This data represents a 1-dimensional turbine and resembles the results from a mean line analysis. Radial and tangential variations are unknown and this might give inaccuracies in the data. The sets of data used in this thesis are

- *Global data* for stage 4b.  $\Pi_{ts} = 1.23$ , with and without purge flow
- *Global data* for stage 4b.  $\Pi_{ts} = 2.06$
- *Global data* for stage 5.  $\Pi_{ts} = 1.23$
- *Traversed data* for stage 4b,  $\Pi_{ts} = 1.23$ , with and without purge flow. Available as 1-dimensional averages and as raw measurement data

### 6.1 Global and traversed data comparison

A comparison was made between the global and 1-dimensionally averaged traversed data. This was made to verify how well the two sets of data agree with each other. The comparison was made between the most important turbine characteristics such as efficiency and degree of reaction.

Figure 6.1a and 6.1c show how the global and traverse data compare to one another when it comes to efficiency and degree of reaction. The efficiency seems to be quite similar between the two measurement methods and should not pose a big problem in the continued comparisons. For the degree of reaction however,

it is clearly visible that the shape for the traversed data is more curved, and also that the absolute value is higher. This might be from a flaw in the measurements, something that will be further explained in the following section.

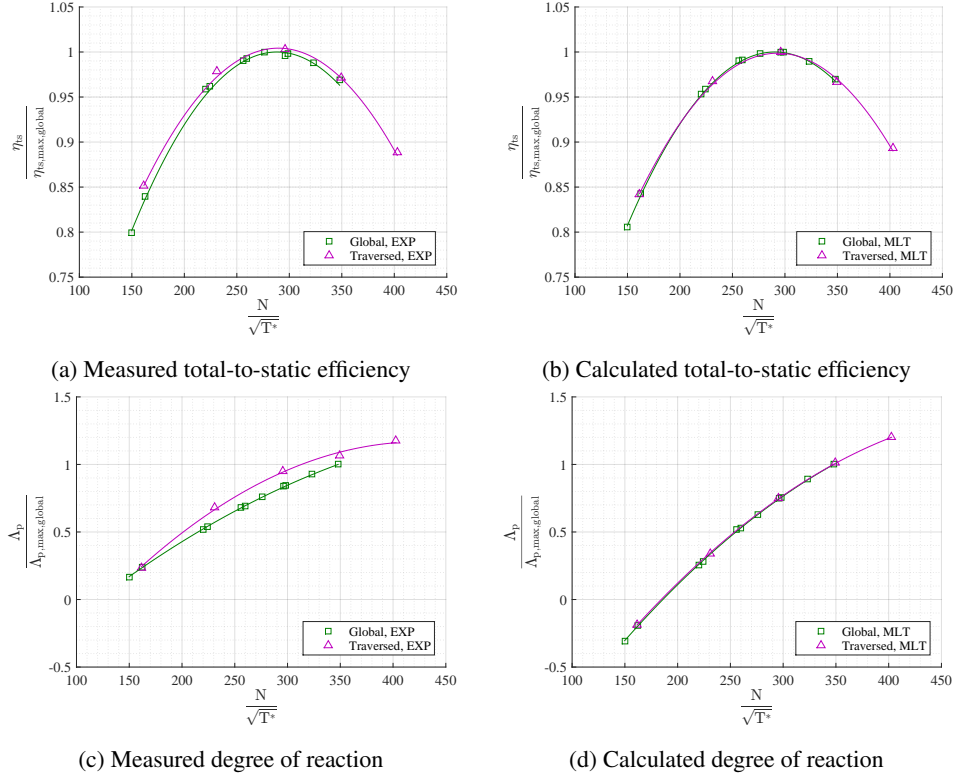


Figure 6.1: Comparison between datasets for stage 4b,  $\Pi \approx 1.23$

## 6.2 Traverse data errors

In the closing weeks of this thesis, it was discovered that the traversed measurements might not be as accurate as originally thought. This was discovered while a comparison of calculated and measured radial static pressure distribution was made. Since global measurements are fast to make they are used in many experiments. However, the profiling of the stator gives an outlet static pressure distribution with a "bubble" shape as presented in Figure 6.2b and not the traditional straight line the radial equilibrium equation would suggest. Global measurements use the pressure taps in the walls and can therefore not capture this shape and will therefore return a mean static pressure lower than the actual value. To overcome this, the bubble shape is captured by fitting a 3rd degree polynomial to the end points. With this, a more correct mean static pressure is calculated as explained



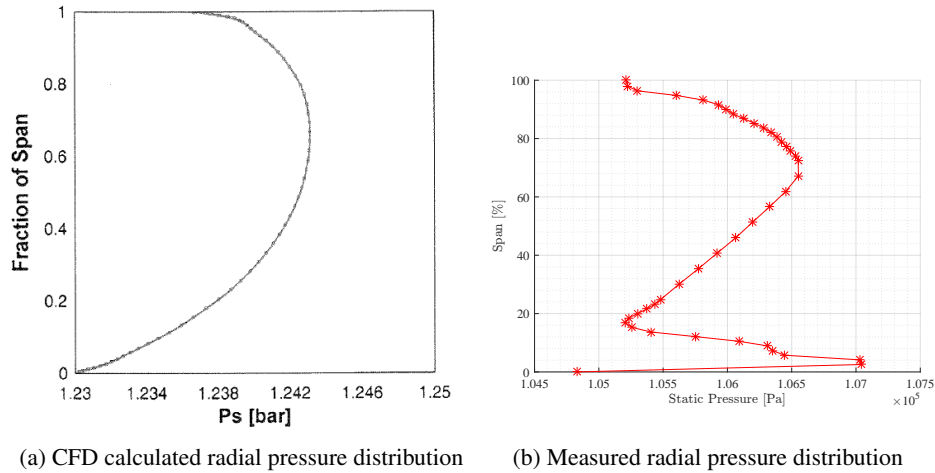


Figure 6.2: Comparison between predicted and measured radial pressure distribution

in [26]. The CFD calculations described in [27] has been used to create this polynomial. Since Figure 6.1 shows a difference between measurements that is not present in the calculated distribution it was suspected the polynomial was inaccurate. In order to evaluate this, a comparison between a radial distribution calculated by [27] and 2-dimensionally averaged experiment data was made. This comparison is presented in Figure 6.2. It can be seen that the peak pressure is located at 70 % span in both the calculations and in the measurements. The overall shape seems quite accurate, but the radial distribution shows a strange behavior close to the hub wall, probably due to probe and wall interaction. This makes the reliability of the entire dataset questionable. It is unknown how this interaction affects all other results such as loss coefficients, measured velocities and mass flows. The errors are however isolated to the stator exit, and should therefore not affect the global stage parameters such as isentropic velocity ratio, efficiency or total mass flow. Also, the *global measurements* are not effected since the probe is not used for these.

To get an estimate of how much error this results in, a comparison between the expansion based on global measurements and loss coefficients from traversed data was plotted and is presented in Figure 6.3. Calculating the efficiencies for the stage using the definition in Equation (3.25) gives an efficiency of around 85 % for the global expansion and about 3 p.p. higher if the measured loss coefficients are applied. The efficiency calculated from traversed loss coefficients is very close to the measured. In fact, it is better than the global calculation. However, based on results from previous work in [25] the global measurements are thought to be the most accurate available. The good agreement between measurement and calculations based on loss coefficients are thought to be coincidental.

It has also been discovered that the stator position has been slightly wrong for the measurements of the global data, leading to a possible error in the measuring of static pressure between the stator and rotor. The impact of this error has been studied in [26]. A figure from this paper is shown in Figure 6.4 and illustrates how large the error from different stator positions can be. The error is noticeable, but not large enough to explain all the difference observed in the end results.

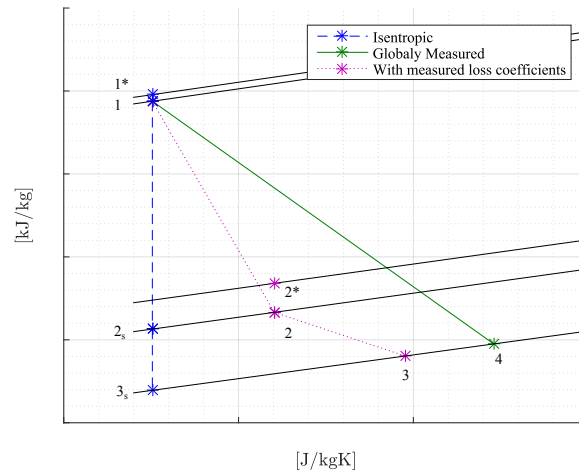


Figure 6.3: Expansion calculated from global measurements and measured loss coefficients for stage 4b's rotor and stator,  $\Pi_{ts} \approx 1.23$  and  $v_{ts} \approx 0.55$

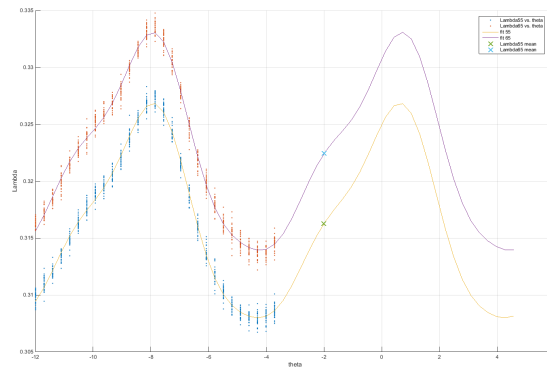


Figure 6.4: Impact of stator tangential position on measured global reaction

# Chapter 7

## Results

### 7.1 TIT scaling

In order to determine a scaling temperature, a study of when MLT starts returning correct results was made as described in section 2.2. The results of this study is presented in Figure 7.1 and clearly shows that the efficiency is rapidly approaching a realistic value for a single stage turbine. Beyond 340 K the efficiency vary only slightly, suggesting that MLT will converge properly if the temperature can be increased just slightly from the experimental value. The sharp breaking point also suggests that the simulation does not slowly approach a valid value; instead it will almost immediately find a valid answer as soon as it delivers physically realistic results. With these figures in mind, the experimental results will be evaluated by scaling the turbine speed to 345 K TIT. The same study has been made for stage 5 since the different degrees of reaction gives different expansions. The graphs from this study are however not presented here since they are practically the same. The scaling temperature for stage 5's pressure ratio sweep was set to 350 K.

By using Equation (3.43) with these two temperatures, Tables 7.1 and 7.2 can be constructed. The tables presents the new turbine speeds to be used for the elevated temperatures.

Experimental Values		Scaled Values	
Total Temperature [K]	Speed [rpm]	Total Temperature [K]	Speed [rpm]
335.12 K	5299.91 rpm	345 K	5377.43 rpm
335.09 K	6221.00 rpm	345 K	6312.35 rpm
334.57 K	7366.11 rpm	345 K	7480.10 rpm
334.31 K	8333.55 rpm	345 K	8465.79 rpm
334.43 K	8568.40 rpm	345 K	8702.75 rpm
334.67 K	9699.30 rpm	345 K	9847.79 rpm
334.44 K	9800.16 rpm	345 K	9953.61 rpm
334.47 K	10715.37 rpm	345 K	10882.78 rpm
334.56 K	11479.53 rpm	345 K	11657.20 rpm

Table 7.1: Scaled non-dimensional turbine speed for the speed sweep, stage 4b,  $\Pi \approx 2.06$

Experimental Values		Scaled Values	
Total Temperature [K]	Speed [rpm]	Total Temperature [K]	Speed [rpm]
341.75 K	10304.70 rpm	350 K	10428.37 rpm
341.61 K	10304.08 rpm	350 K	10429.92 rpm
341.40 K	10303.36 rpm	350 K	10432.29 rpm
341.17 K	10302.43 rpm	350 K	10434.85 rpm
340.89 K	10301.37 rpm	350 K	10438.18 rpm
339.07 K	10301.11 rpm	350 K	10465.78 rpm

Table 7.2: Scaled non-dimensional turbine speed for the pressure ratio sweep, stage 5

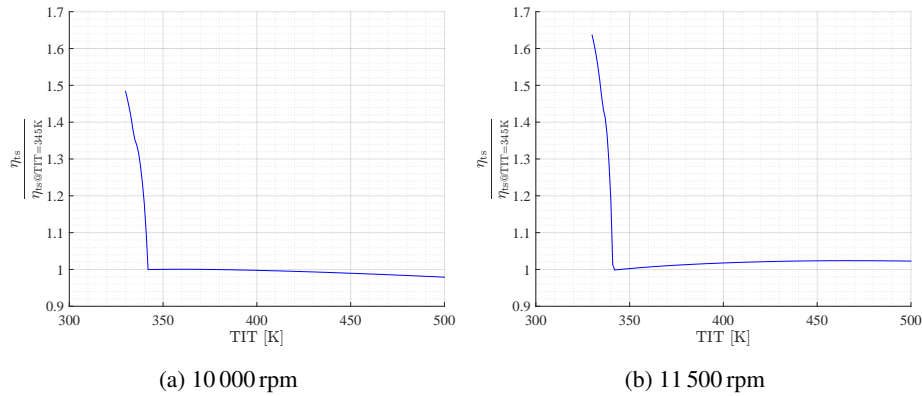
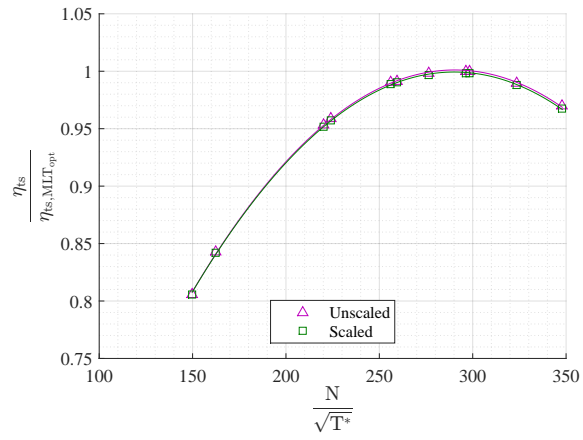


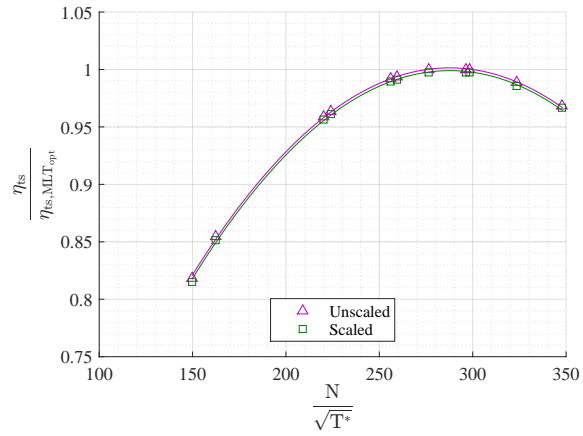
Figure 7.1: Varying temperatures at two different turbine speeds,  $\Pi \approx 2.06$ , stage 4b

### 7.1.1 Scaling method validation

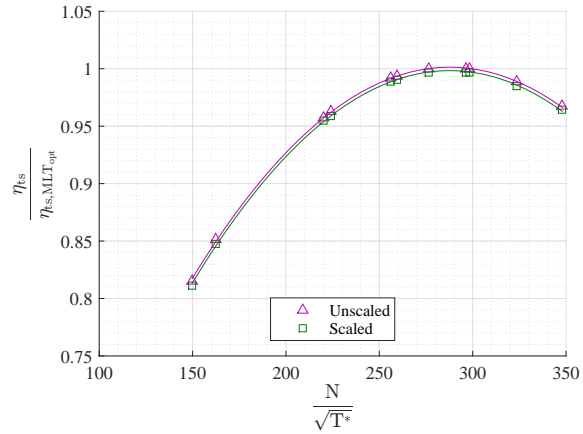
The results of the scaling validation are presented in Figures 7.2 to 7.4. A comparison of the relative differences between all of the models is presented in Figure 7.5. The comparison clearly shows a good agreement for all models, hence all of them should work for the purpose of this thesis. However, the relative error is the smallest for the correlation based model and it was therefore selected as the main model for this thesis. It should be noted that the impact of the chosen model is small and also diminishes as turbine speed is increased. The results are deemed satisfactory and scaling will therefore be used for cases where convergence problems arise.

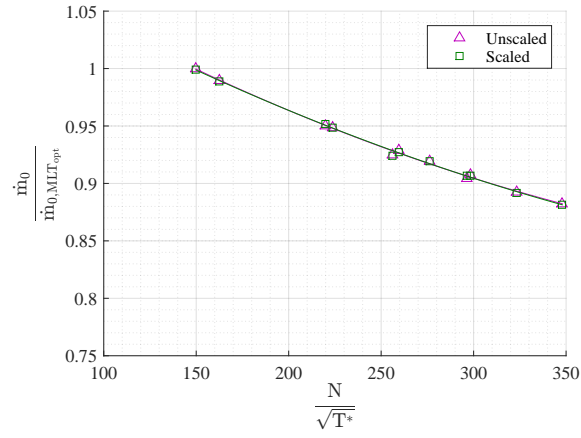


(a) Correlation based loss model

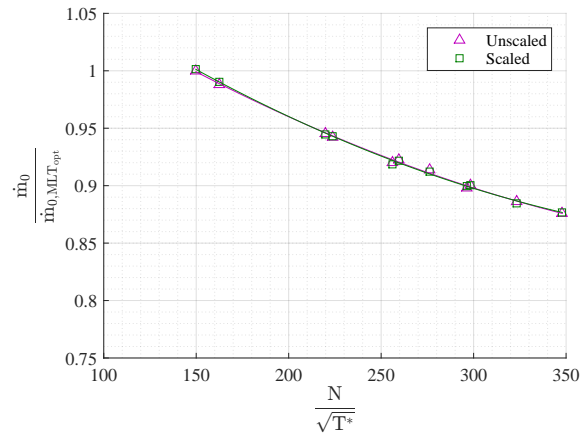


(b) Boundary layer based loss model, default settings

(c) Boundary layer based loss model, forced transition at  $s/s_{max} = 0.1$ Figure 7.2: Comparison of scaling accuracy for total-to-static efficiency, stage 4b,  $\Pi_{ts} \approx 1.23$



(a) Correlation based model



(b) Boundary based loss model, default settings

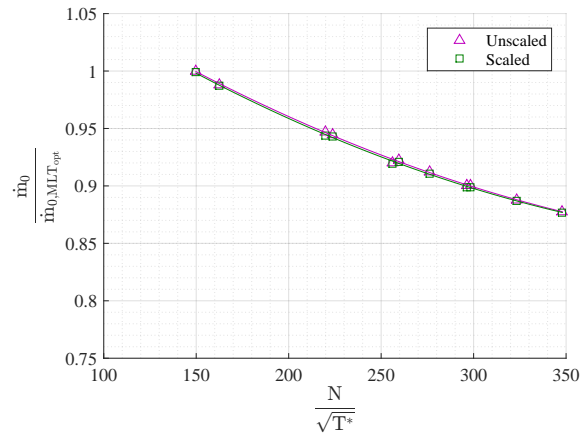
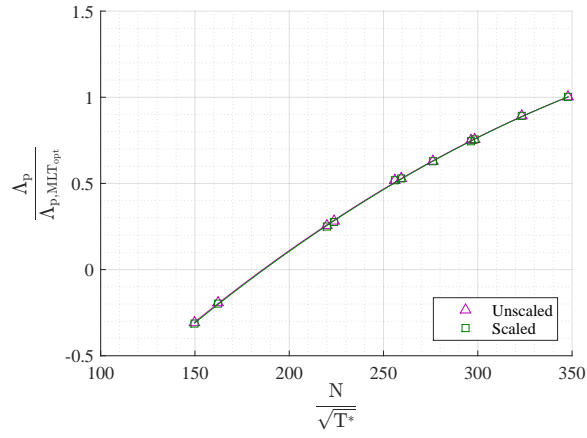
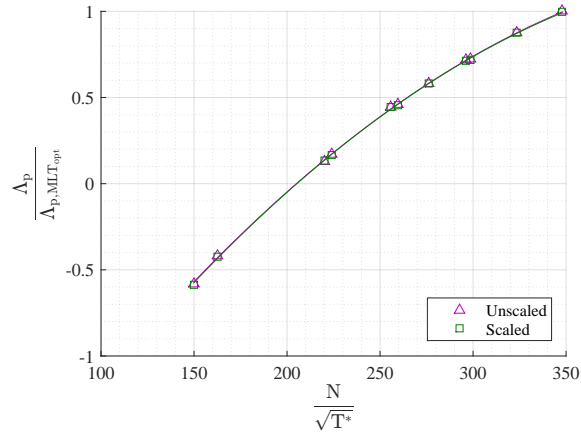
(c) Boundary based loss model, forced transition at  $s/s_{max}$ 

Figure 7.3: Comparison of scaling accuracy for total-to-static efficiency, stage 4b,  $\Pi_{ts} \approx 1.23$



(a) Correlation based model



(b) Boundary based loss model, default settings

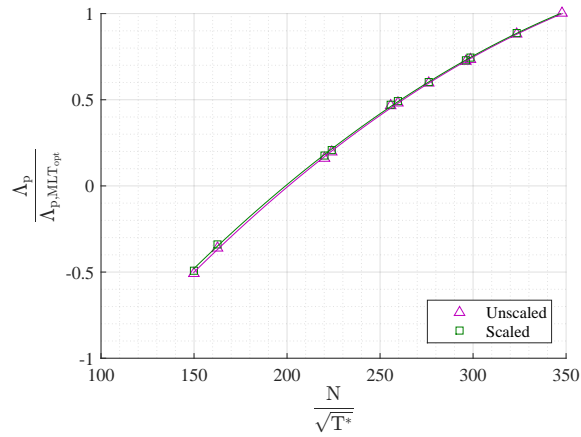
(c) Boundary based loss model, forced transition at  $s/s_{max}$ 

Figure 7.4: Comparison of scaling accuracy for total-to-static efficiency, stage 4b,  $\Pi_{ts} \approx 1.23$



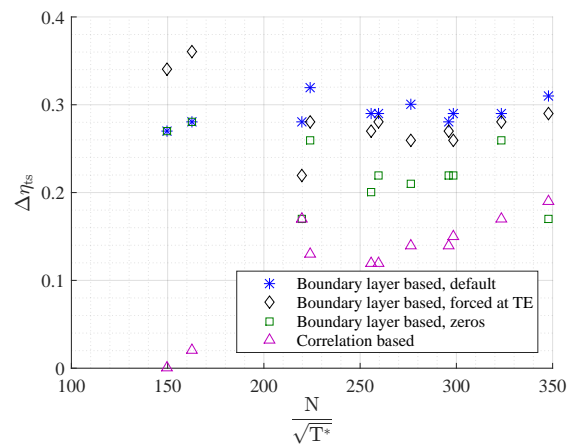


Figure 7.5: Differences between scaled and unscaled simulation using different loss models, stage 4b,  $\Pi_{fs} \approx 1.23$

## 7.2 Stage 4b

### 7.2.1 Global evaluation – PR = 1.23

Global stage performance was evaluated first since it can tell a lot about model performance, but without requiring too much data. The calculations in this section are made with 1-dimensionally averaged traverse data as input since further analysis will be easier if the data sets are equal. In the initial analysis, the model prediction for max efficiency is off with about 4 p.p. and predict the efficiency more accurately at low turbine speeds as can be seen in Figure 7.6. However, the prediction of important characteristics such as dimensionless mass flow and degree of reaction are predicted worse at low speeds and improve until the upper part of the high speed range where the calculations pass experimental values as evident in Figures 7.7 and 7.8. It could be considered a bit surprising that the most accurate prediction of efficiency coincide with worst performance on the other important characteristics. This could suggest that the accurate prediction is coincidental and the result of erroneous calculations adding up to a more accurate result. In order to evaluate whether this is the case or not, the losses need to be split up in more basic components. The stage velocities and flow angles also need to be studied to pinpoint the cause of the observed behavior. This split will be done later on in section 7.2.3.

#### Total-to-static efficiency

The total-to-static efficiency as function of dimensionless speed is presented in Figure 7.6. It can be seen that the total-to-static efficiency is predicted to be higher than the experimental values. The difference is least in the lowest speed point and grows as the turbine speed increases. The relative error is varying between 3.6 and 5.4 %.

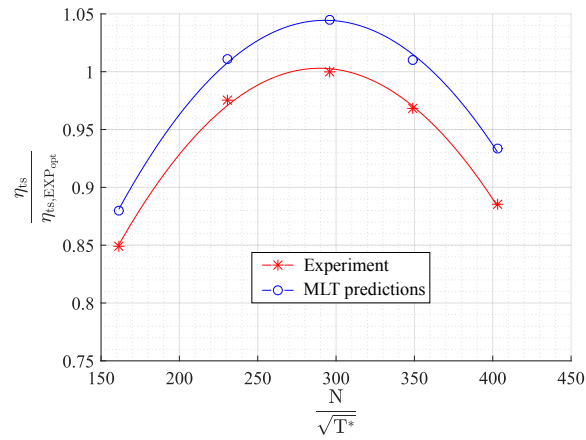


Figure 7.6: Total-to-static efficiency for stage 4b,  $\Pi \approx 1.23$

### Degree of reaction

The degree of reaction as function of dimensionless speed is presented in Figure 7.7. The low speed range shows an underpredicted value. The predicted degree of reaction is even predicted to be negative, meaning a static pressure *increase* over the rotor. The degree of reaction rises as the turbine speed increases, but the predicted values rise faster and at near highest speed, the predicted value passes the measured value. The curvature of the predicted curve seems flatter with higher sensitivity to increased turbine speed in the high speed region of the test envelope compared to the measured data.

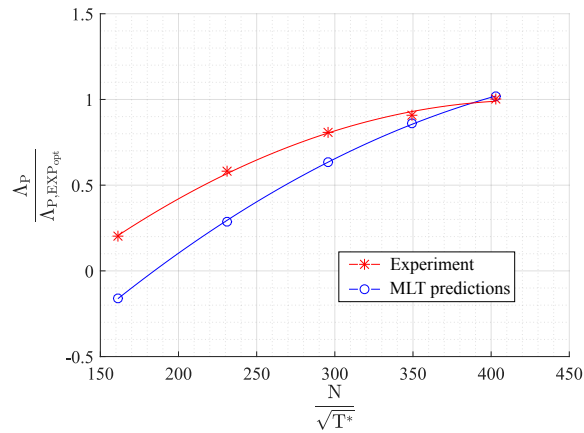


Figure 7.7: Pressure based degree of reaction as function of dimensionless speed, stage 4b,  $\Pi \approx 1.23$

### Dimensionless massflow

The dimensionless mass flow as function of dimensionless speed is presented in Figure 7.8. The dimensionless mass flow is predicted higher for the turbine, but the curves for experiment and calculations approach each other and are at almost the same value at the highest measured speed. As for degree of reaction, the curve appears flatter. This higher mass flow rate suggest that some part of the turbine is predicted as being too open, or alternatively that the throat areas in some part of the turbine are not accurately manufactured.

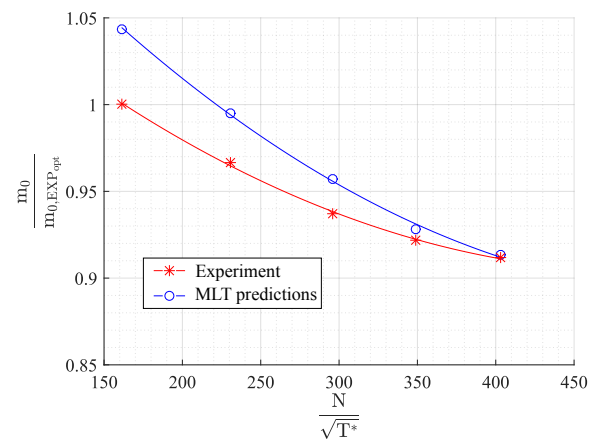


Figure 7.8: Dimensionless mass flow as function of dimensionless speed, stage 4b,  $\Pi \approx 1.23$

## 7.2.2 Global stage evaluation – PR = 2.06

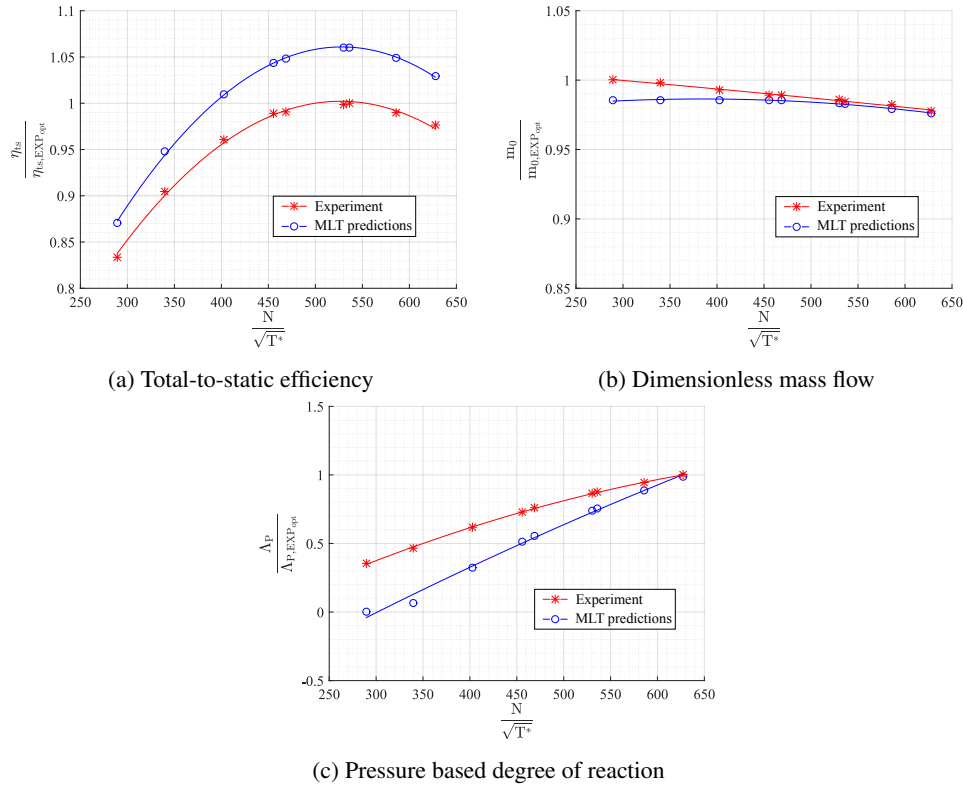


Figure 7.9: Turbine characteristics as function of dimensionless speed, stage 4b,  $\Pi \approx 2.06$ , correlation based loss, TIT scaled to 345 K

Figure 7.9 show turbine characteristics as a function of dimensionless speed for the high pressure ratio. A few phenomena can be seen. First of all, the efficiency curve has a worse shape then what was observed for the low pressure ratio. Moreover and more alarming is the mass flow curve. It is very evident that something is wrong. Closer scrutiny of the predicted values for speeds lower than 450 show that MLT predicts the same dimensionless mass flow for a turbine speed of 450 and lower. This means that the stator has choked, something that obviously does not happen in the real, measured turbine since the dimensionless mass flow keeps increasing as turbine speed decreases. It is suspected that the over acceleration observed for the low pressure ratio is behind this. The static pressure drop over the stator is over predicted as evident by the degree of reaction curve. In combination with cool gas, it is very easy to see why the stator chokes. The high stator pressure ratio gives a high driving pressure through the lattice. In combination with low gas temperatures, the Mach number in the throat increases fast and will reach

sonic conditions very easily. It should also be noted that scaling was needed to get proper model convergence. Without scaling, predicted efficiencies above 140 % were obtained. The observed worsening in prediction of efficiency as mass flow and reaction improves is surprising and will require more investigation.

### 7.2.3 Traversed data analysis – PR = 1.23

#### Stage pressure levels

The pressure before the stator will of course be the same for both experiment and calculations since the measured static and total states before the stator were used as boundary conditions for the mean line analysis. The same is true for static pressure out of the turbine stage since the pressure ratio is equal. However, the static pressure within the stage can be both measured and calculated. The pressure level between the rotor and stator is not decided explicitly so the pressure levels might very well differ between measurements and calculations. The static pressure in between the stator and rotor is illustrated in Figure 7.10a. It can be seen that the static pressure from the calculations is lower than the real stage up until  $\frac{N}{\sqrt{T^*}} \approx 350$  when it passes. This is not so surprising, since the degree of reaction has this pressure as part of its definition meaning they are tied to each other. The total pressure out of the stator can be used to estimate stator losses. From Figure 7.10b it can be seen that the total pressure at stator exit is always higher for the calculations, suggesting the stator is more efficient in the in-house codes compared to measurements.

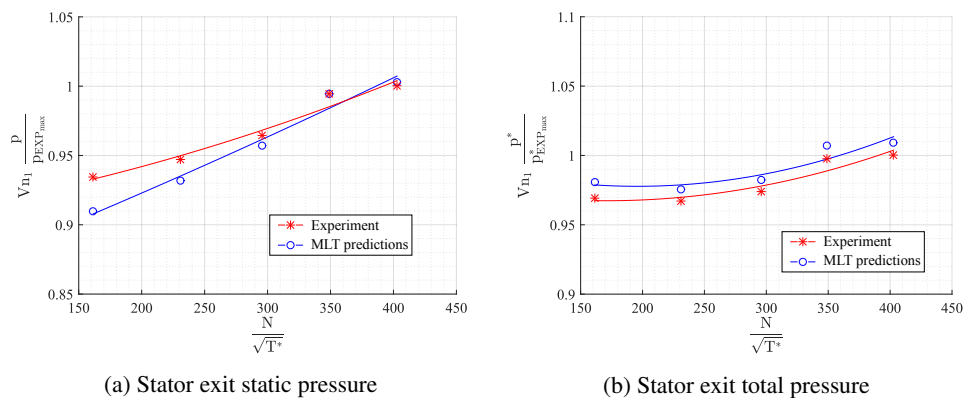


Figure 7.10: Pressures within stage 4b,  $\Pi \approx 1.23$

### Stage velocities

Figure 7.11 shows the stator total exit velocity. The predicted stator velocity is higher for all turbine speeds, with the difference becoming smaller with increasing turbine speed. The expansion over the stator is determined by the exit static pressure. Figure 7.10a shows that the predicted static pressure at stator exit rises above the measurements, but the exit velocity is still over predicted. This indicates under-predicted stator losses as stated before. This velocity difference probably explains the observed difference in dimensionless mass flow.

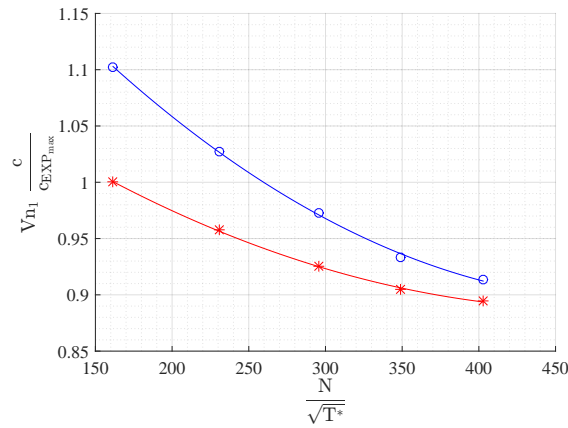


Figure 7.11: Total stator exit velocity for stage 4b ,  $\Pi \approx 1.23$

### 7.2.4 Analysis of radial distribution - Stator

Traverse data give the possibility to check how the flow behaves radially and span-wise. This information could be used to check how large the secondary vortices are and to estimate if the given values from MLT are realistic or not. It will also show how the static pressure is varying which could give an explanation to the error in degree of reaction as well. The radial distribution is averaged span-wise using Dzung averaging method. A contour plot with iso-lines is also created to better estimate the size of secondary vortices and is presented in figure 7.13a. The plot clearly shows the 2-dimensional flow region in the mid-section, while also showing the wake formed by the blades. In close proximity, there are two strong secondary vortices characterized by regions of much lower velocity and higher static pressure. These vortices takes up about 37 % of the total channel height. The vortex position shows the under-turning that the fluid will experience, causing incidence other than intended design flow angle at a significant portion of the blade height. Figure 7.12b show the radial distribution for the static pressure out of the stator. The error induced by the probe-wall interaction as explained in section 6.2 is clearly visible in the last 20 % of the span.



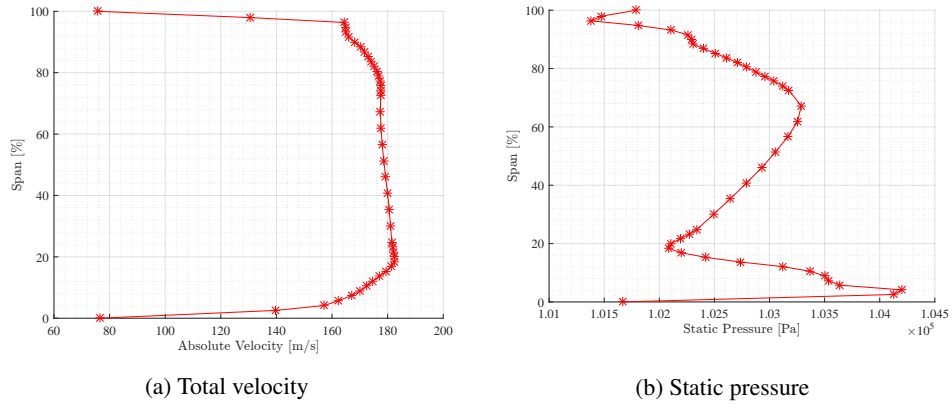


Figure 7.12: Radial distribution at stator exit, stage 4b,  $\frac{N}{\sqrt{T^*}} = 161$ ,  $\Pi \approx 1.23$

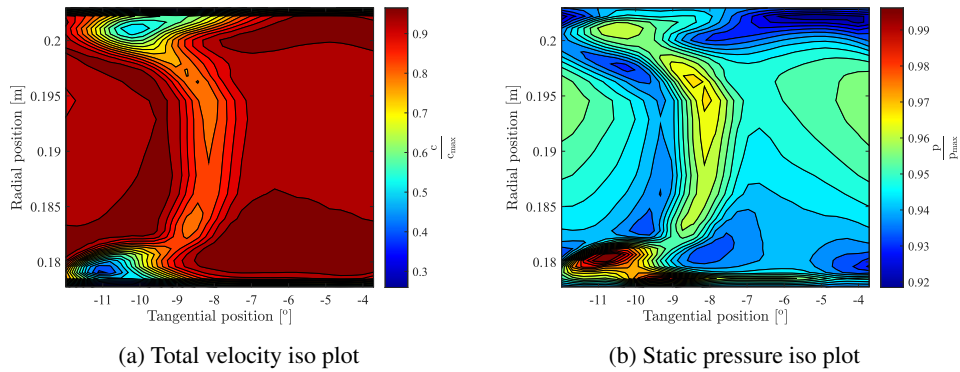


Figure 7.13: Radial distribution and iso plots over the stator exit, stage 4b,  $\Pi \approx 1.23$

### 7.2.5 Rotor and stator loss coefficients

#### Total loss coefficients

In order to start the loss breakdown, the loss coefficients for rotor and stator were plotted. These losses are available in both the traversed stage 4b experiment and MLT calculations and can thus easily be compared. The result of this comparison is presented in Figure 7.14. As can clearly be seen in the figure, both the stator and rotor coefficients are underpredicted for the optimum point, and stator losses are more or less constantly predicted far too low. The rotor in turn shows an underpredicted optimum point loss, but then a sharp increase at off design conditions. This increase is also noticeable in the experiment, but the curve is much shallower. It is suspected that this is the effect of an over predicted sensitivity to incidence. This over predicted sensitivity has already been subject to scrutiny by SIT and is further described in [28]. The conclusion of the referenced report is that incidence sensitivity is over predicted for profiles similar to the 4b rotor.

Figure 7.16a shows this behavior for the secondary loss. From these figures it seems like the "baseline" loss at stage optimum is too low, and more work needs to be done to evaluate the cause of this discrepancy. Possible causes of action would be to do an analysis based on CFD in 2- or 3-dimensions. A 2-D analysis might be best suited for its ease of setup, low computational time and ease of result evaluation. It might also be good to perform an analysis of stage 5 since it represents a typical SIT gas turbine profile for which the mean-line tools are tailored. Both of these analyses will be performed in Section 7.3 and 7.5 respectively.

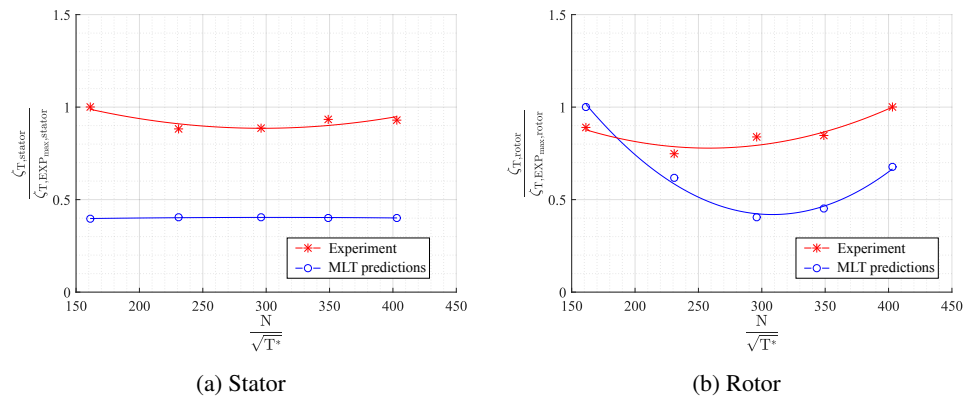


Figure 7.14: Total loss coefficients for the uncooled 4b stage,  $\Pi \approx 1.23$

### **Incidence loss**

The incidence loss is presented in figure 7.16b and shows the same sharp increase as the total loss does. However, there is no experimental data available for this loss coefficient since it is impossible to accurately split the component loss (i.e. stator and rotor) in more specific loss coefficients. The secondary loss should also be increased by the increased incidence loss as it is a component of the secondary loss modelling.

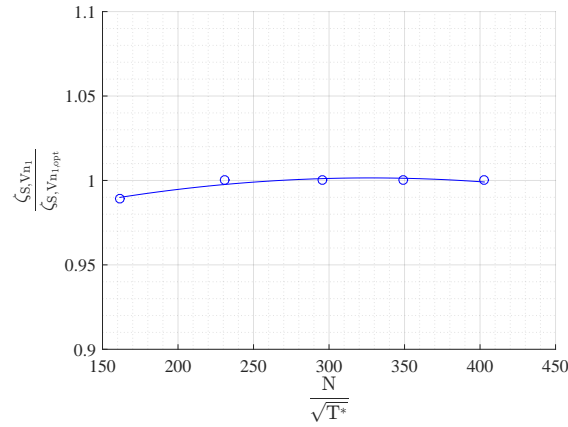
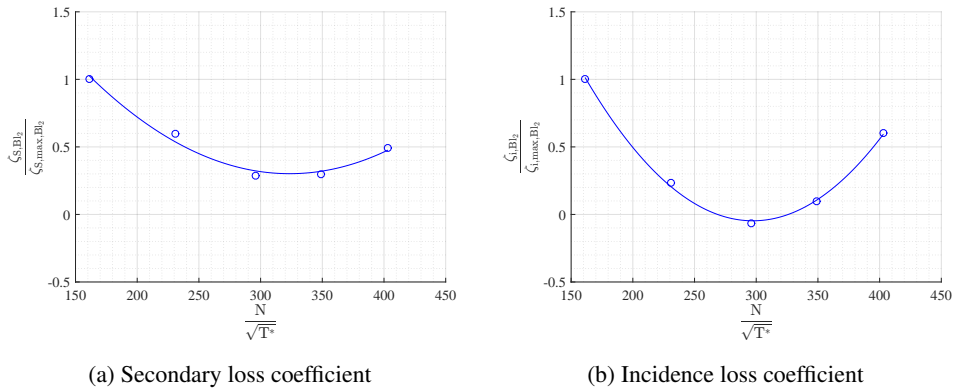
### **Profile loss**

The low stator and rotor loss at design conditions indicate that losses associated with the blade profile are underpredicted. This should also indicate that secondary losses are too low, since SIT models uses the profile loss as a factor in secondary loss. Because of this, it seems natural to begin with the profile losses. If this loss is underpredicted as suspected, the secondary loss will follow. In SIT in-house codes, what is considered profile loss is the loss from the airfoil skin friction. Losses from trailing edge, surface roughness and Reynolds number are presented separately. This separation of loss mechanisms is impossible in reality, since they can only be measured as a group. However, secondary, endwall and incidence losses can be eliminated. In order to do this, the profile loss needs to be studied in a 2-dimensional flow region. This is probably the case in the mid-section of the blade where endwall impact is small.

In order to get data to compare with, a 2-D blade to blade analysis tool "MISES" was used. MISES analyze the blade in 2-dimensions, effectively removing the impact of secondary flows. Incidence loss is accounted for my MISES calculations and if it is erroneously predicted, it should be evident from the trend for off design speeds. The minimum loss is then only profile loss. This was studied by plotting of Traupel's loss coefficient from MISES together with the sum of all loss coefficients from MLT with the exception of secondary loss. The results from this is presented in Figure 7.26.

### **Secondary loss**

The secondary loss is as mentioned in section 3.7.3 a large contributor to the total loss in a gas turbine stage. The results seen in Figure 7.15 suggests a very low turbine speed dependence for the stator. The total level is low, according to [29], a secondary loss coefficient almost 300 % higher is predicted when using SIT steam turbine code AXIAL. This low stator secondary loss indicates that the modelling of secondary losses are too low and probably should increase by a large amount. The secondary loss coefficient in the rotor presented in Figure 7.16a show a much more realistic value at optimal speed. However, the large loss coefficient seen at higher

Figure 7.15: Secondary loss coefficient, stage 4b stator,  $\Pi \approx 1.23$ Figure 7.16: Loss coefficients for stage 4b rotor,  $\Pi \approx 1.23$ 

and lower speeds are probably due to over predicted incidence loss and might not reflect reality accurately. The result from the stator strongly suggests a flaw in the secondary loss models, something that will require further investigation.

### 7.2.6 Extra loss addition – PR = 1.23

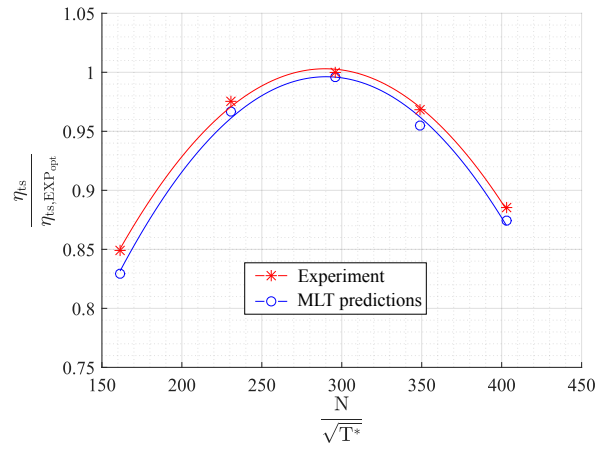
As can be seen in section 7.2.3, the losses for both rotor and stator are underpredicted by a large margin. This underprediction probably causes at least parts of the behavior seen in section 7.2.5 with overpredicted efficiency and with degree of reaction and dimensionless mass flow with erroneous trends. Figure 7.17 show how the total-to-static efficiency reacts to an addition of losses. The figure clearly shows that a constant addition of 4.6 % loss on the stator is giving the best results, although both of the other techniques are more or less successful. An addition of loss on the rotor instead of the stator give a bit to "sharp" curve with predictions

that falls further of the mark the further away from the optimum point the turbine is operating. A stator loss coefficient matched to experiments gives a good shape agreement, but the added loss is a bit too much, making the predicted efficiency fall a bit under the measured one.

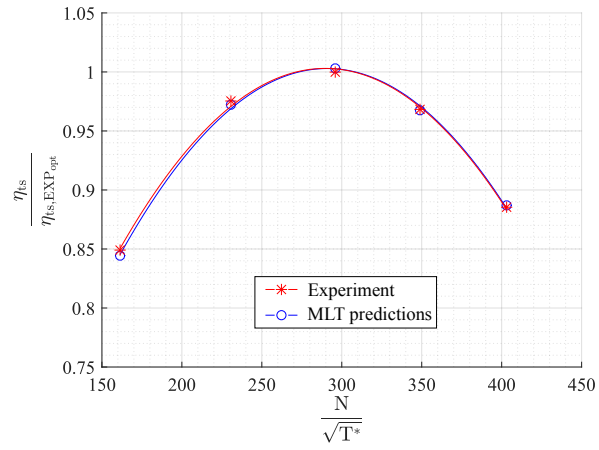
Figure 7.18 shows the degree of reaction for stage 4b with extra loss added. As can be seen from the figure, the stator loss has an insignificant impact on the stage degree of reaction. The rotor has a much larger impact, with the degree of reaction becoming much better predicted, especially for low turbine speeds. The shape is however a bit off, and the highest speed part becomes over predicted.

The dimensionless mass flow with different extra losses is presented in Figure 7.19. It can be seen that the flow capacity is not affected much by rotor loss, instead, the stator loss has an effect on the flow capacity. The impact is not very large, and mostly moves the predicted curve up or down the y-axis. The error in shape persists and seems to be rather unchanged for all cases.

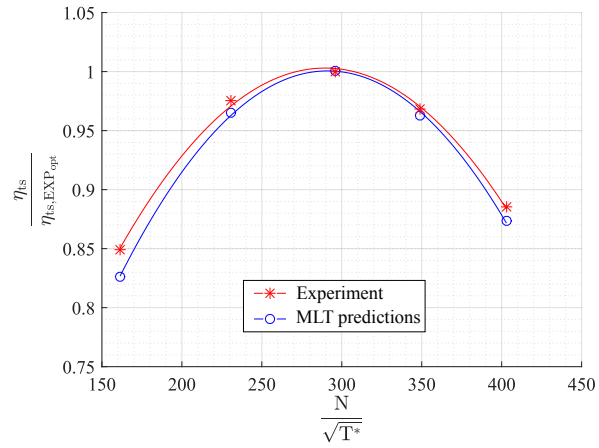
If the same method is applied to the rotor, a slightly different trend can be seen. Figure 7.17c show that the level in peak efficiency is correct, but the shape of the curve is wrong. The efficiency curve becomes a bit too "sharp", suggesting a still too high impact of incidence. However, when it comes to degree of reaction prediction presented in Figure 7.18c, the performance is better than for when loss is added to the stator. This suggests rotor losses have a bigger impact on the pressure level behind the stator. The results from these calculations show that a combination of rotor and stator loss is probably what is needed.



(a) Matched stator loss

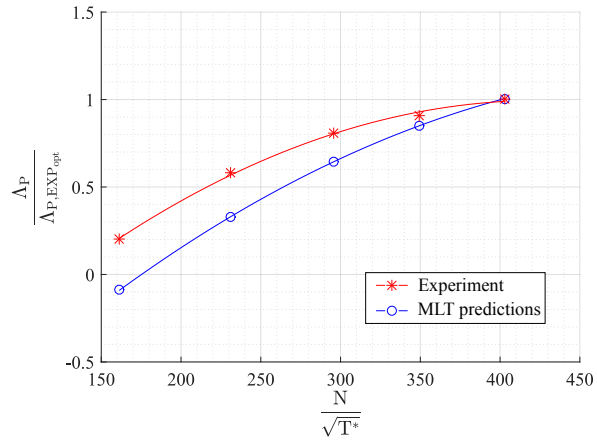


(b) 4.6% extra stator loss

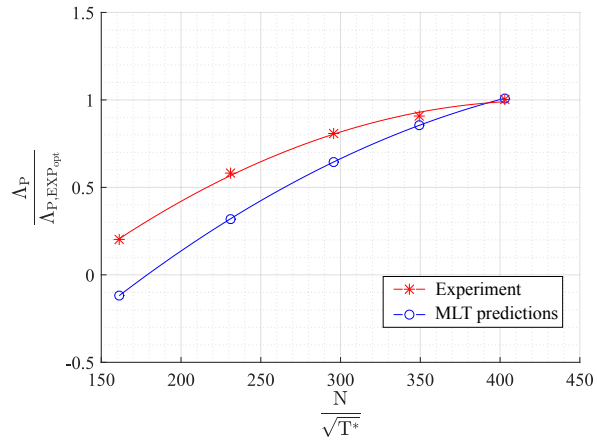


(c) 10.6% extra rotor loss

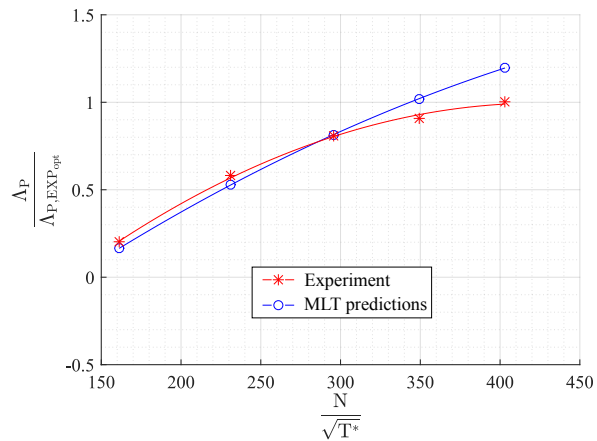
Figure 7.17: Total-to-static efficiencies for different extra loss additions, stage 4b,  $\Pi \approx 1.23$



(a) Matched stator loss

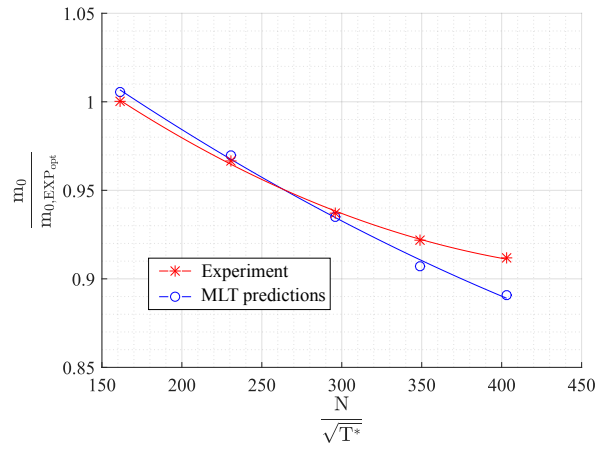


(b) 4.6% extra stator loss

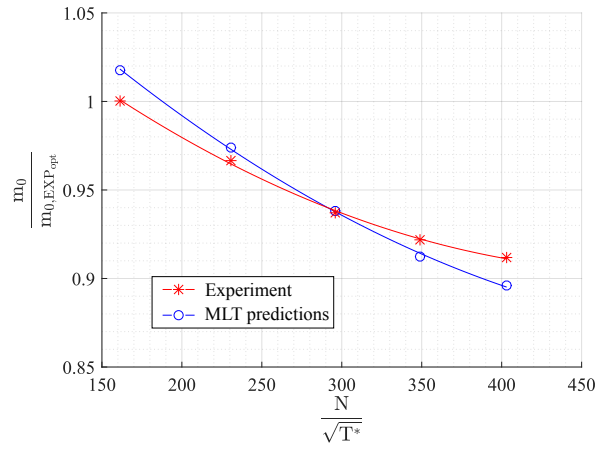


(c) 10.6% extra rotor loss

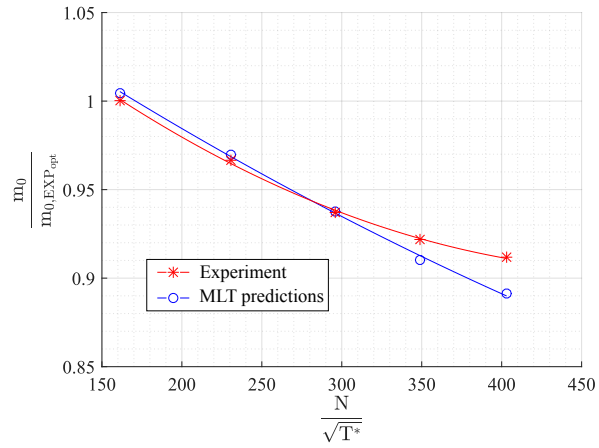
Figure 7.18: Pressure degree of reaction for different extra loss additions, stage 4b,  $\Pi \approx 1.23$



(a) Matched stator loss



(b) 4.6% extra stator loss



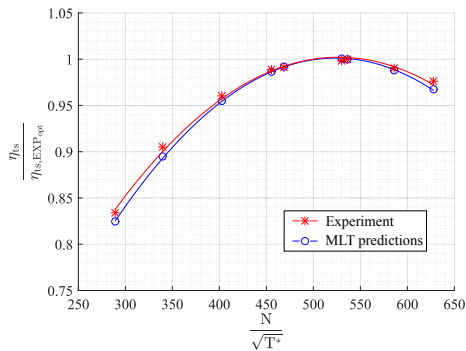
(c) 10.6% extra rotor loss

Figure 7.19: Dimensionless mass flow for different extra loss additions, stage 4b,  $\Pi \approx 1.23$

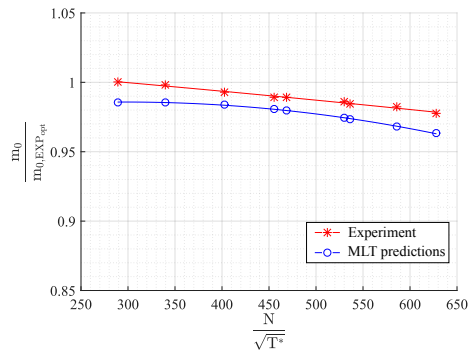


### 7.2.7 Extra loss addition – PR = 2.06

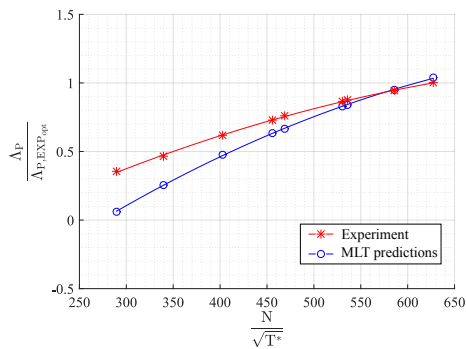
Extra losses were also added to the high pressure ratio case. Since no traverse data was available, only the method of trying to match efficiency at optimal conditions was used. The amount of extra loss needed is higher for the high pressure ratio case, 7.23 % compared to 6.4 % for the low pressure case. Figure 7.20b shows that adding extra loss delays the choking to the last operating point, however, it does not give accurate results for mass flow or degree of reaction. The total-to-static efficiency is quite good, which is to be expected since it was used to decide the amount of added loss. The trend seems to be quite good, although it predicts a slightly too "narrow" efficiency curve.



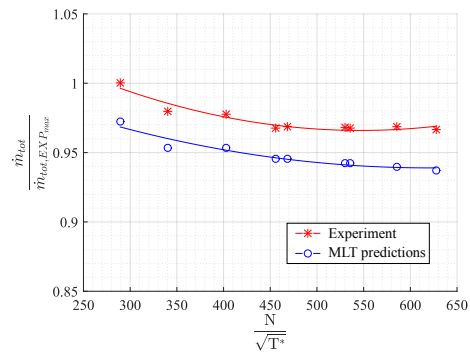
(a) Total-to-static efficiency as function of dimensionless speed



(b) Dimensionless mass flow as function of dimensionless speed



(c)  $\Lambda_P$  as function of dimensionless speed



(d) Total mass flow as function of dimensionless speed

Figure 7.20: Turbine characteristics with 7.23 % extra loss in the rotor, stage 4b,  $\Pi_{ts} = 2.06$

### 7.3 Global evaluation of stage 5 – PR = 1.23

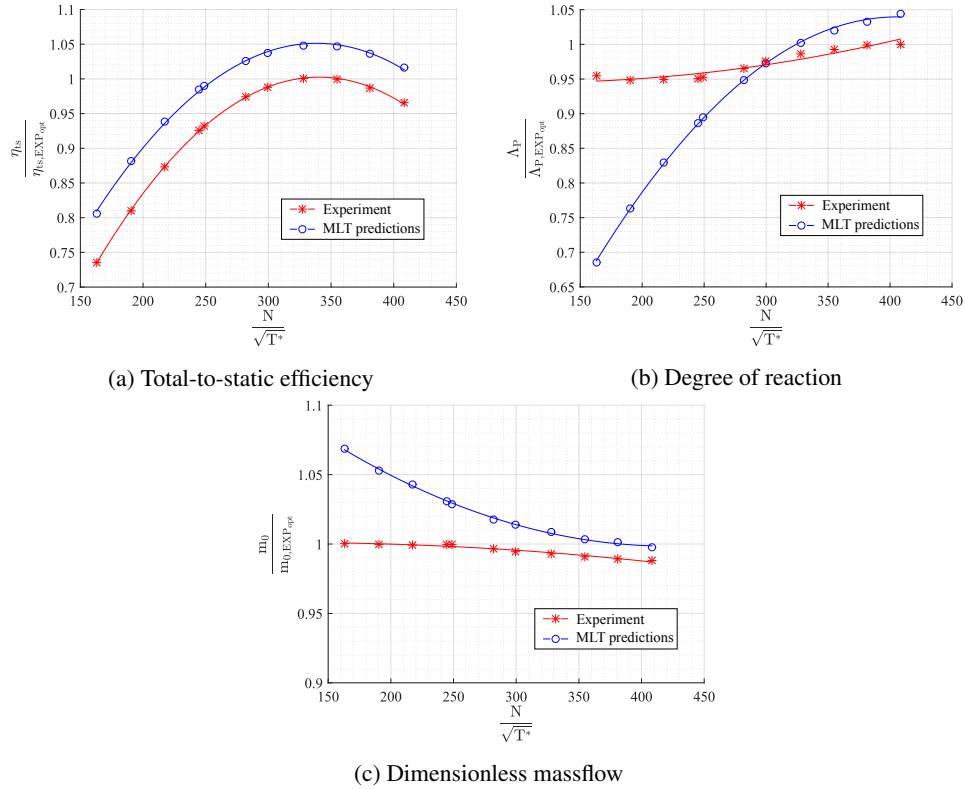


Figure 7.21: Turbine characteristics for stage 5 as function of dimensionless speed,  $\Pi_{ts} \approx 1.23$

The results from the stage 5 geometry will not be as extensive since experiment data is not available in such abundance as for stage 4b. From Figure 7.21a it is clear that the models are better tailored to gas turbine geometries when it comes to efficiency. The shape is very accurate but the level is off by about 4 p.p. However, the same cannot be said for parameters such as mass flow and degree of reaction presented in Figures 7.21b and 7.21c. The behavior of these two parameters is as bad as earlier predictions for stage 4b. Again, it seems like mass flow and degree of reaction predictions are tied together. While looking at these results, it should be observed that the range where measurements were made is not in the operating range of the turbine.

Stage 5 has a significantly higher design speed and the range with poor prediction is in the hard to predict, low speed range. During the writing of this thesis, the experiment data did not contain the entire operating range. It is however very

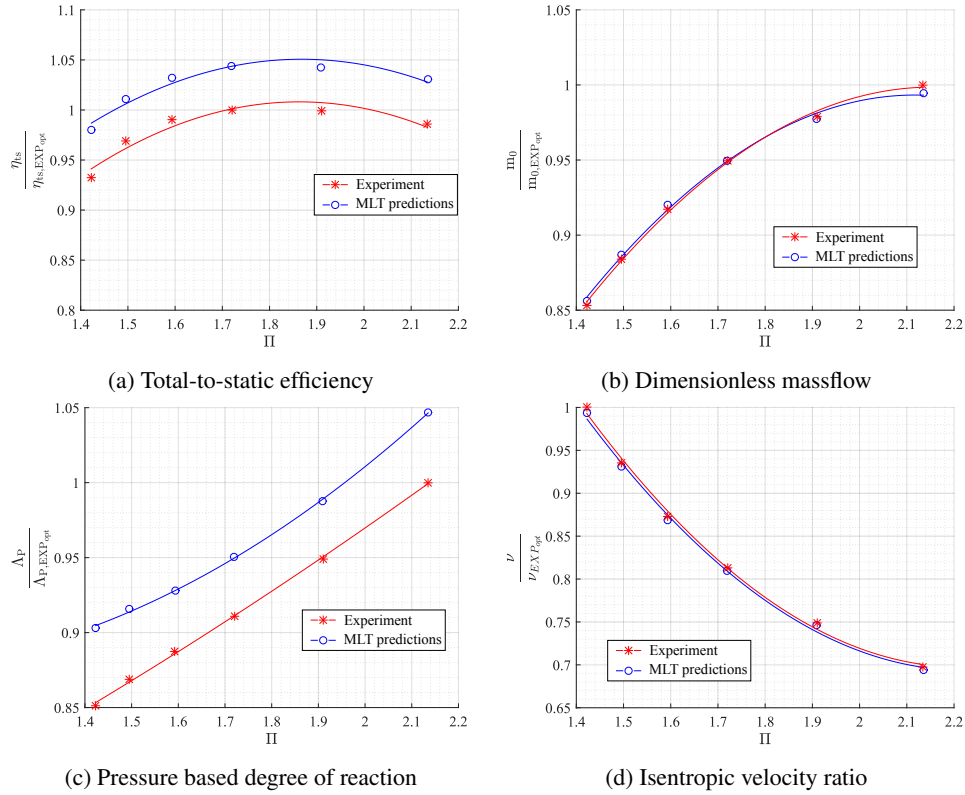


Figure 7.22: Stage 5 characteristics as function of pressure ratio,  $\frac{N}{\sqrt{T^*}} \approx 577$ , scaled to  $T^* = 350$  K

possible that the prediction is better in the high speed range. A more detailed analysis is hard to make since traversed data will not be available before the end of this thesis. However, it seems accurate to conclude that SIT models perform better for this higher reaction stage, as long as the turbine speed is in the normal operating range. Figure 7.22 show turbine characteristics for constant turbine speed and varying pressure ratios. Note that the turbine speed here is much higher than what is shown in Figure 7.21. These results indicate that the mass flow will be very accurate at high turbine speed and that the degree of reaction will be somewhat accurate, although still a bit overpredicted. Since this is only one operating point, it is too soon to draw final conclusions, but in conjunction with Figure 7.21 it does look like MLT is accurate for higher speeds, and not diverging again as was feared from the speed sweep measurements. The case needed to be scaled since the high pressure ratio would give negative enthalpy and non-valid answers if no preventive steps were taken. The method used for scaling is described in section 3.5.7.

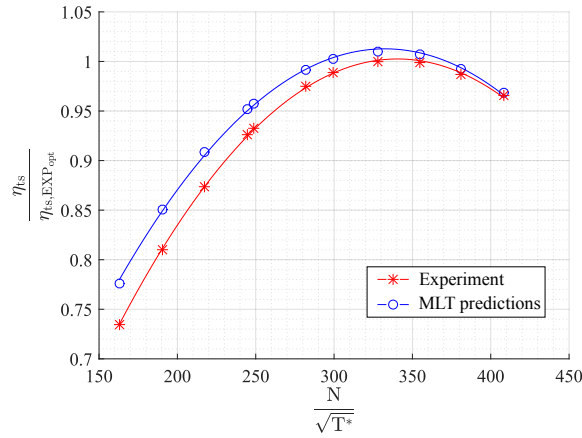


Figure 7.23: Total-to-static efficiency for stage 5 with stator losses matched to stage 4b,  $\Pi_{ts} \approx 1.23$

### 7.3.1 Extra losses

The performance for stage 5 is marginally better predicted than for stage 4b. The efficiency is off by about 4.6 p.p. and is almost constant over the measured speed range. Since traverse data of the stage were delayed to after the conclusion of this thesis, the real stator and rotor losses were unknown. As a substitute, an approximate solution was used to obtain approximate results. Since the stator is the same for both stage 5 and 4b, it was assumed that it could be approximated by values from the 4b measurements. Extra losses were added until stage 5 stator matched the measured values from 4b using the same method as described in section 7.2.6. The result from this corrected calculation is presented in Figure 7.23. The level at optimal operation is significantly better predicted, but the trend is actually worse compared to the uncorrected case. This would suggest that the results seen earlier with increased stator loss making more accurate predictions are not due to a better predicted stator, but something else might be wrongfully correcting the results. The reasoning behind this is that stage 4b is a steam turbine stage known to cause trouble when evaluating the rotor. Stage 5 is a gas turbine inspired stage, deemed more accurately predicted by MLT. The assumption that stator losses could simply be moved between the two stages might also be incorrect.

## 7.4 Comparison between stage 5 and 4b – PR = 1.23

### 7.4.1 Total-to-static efficiency

Figure 7.24 presents a comparison between stage performance for stage 4b and stage 5. The figure clearly shows the difference in operating speed between the two.

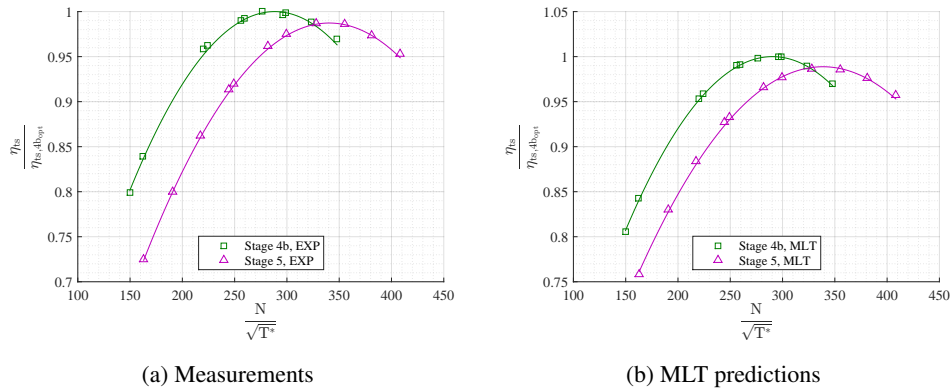


Figure 7.24: Comparison of total-to-static efficiency between stage 5 and stage 4b,  $\Pi_{ts} \approx 1.23$

The higher reaction stage 5 has a significantly higher optimal speed compared to stage 4b. Surprisingly, both measurements and predictions show a higher efficiency for the low reaction stage, and the difference between the two concepts is fairly similar for both experiments and predictions. This suggests the models are still adequately predicting differences between concepts. This is good news for SIT, since accuracy between concepts is of great importance in early design phases. The measured difference between the two at design speed is 1.07 p.p. while the difference for predictions is slightly lower at 0.99 p.p.

#### 7.4.2 Total-to-total efficiency

The total-to-total efficiency for both stages as function of dimensionless speed is presented in Figure 7.25. It can be seen that stage 5 has a higher total-to-total efficiency than stage 4b, opposite of how the total-to-static efficiency compares to one another.

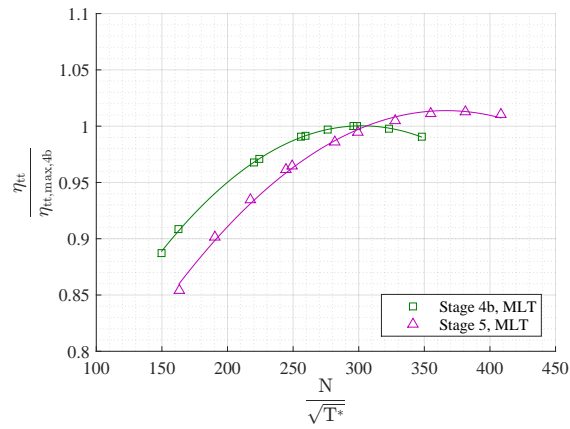


Figure 7.25: Total-to-total efficiency as function of dimensionless speed,  $\Pi_{ts} \approx 1.23$

## 7.5 Profile loss validation

The results from MISES show good, but not perfect agreement with MLT at operating conditions. It should be observed however, that MISES does the same overprediction of the off design loss. This is unexpected since MISES is generally regarded as accurate. The implications from MISES is still that profile loss is accurately captured by MLT, as can be seen from Figure 7.26, and that the error in loss must be from secondary flows. To confirm this, further investigation is necessary.

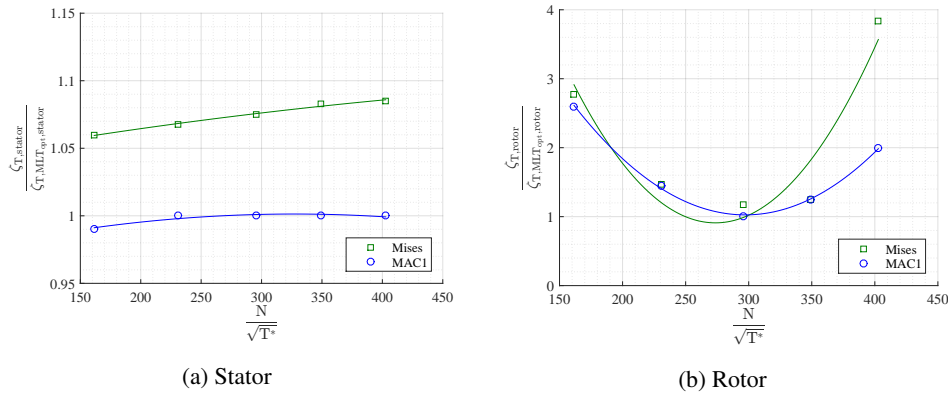


Figure 7.26: Traupel's and MLT profile loss, AVDR compensated, stage 4b,  $\Pi \approx 1.23$

## 7.6 Alternative secondary loss models

All data up to this point implies underpredicted secondary losses. This has also been previously implied by [20, ch 4.3 – p. 91, pp.95–96], in-house codes predict very low secondary losses in comparison to models available in the open literature. Differences in between 50–200 % higher for other models can be found depending on operating conditions. However, the total losses are on the same level since their losses are generally higher for MLT. In order to evaluate if this is the reason behind the results seen previously in this thesis, different loss models available in the open literature have been studied and tested. The models tested here are chosen based on merit, age, ease of implementation and suggestions made in [20]. Sections 7.6.1 to 7.6.4 presents the predictions with the different secondary loss models applied. The sections present comparisons for measured, old and new loss coefficients and also the effects on the stage in terms of degree of reaction and total-to-static efficiency for stage 4b with a pressure ratio of 1.23.

### 7.6.1 BSM

Figure 7.27 and 7.28 show the results of implementing the BSM models into MLT. There is a increase in secondary loss for the stator and the rotor show a increase at opimal conditions without increasing it for the low and high speeds, suggesting a lower impact of incidence which matches the measured losses more accurately. The effect of this is seen in Figure 7.28 with a much closer approximation of the efficiency curve, especially for the optimal point where the difference is less then half of the unmodified MLT model without making the lowest and highest speed points suffer. The degree of reaction is a bit increased for the optimum point, but the difference is very slight and the big discrepancy is still present.

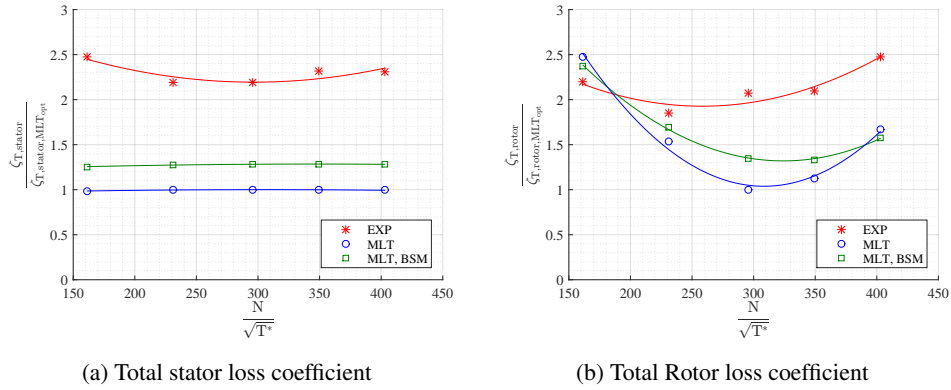


Figure 7.27: Total loss coefficients with BSM's secondary loss model, stage 4b,  $\Pi_{ts} \approx 1.23$

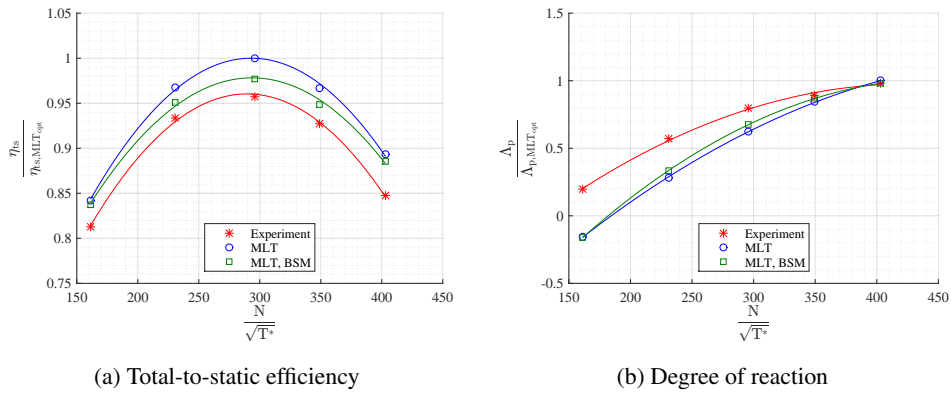
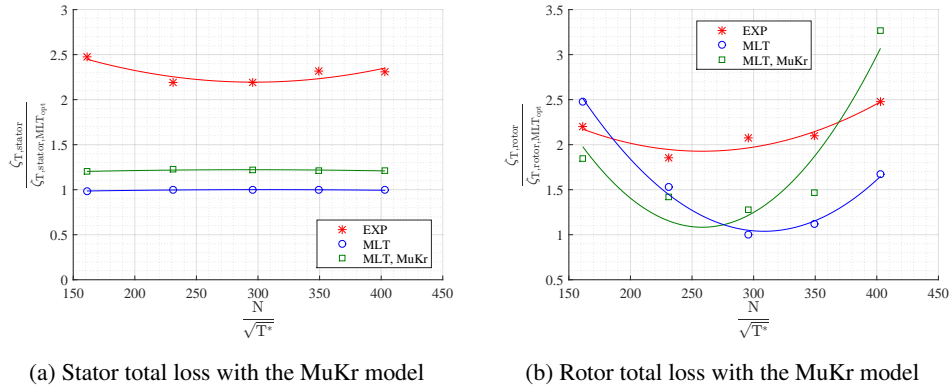
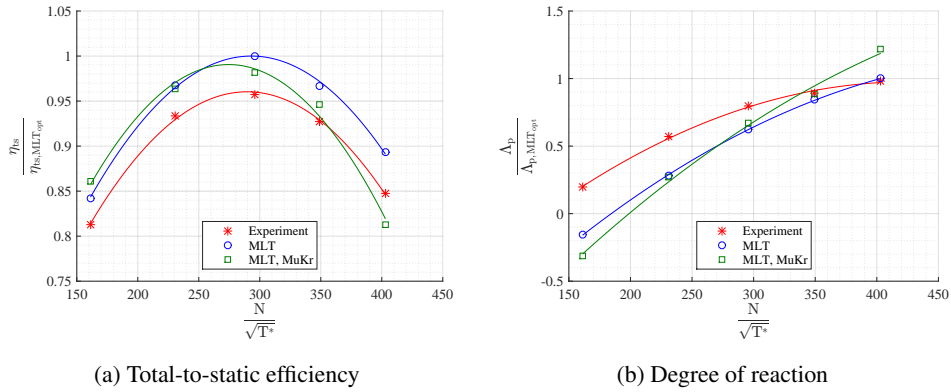


Figure 7.28: Turbine characteristics with BSM's loss model for the stator, stage 4b,  $\Pi_{ts} \approx 1.23$

### 7.6.2 MuKr

Figures 7.29a and 7.29b are showing a significantly higher secondary loss for the stator with the use of the MuKr model. The levels are not on par with the levels predicted by AXIAL, and a bit lower than predicted by BSM, but still a lot higher than what has been predicted by MLT. The MuKr model operates in the same way as the models used at SIT today, using profile and flow angle as input with corrections for incidence. The rotor looks much more accurate, but with a lower sensitivity for incidence as has already been observed to be over predicted by SIT in-house models, further confirming this hypothesis.



Figure 7.29: Total loss coefficients for the MuKr model, stage 4b,  $\Pi_{ts} \approx 1.23$ Figure 7.30: Comparison between experiment, unmodified MLT and MLT with MuKr's secondary loss model, stage 4b,  $\Pi_{ts} \approx 1.23$ 

### 7.6.3 Traupel

The results from implementing Traupel's secondary loss model is shown in Figures 7.32 to 7.31. The results show a very accurate prediction of the optimal efficiency, a significant improvement over MLT's prediction. The optimal point is however slightly moved towards higher turbine speeds. Traupel's loss model also shows a significant improvement in the prediction of degree of reaction. The curve has the flatter appearance observed in measurements and also a higher lowest reaction while simultaneously not over predicting high turbine speeds. Figure 7.33 show where on Traupel's secondary loss graph the stator and rotor are placed.

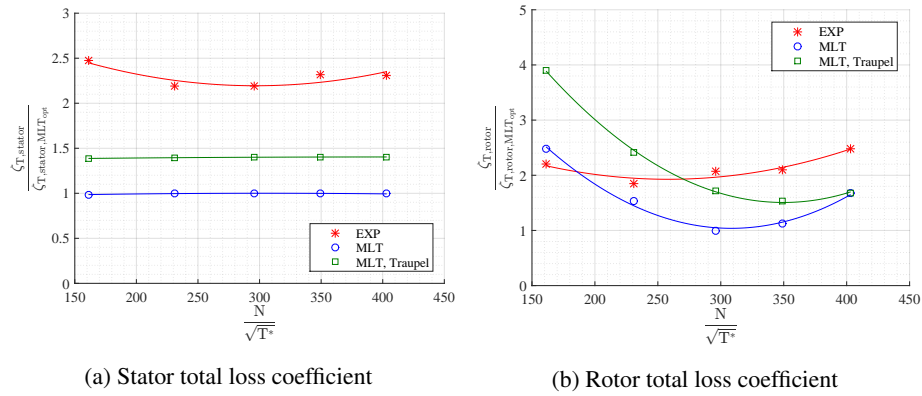


Figure 7.31: Total loss coefficients with Traupel's secondary loss model,  $\Pi_{tS} \approx 1.23$

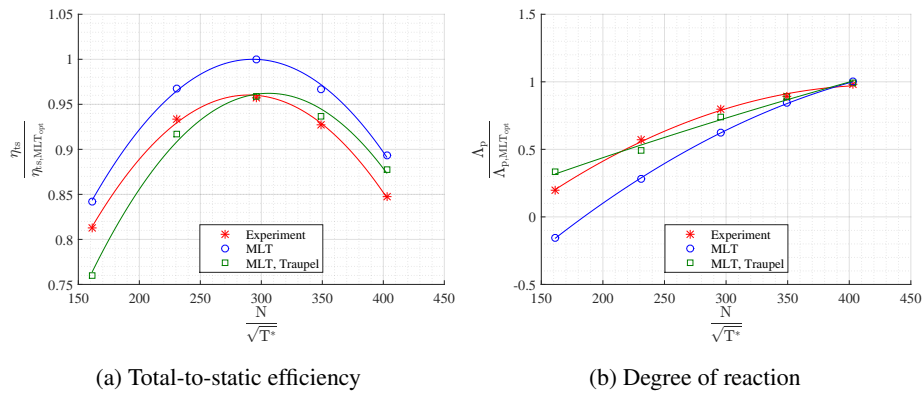


Figure 7.32: Comparison between experiment, unmodified MLT and MLT with Traupel's secondary loss model, stage 4b,  $\Pi_{tS} \approx 1.23$

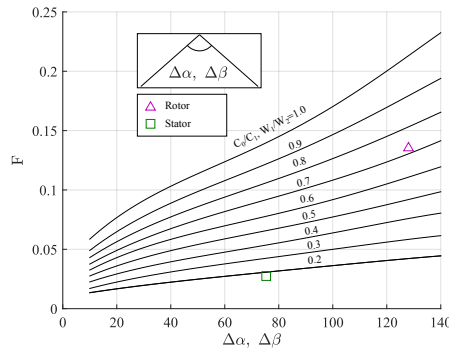


Figure 7.33: Traupel’s secondary loss graph with stator and rotor operating points marked, stage 4b,  $\Pi \approx 1.23$ ,  $\frac{N}{\sqrt{T^*}} \approx 295$

### 7.6.4 ShBu

Figures 7.34 to 7.35 show results from implementing ShBu’s loss model for secondary loss. The loss model has a strong impact on the efficiency as can be observed in Figure 7.35. With this secondary loss model, the total-to-static efficiency is constantly underpredicted, especially for low turbine speeds. The degree of reaction is very significantly affected, and shows an almost reversed trend at low speeds with increasing rather than decreasing degree of reaction at the lowest speeds. This gives a trend that is going in the opposite direction compared to both the original MLT model and measured values. ShBu’s predictions for loss coefficient in the rotor grow very rapidly as the turbine speed decreases. In fact, the lowest operating point needed to be capped to not crash MLT. The total stator loss however is predicted higher with ShBu than MLT, but still a bit under the experimentally measured value.

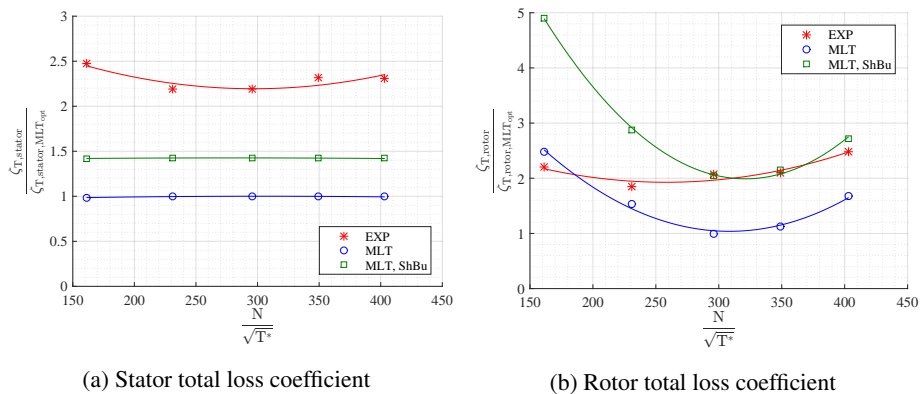


Figure 7.34: Total loss coefficients with ShBu secondary loss model, stage 4b,  $\Pi_{t,s} \approx 1.23$

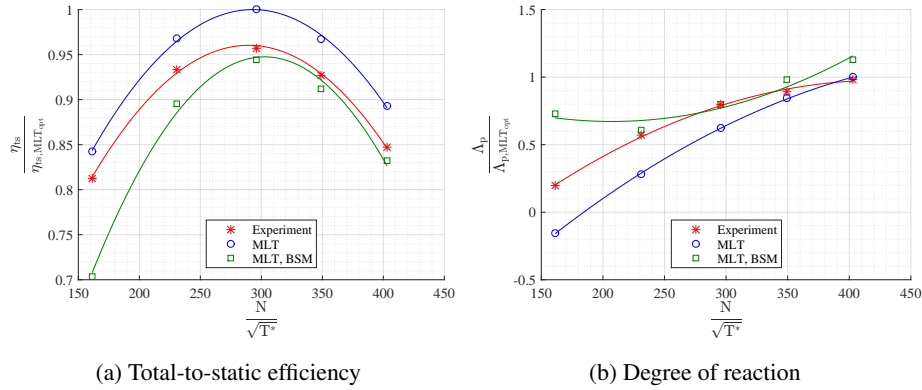


Figure 7.35: Comparison between experiment, unmodified MLT and MLT with ShBu's secondary loss model, stage 4b,  $\Pi_{ts} \approx 1.23$

### 7.6.5 Comparison between secondary loss models

Figure 7.36 show a clear improvement over MLT for all tested secondary loss models, especially for high turbine speeds. The low speed area is a bit worse for all tested models, especially MuKr and ShBu. MuKr in general seems to poorly predict this type of turbine stage and show a clear over estimation of incidence at high speeds. It should however be noted that the low amount of experimental data points have had a detrimental effect on the curve fit of the data points for this model, and the peak efficiency point has been skewed towards lower turbine speeds. A higher number of measurement points would probably smooth out the shape, but the high speed performance would still suffer. ShBu is showing a fast drop in efficiency at low speeds, but has a good precision at near optimal point and high speeds. Both BSM and Traupel's show an improvement over standard MLT over nearly the entire speed range, suggesting improvements could be made with inspiration from these modelling systems. However, Figure 7.37 which show degree of reaction show a concerning and confusing worsening of prediction performance, at least at low speeds. At just under design speed and higher, BSM and Traupel's models predict a bit better than MLT. MuKr again seems to be performing worse. Due to time constraint, this will not be investigated further.

Figure 7.38 show total-to-static efficiency for stage 5. A smaller difference between models is observed compared to stage 4b, possibly because the in-house codes are more tailored to these kinds of geometries. MLT has a very accurate shape, but lacking in absolute level. The most obvious difference can be observed for ShBu where the low performance again is very poor, but from close to optimal point to high speeds is very accurately predicted. MuKr, BSM and Traupel's models look very similar to MLT, with the biggest difference at low turbine speeds. At

close to optimal point and at high speeds, they all perform better than MLT and predicts closer and closer to measured values as speed is increased.

Figure 7.40 show the total-to-static efficiency for stage 4b at  $\Pi_{ts} \approx 2.06$  with all five loss models implemented. Just as has been seen for the lower pressure level, the open literature loss models in general show improvements over the currently used. The tested models all follow one another closely, with BSM showing a bit different trend with better prediction in the lower end and a bit worse at higher speeds. In general, it seems like the BSM model follow the experimental data very closely, just at a bit higher value. Both MuKr and Traupel's models show the same behavior with excess over prediction at low speeds, and close prediction at high, although it seems like the drop at overspeed is a bit too fast and that it might start under predicting at even higher speeds. ShBu is again severely underpredicting at low speeds but compensates by being very accurate at close to optimum and above. All of the alternative models are however almost always between MLT and the experimental data.

Figure 7.41 shows that most models are not good at predicting the degree of reaction, with all but MuKr showing poor performance at speeds far from the optimum point. ShBu especially show a strange behavior by having a completely different shape compared to the other models. ShBu overpredicts at both low and high speeds, something it is the only model to do.

The pressure ratio sweep for stage 5 continues to show that a higher reaction stage is better predicted by the models. The shapes for efficiency presented in Figure 7.42 are good for all models, with ShBu drifting away at higher pressure ratios. Despite this drift, it is still the model that consistently predict closest to the measured value. The degree of reaction for the pressure ratio sweep presented in Figure 7.43 show good shapes for all models. All models are also predicting very close to each other, but over predicts for all investigated pressure ratios.

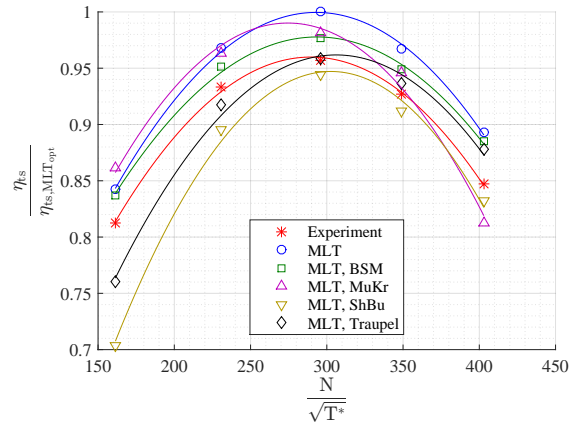


Figure 7.36: Total-to-static efficiency for stage 4b,  $\Pi_{ts} \approx 1.23$  with 4 different loss models

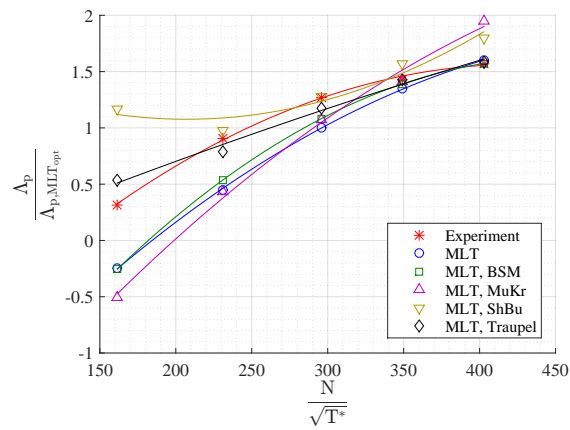


Figure 7.37: Degree of reaction for stage 4b,  $\Pi_{ts} \approx 1.23$  with 4 different loss models

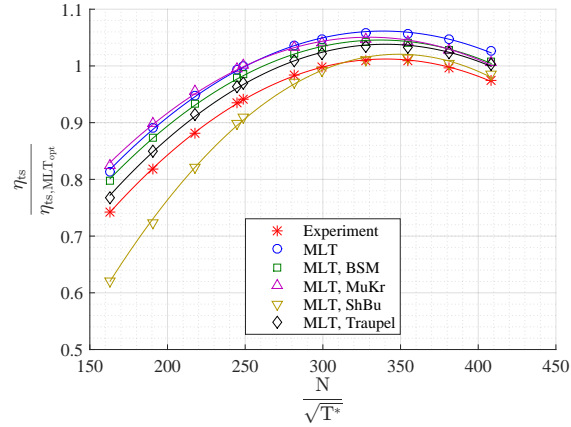


Figure 7.38: Total-to-static efficiency for stage 5,  $\Pi_{ts} \approx 1.23$  with 4 different loss models

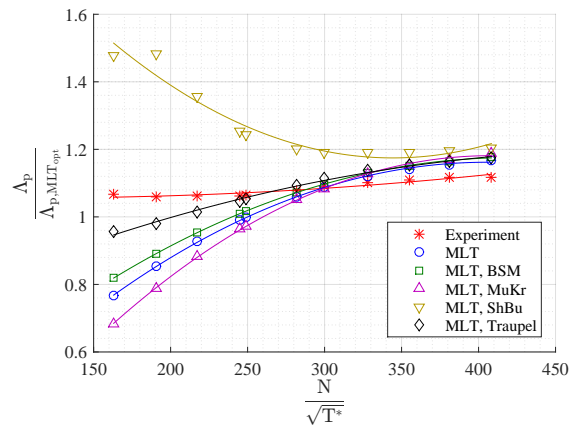


Figure 7.39: Degree of reaction for stage 5,  $\Pi_{ts} \approx 1.23$  with 4 different loss models

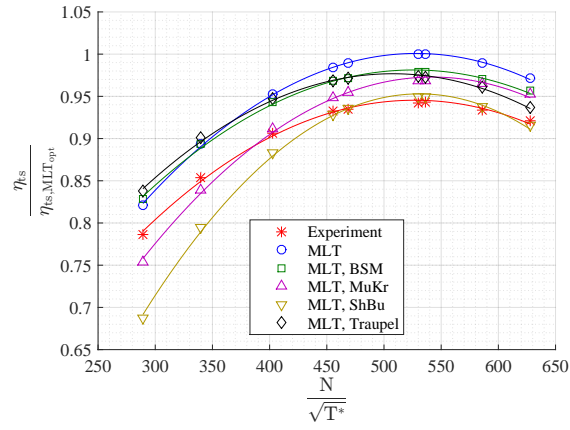


Figure 7.40: Total-to-static efficiency for stage 4b,  $\Pi_{ts} \approx 2.06$  with 4 different loss models

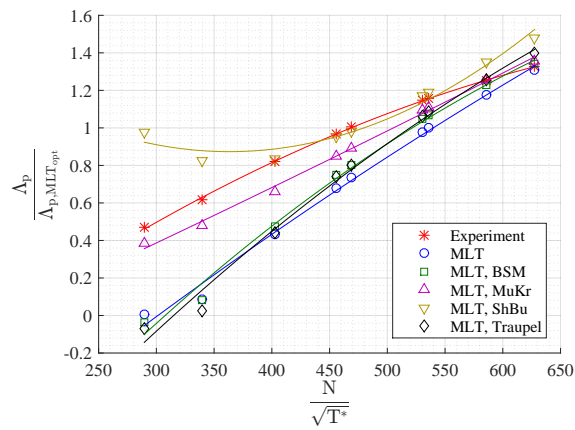


Figure 7.41: Degree of reaction for stage 4b,  $\Pi_{ts} \approx 2.06$  with 4 different loss models



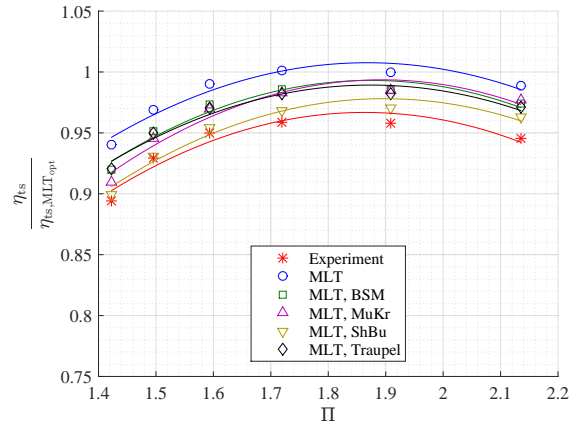


Figure 7.42: Total-to-static efficiency as function of  $\Pi_{t5}$ , stage 5,  $\frac{N}{\sqrt{T^*}} \approx 560$

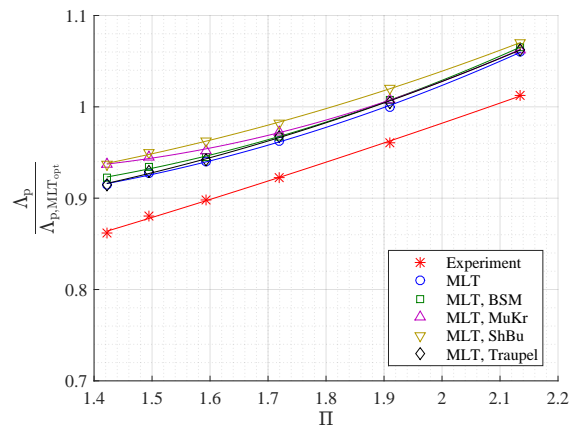


Figure 7.43: Degree of reaction as function of  $\Pi_{t5}$ , stage 5,  $\frac{N}{\sqrt{T^*}} \approx 560$

### 7.6.6 Secondary loss investigation

To get a more detailed picture of how MLT's model for secondary loss perform in comparison to models in the open literature, a parametric study was made to evaluate whether the in-house model show a significantly different trend if certain blade row parameters are changed. In order to do this, the already presented secondary loss models available in open literature were implemented in MATLAB and compared. In this study, two parameters were varied, the aspect ratio by altering blade height and the exit angle out of the blade row. The study was made for the stator and both stage 4b's and 5's rotor. The variation of aspect ratio is presented in Figures 7.44, 7.46 and 7.48. They all show that MLT is predicting the lowest secondary losses compared to all the other tested models. The figures also show that MLT has the weakest dependence on aspect ratio, indicating something in the model is underestimating the impact of having a short blade. The difference is most evident in the stator and for the impulse type blade. For the high reaction stage 5 blade, the weak dependence seems to be gone. However, even for the high reaction blade, a low initial value can be observed, suggesting not only the aspect ratio dependence but also the general level is not accurately predicted. Figures 7.45, 7.47 and 7.49 show the dependence on outlet angle. A smaller outlet angle will give a smaller throat, but also increase the stage turning. MLT seems to follow a good trend for angle dependence, but the level is too low as explained earlier. It should be observed that Traupel's secondary loss model is basically linear for all varied angles because of how it works. The greatest difference in outlet angle dependence seems to be for stage 5's high reaction blade, a geometry that showed the best agreement when aspect ratio was evaluated.

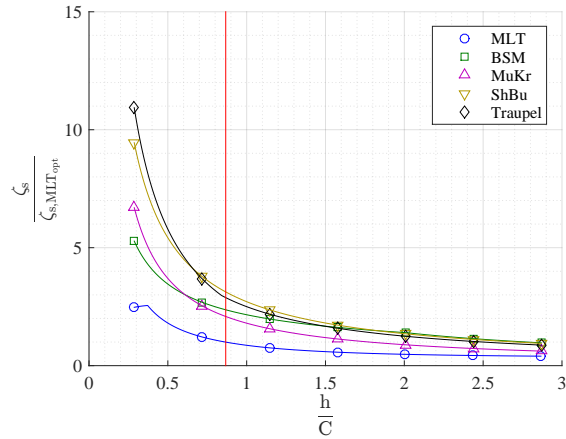


Figure 7.44: Comparison between secondary loss coefficients with varying aspect ratio for stage 4b's stator

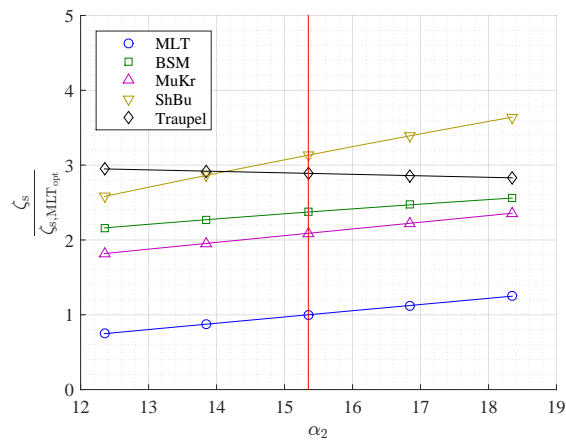


Figure 7.45: Comparison between secondary loss coefficients with varying exit angle for stage 4b's stator

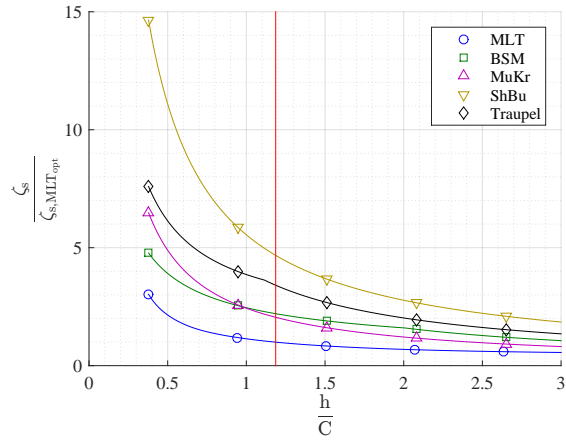


Figure 7.46: Comparison between secondary loss coefficients with varying aspect ratio for stage 4b's rotor

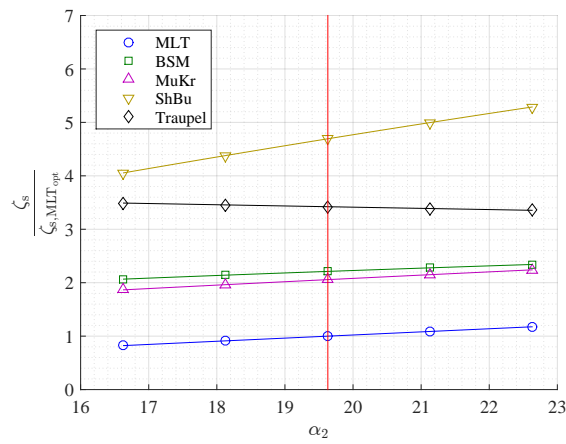


Figure 7.47: Comparison between secondary loss coefficients with varying exit angle for stage 4b's rotor

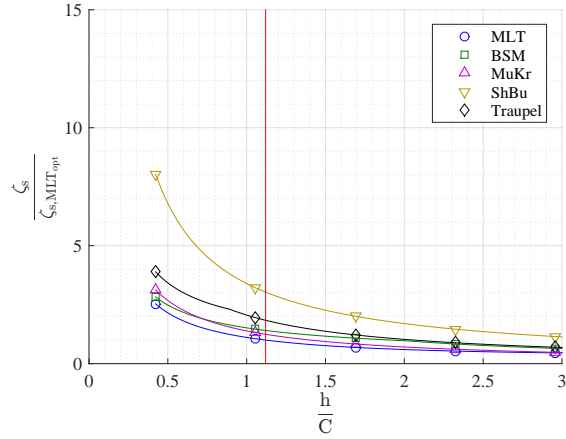


Figure 7.48: Comparison between secondary loss coefficients with varying aspect ratio for stage 5's rotor

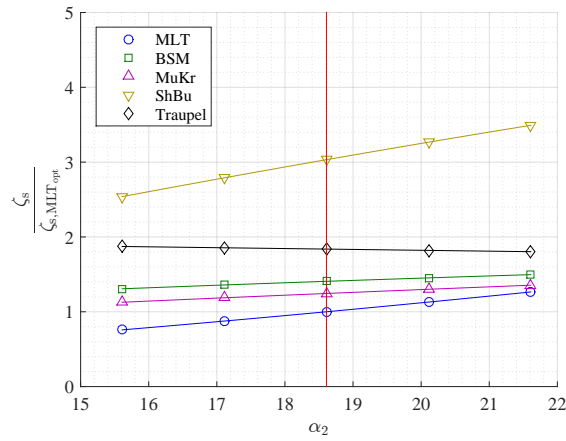


Figure 7.49: Comparison between secondary loss coefficients with varying exit angle for stage 5's rotor

## 7.7 Cavity purge flow impact

Figure 7.50 shows the effect of cavity purge flow. As can clearly be seen from it, MLT underestimates the impact of cavity purge flow. It should be noted that for SIT, the interesting range is up to about 3 % purge flow, meaning just a part of the total measured range is of interest. The number of measured points is small, but it does seem like the impact of cavity flow is linear. In the range were SIT turbines operate, the efficiency drop is underpredicted with about 1.1 p.p. as can be seen in Figure 7.50a. From this, it can be suspected that cavity purge flows are not getting the attention they should since the impact on efficiency is not seen as severe as in reality. Figure 7.50b show an overpredicted dependence for degree of reaction. There is however uncertainties of how the impulse blade reacts in comparison to a reaction blade in the in-house models. It should also be noted the available dataset is really small, both in terms of data-points and in terms of tested objects since only one has been tested. This makes it unwise to draw any broader conclusions; instead, it should be seen as a hint of what might be discovered with closer scrutiny.

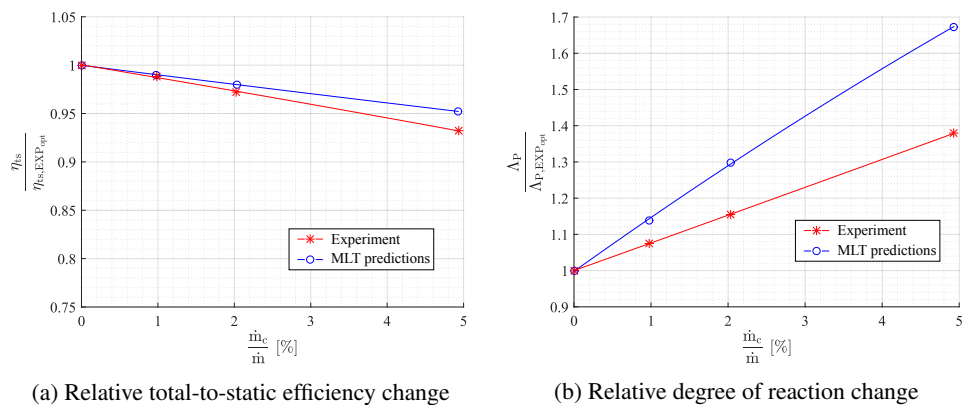


Figure 7.50: Impact of cavity purge flow, stage 4b,  $v_{tS} \approx 0.47$

# Chapter 8

## Discussion

### 8.1 Conclusions

This thesis has been focused on validating the new 1-D code MLT against a small scale test turbine. The validation has showed that the models used in MLT do not agree well with the measurements from the test turbine. MLT in general over predicts the efficiency for both tested geometries and a reason for this have been searched. Turbine characteristics such as degree of reaction and flow capacity are also not predicted very well. It has been concluded that the secondary losses are underpredicted by MLT and alternative secondary loss models have therefore been tested to find possibilities for improvements. No conclusion has been reached as to which of the alternative models performs best. However it is evident that they in general give more reasonable predictions than the model used in MLT today. It is highly suspected that the models with a more modern approach, utilizing boundary layers, are more accurate and versatile. It has also been observed that the high reaction blade tested showed less variation in between the models, and the predictions in general was much closer to measurements. There are still loss sources such as tip leakage and cavity interactions left to be investigated and validated. The possible impact of these loss sources is unknown.

As previously stated, the secondary losses in the current models seem to be underpredicted. This is supported by studying of open literature and experimental results. The reason behind this under prediction is hard to pin down since the current loss model system used in MLT is complex and interweaved with other loss coefficients. However, the results suggests an underpredicted impact of aspect ratio might be a reason behind the observed behavior. The over estimation of test turbine performance in conjunction with exclusion of other error sources makes it clear that the secondary loss system need significant rework.

The number of turbine geometries and operating conditions tested in this thesis are very few, and to draw a general conclusion applicable for all turbine geometries is not possible at this point. However, a few conclusions about the geometries investigated in this thesis are possible. The conclusions are listed below. Even though a few conclusions can be drawn, there is only enough data to hint at what is the underlying cause to the bad predictions. It was also discovered that there was certain problems regarding the accuracy of the traverse measurements caused by wall interference between wall and measuring probe. This has resulted in uncertainty for the gas state within the stage, which in turn has affected velocities and losses in this measurement plane. Exactly how large these possible errors are yet to be determined. However, since the global measurements has not been affected by this error source, the general conclusions are still thought to be valid.

- **The Test Data**

- There might be a difference in the specifications the stator was designed to have and the one it ended up being manufactured with.
- Interference between the wall and traverse probe has affected the acquired test data.

- **Computational predictions**

- Both MLT and open literature models perform better for a high reaction stage.
- Secondary losses are underpredicted. This is especially true for impulse blades, but also for the high reaction stage.
- Some of the loss models available in the open literature seems to offer improvements over the in-house tools used today.
- MLT is good at comparing concepts.
- It seems like the in-house models under predict the impact of cavity purge flow, possibly due to no care being taken to adjust for impact other than mixing losses.
- A brief investigation in cavity purge flow loss show an underpredicted impact on the total-to-static efficiency.
- Very low turbine speeds seems to have a large impact on total-to-static efficiency.
- High pressure ratio and low rotor speeds with the low temperatures seen in test turbine environments are problematic for the in-house codes in terms of convergence and physical results.



- The in house codes are over predicting the impact of incidence.

## 8.2 Future work

The conclusions from this thesis leave a lot of future work. Because of the large discrepancies in secondary losses for some cases, the secondary loss models need significant work with tuning, or possibly be re-implemented using a more modern approach. Since the complete loss system is tuned to give good agreement for full scale machines, any alteration in secondary loss modelling will need to be validated and also probably be compensated by altering other loss sources. Identifying other loss sources that might be falsely predicted will require a large amount of work. A creation of a new loss system or a substantial update of the current will also require extensive validation, both on the test turbine and production machines. The errors caused by measurement equipment is a cause for concern and more work is needed to try and evaluate how much it has impacted the results in this thesis. A short list of suggested future work follows below

- Investigate reason behind discrepancy in prediction of degree of reaction.
- Further investigation of secondary loss systems to determine cause behind observed behavior.
- Further investigation of incidence modelling.
- Validate modelling of tip leakage and cavity interaction.
- Implement changes in loss prediction and re-validate the new loss system.
- Check accuracy of the manufactured stator and rotor geometry.
- Estimate the impact of the errors in traverse measurements.

# Bibliography

- [1] Y. A. Cengel and M. A. Boles, *Thermodynamics An Engineering Approach*. New York, USA: McGraw-Hill, 2011, ISBN:978-007-131111-3.
- [2] S. L. Dixon and C. A. Hall, *Fluid Mechanics and Thermodynamics of Turbomachinery*. Oxford, UK: Butterworth-Heinemann, 2014, ISBN:978-0-12-415954-9.
- [3] C. Hjalmarsson, N. Mikailian, and K. Flydalen, *Description of aerodynamical loss models in 1D/2D Aero-codes (MAC & Beta)*. SIT Technical Report, 2014, RT\_AERO\_006\_14.
- [4] H. Moustapha, M. H. Zelesky, N. C. Baines, and D. Japikse, *Axial And Radial Turbines*. Vermont, USA: Concepts NREC, 2003, ISBN:0-933283-12-0.
- [5] J. D. Denton and L. Xu, “The exploitation of three-dimensional flow in turbomachinery design,” *Journal of Mechanical Engineering Science*, vol. 213, no. 2, pp. 125–137, February 1998.
- [6] J. P. Longley, “Introduction to 3–D Flows in Turbomachinery,” in *Cambridge Turbomachinery Course 2012*. CTC, June 2012, vol. 1.
- [7] A. Persson, “Medidional profiling in VAXII,” November 1995, RT TEF 3395.
- [8] H. P. Hodson, “Blade to Blade Flowfields in Axial Flow Turbomachines,” in *Cambridge Turbomachinery Course 2012*. CTC, June 2012, vol. 1.
- [9] L. S. Dzung, “Konsistente Mittelwerte in der Theorie der Turbomaschinen für Kompressible Medien,” *Brown Boveri Mitteilungen*, pp. 485–492, 1971.
- [10] H. I. H. Saravanamuttoo, G. F. C. Rogers, H. Cohen, and P. V. Straznicky, *Gas Turbine Theory*. Essex, England: Pearson Education Limited, 2009, ISBN:978-91-637-4473-0.
- [11] D. F. Young, B. R. Munson, T. H. Okiishi, and W. W. Heubsch, *Introduction to Fluid Mechanics*, 5th ed. John Wiley & Sons, 2012, ISBN 9780470902158.

- [12] J. D. Denton, "Introductory Review of Basic Principles," in *Cambridge Turbomachinery Course 2012*. CTC, June 2012, vol. 1.
- [13] A. H. Shapiro, *The dynamics and thermodynamics of compressible fluid flow*. The Ronald press company, 1953, vol. 1.
- [14] M. Persson, *Highly loaded HPT blading in the KTH test turbine - An attempt to reduce the number of blades in the first stage in a high pressure turbine*. SIT internal report, 2015, RT\_AERO\_009\_15.
- [15] Y. A. Cengel and J. Cimbala, *Fluid Mechanics – Fundamentals and Applications*. McGraw-Hill Education, January 2013, ISBN 978-0073380322.
- [16] J. D. Denton and R. J. Miller, "Loss Mechanisms in Turbomachines," in *Cambridge Turbomachinery Course 2012*. CTC, June 2012, vol. 1.
- [17] M. W. Benner, S. A. Sjolander, and S. H. Moustapha, "An Empirical Prediction Method for Secondary Losses in Turbines – Part II: A New Secondary Loss Correlation," *Journal of Turbomachinery*, vol. 128, pp. 281–291, april 2006.
- [18] E. M. Greitzer, C. S. Tan, and M. Graf, *Internal Flow Concepts and Applications*. Camebridge university press, 2004.
- [19] M. W. Benner, S. A. Sjolander, and S. H. Moustapha, "An Empirical Prediction Method for Secondary Losses in Turbines – Part I: A New Loss Breakdown Scheme and Penetration Depth Correlation," *Journal of Turbomachinery*, vol. 128, pp. 273–280, april 2006.
- [20] A. N. Dahlquist, "Investigation of Losses Prediction Methods in 1D for Axial Gas Turbines," Master's thesis, Lund University, Lund Sweden, November 2008.
- [21] W. Traupel, *Thermische Turbomachinen*, 3rd ed. Springer-Verlag, 1977, vol. 1, ISBN 3-540-07939-4.
- [22] Å. Göransson, L. Hedlund, P. Hirsch, and C. Watzelt, *The PGI loss model for steam turbine performance calculations, a status report*, 1st ed. SIT internal report, December 1997, RT ATP 1697.
- [23] O. P. Sharma and T. L. Butler, "Prediction of Endwall Losses and Secondary Flows in Axial Flow Turbine Cascades," *Journal of Turbomachinery*, vol. 109, pp. 229–235, april 1987.
- [24] M. Drela and H. Youngren, "A user's guide to mises 2.63," <http://web.mit.edu/drela/Public/web/mises/mises.pdf>, 2008, [Online; accessed 29-March-2016].
- [25] N. Mikailian, *Test turbine measurements and comparison with mean-line and throughflow calculations*. SIT internal report, 2012, RT\_AERO\_033\_12.

- 
- [26] L. Hedlund, *Test turbine tests with profiles P21 and P20 compared with AX-IAL calculations*. SIT Technical Report, 2012, RT DA 21/04.
- [27] J. Wickholm, *Investigation of the Spanwise Transport in a Turbine Stage*. SIT Technical Report, 1999, RT RTF 009/99.
- [28] K. Flydalen, T. Pihlstrand, and C. Hjalmarsson, *Investigation of ID incidence losses*. SIT Technical Report, 2011, RT\_GRCTA\_022\_11.
- [29] L. Hedlund, April 2016, private Conversation.